공학박사 학위논문

Capturability Analysis of Missile Guidance Laws Considering Seeker's Field-of-View Limit

탐색기의 시야각 제한을 고려한 유도탄 유도기법의 요격영역 분석

2019 년 8 월

서울대학교 대학원

기계항공공학부

이 석 원

Capturability Analysis of Missile Guidance Laws Considering Seeker's Field-of-View Limit

탐색기의 시야각 제한을 고려한 유도탄 유도기법의 요격영역 분석

지도교수 김 유 단

이 논문을 공학박사 학위논문으로 제출함

2019 년 6 월

서울대학교 대학원

기계항공공학부

이 석 원

이석원의 공학박사 학위논문을 인준함

2019 년 6 월

위 원 장 박 찬 국 (인)

부위원장 김 유 단 (인)

위 원 김 현 진 (인)

위 원 탁 민 제 (인)

위 원 유 창 경 (인)

Capturability Analysis of Missile Guidance Laws Considering Seeker's Field-of-View Limit

by

Seokwon Lee

Submitted to the Graduate School of
Seoul National University
in partial fulfillment of the requirements for the degree of

Doctor of Philosophy

Department of Mechanical and Aerospace Engineering
Seoul National University

Advisor: Prof. Youdan Kim

August 2019

Capturability Analysis of Missile Guidance Laws Considering Seeker's Field-of-View Limit

by

Seokwon Lee

Approved as to style and content by:

Chan Gook Park, Chair, Ph.D.

Youdan Kim, Vice-Chair, Ph.D.

H. Jin Kim, Member, Ph.D.

Min Jea Tahk, Member, Ph.D.

Chang Kyung Ryoo, Member, Ph.D.

With great love to my family.

Abstract

Capturability Analysis of Missile Guidance Laws Considering Seeker's Field-of-View Limit

Seokwon Lee
Department of Mechanical and Aerospace Engineering
The Graduate School
Seoul National University

A capturability analysis of missile guidance laws with constraints on the seeker's field-of-view limit is proposed against moving targets. The capture region is expressed in the initial position space to facilitate the integration with midcourse guidance, where physical constraints including the seeker's field-of-view limit and maximum acceleration are taken into account in the derivation process. Missile guidance laws are classified into two categories depending on the guidance objectives: guidance law for target interception and impact-angle-control guidance law. On the basis of the capture region, the characteristics of the guidance laws according to the reduction of the field-of-view limit are analyzed. The capture region of guidance laws is derived for guidance laws whose primary objective is to intercept a target. Pure-proportional navigation guidance as well as look-angle constrained composite guidance consisting of pure-proportional navigation and a look-angle control scheme is considered. The capture region is obtained by using an analytical solution of the trajectories and by considering the phase portraits of the proportional navigation and the deviated pure pursuit.

The capture region of the impact-angle control guidance law is also analyzed. To analyze the capture region of the impact angle control guidance law,

a composite guidance method is considered in which the deviated pure pursuit is performed in the initial phase and proportional navigation guidance is performed in the terminal phase. In addition, a modified impact-angle-control guidance scheme is proposed, where the look angle command is modified in the initial phase to improve the performance of the existing impact-angle control composite guidance. Then, the capture region of the proposed guidance law is obtained. The capture region of the impact-angle control composite guidance is analyzed by several sub-regions including the impact angle set according to the initial distance and the initial line-of-sight angle, and the initial position to satisfy a specific impact-angle constraint.

The characteristics of the guidance laws are analyzed on the basis of the capture regions. Because of the reduction of the field-of-view limit, the capture region of the guidance laws becomes narrower and is divided according to the head-on and tail-chase engagement geometries. In the case of the look-angle constrained composite guidance, the capture region is expanded as compared to the proportional navigation guidance because of the maneuver that maintains its look angle within the field-of-view. In the case of impact-angle control guidance, the confined achievable impact angle is analyzed, and the capture region expanded over the existing method is discussed. Finally, numerical simulations for air-to-air engagement are carried out to verify the capture region and to compare the performance of the guidance laws.

Keywords: Missile Guidance, Capturability Analysis, Pure Proportional Navigation, Look Angle Control, Field-of-View

Student Number: 2012-20690

Contents

List of Tables

List of Figures

Chapter 1

Introduction

1.1 Background and Motivation

Since World War II, the weapon technology has been advanced, and the recent warfare has diverse and challenging requirements for guided weapons including improved lethality, tactical flexibility, and low-cost efficiency. With the increased demands, a precision strike missile system with the lightweight capability was developed to replace formal weapon systems [1]. One of the examples is the anti-tank guided munitions (ATGMs) for relatively short-range engagement, where shoulder-launched weapon systems adopted a "fire-and-forget" strategy to reduce the operational burden.

Most of the existing guided missile systems implement a strap-down seeker, which is rigidly mounted on the missile body without gimbal because of several benefits such as compact structure, high reliability, low cost, and low weight. For example, a strap-down-IR (infrared light) seeker is installed on low-cost guided-imaging rockets [2] and spike missiles [3], and a strap-down laser seeker system is implemented in advanced precision weapon systems (APKWSs) [4]. Joint direct attack munition (JDAM) equipped with an uncooled infrared strap-down seeker (direct attack munition affordable seeker; DAMASK) was developed to replace

laser-guided bombs [5]. Furthermore, there have been increased attempts to apply the strap-down seeker to missile systems for air and missile defense (AMD). Rockheed Martin is developing a small, lightweight weapon seeker to enable smart munitions to engage moving and relocatable targets, where global positioning system (GPS) satellite navigation may not be available as part of the DARPA Seeker Cost Transformation (SECTR) program. In standard missile-3 (SM-3) [6], the IR seeker is mounted on the kill warhead to detect a target in an exo-atmospheric environment, as shown in Fig. 1.1(b).

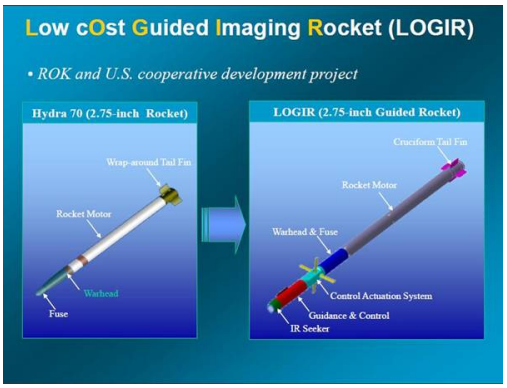

(a) low-cost-guided-imaging-rocket

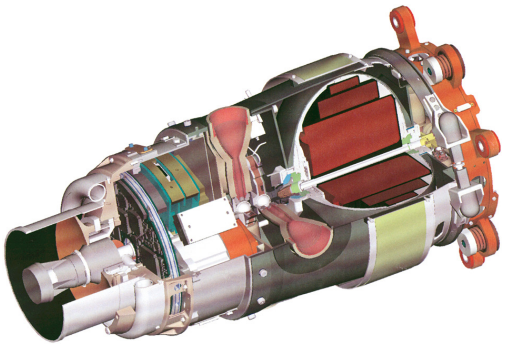

(b) SM-3 kill warhead [6]

Figure 1.1: Examples of Strap-down Seeker Guided Weapons

In regard to the strap-down seeker-guided missiles for the AMD, intercepting a fast-moving target is a challenging but crucial task. Against the moving target, good hit-to-kill performance is essential for the missile to directly destroy the target. Often, the air-to-air engagement needs to be done in a specific configuration together with the hit-to-kill requirement to increase the kill probability, which usually involves a large closing speed. To accomplish the mission, it is required to obtain the initial condition that guarantees the capture of the target. Furthermore, in active-homing missiles, the mission requirements could be even more complicated because the strap-down seeker has to acquire the target and lock on it during the engagement. The missile has to accurately detect the long-range target through the seeker and directly hit the target; therefore, the image resolution of the seeker needs to be improved by narrowing its field-of-view (FOV) for improved detectability.

The strap-down seeker needs to resolve some drawbacks associated with vulnerability to measurements errors, parasite effects, and restrictions on the missile maneuvers. In particular, because of the limited FOV of the seeker, the missile must perform a maneuver while always maintaining the image of the target within the narrow FOV, which may restrict the maneuvers of the missile. A narrow FOV increases the severity of this restriction and results in the failure of target interception at the end of the engagement. This difficulty can be resolved by designing an appropriate guidance law that considers the seeker's FOV limit and by analyzing the capture region of the guidance law.

Meanwhile, capturability analysis is very important, because even FOV-constrained guidance laws may fail to intercept the target if the missile initiates the homing phase outside its capture region. Capturability analysis has

been used to evaluate the performance of the guidance law, and the analysis results can be utilized in the mission analysis to determine the launch condition of the missile and the parameter specification of the guidance law. Usually, capturability analysis is performed by finding the closed-form solution of the relative motion or by obtaining the capture condition of the missile-target for various parameters, including the initial position, velocity, and guidance gain of the missile. However, the relative dynamics between a missile and a target are nonlinear; therefore, it is difficult to obtain the closed-form solution of the relative motion and to analyze the capture condition. More importantly, if the guidance law needs to be designed to satisfy multiple constraints, the analysis is considerably more challenging.

From this aspect, it is necessary to investigate the compatibility of the existing guidance laws for air-to-air engagement under a seeker's narrow FOV limit. Even though there has been considerable research on guidance laws regarding the FOV limit, most of the existing guidance laws have been designed for surface-to-surface engagement, which may be less effective for air-to-air engagement. Unlike the surface targets, the air-to-air missile must intercept a fast-moving target, and the narrow FOV of the strap-down seeker will severely confine the maneuvers of the missile. Consequently, successful interception will be achieved only under restricted initial configurations. In particular, an initial point of the homing missile, which is a handover point between the midcourse and the terminal phases, should be predetermined for the interception considering various harsh conditions.

1.2 Literature Review

The literature review in this section is categorized into two classes; guidance laws considering a seeker's FOV limit, and capturability analysis on the guidance laws.

1.2.1 Guidance Laws Considering Seeker's FOV Limit

To achieve the FOV constraint, the look angle should always be within the seeker's FOV limit, which is called the lock-on condition. The earliest studies on strap-down seeker guidance [7–9] focused on the problem associated with integrating strap-down seekers into the overall guidance system. Willman investigated the effect of the scale factor error on the stability of homing guidance [10]. Further analysis on parasite effects due to the scale factor error and the time delay has been performed by several researchers [2, 11, 12]. Other studies dealing with a guidance filter for the strap-down seeker guidance can be found in [2, 13, 14]. However, the FOV limit because of a strap-down seeker has been rarely investigated.

In recent years, various approaches of the strap-down guidance laws have been proposed for short-range surface-to-surface missiles with a constraint on the seeker's FOV limit. These approaches can be classified into three categories as follows:

Guidance Laws for Target Interception

Earlier studies on FOV-constrained guidance laws have focused on the interception of a target to fulfill the primary objective of the guidance. Thus far, several methods have been proposed for the guidance laws, where different

guidance schemes have been utilized as their main guidance command. These guidance schemes can be classified as follows.

- Proportional Navigation Guidance

  As one of the general and classical guidance schemes, proportional navigation guidance (PNG) has been widely used for modern missile systems. The concept of PNG is to generate an acceleration command proportional to the LOS rate and to form a stable collision geometry. PNG was incorporated as a main guidance law for the FOV-constrained guidance law because of its good compatibility with many guided munitions and moderate effectiveness. For air-to-air applications, Mehra and Ehrich [9] proposed a PNG for short-range air-to-air missiles using an active strap-down seeker under the wide FOV limit. However, pure-proportional navigation (PPN) guidance was designed without considering the FOV limit, and therefore, the strap-down seeker may fail to lock-on the target during the maneuver if the FOV limit is reduced.

- Pursuit-Type Guidance

  Another attempt to design a guidance law is pursuit-type guidance by directly controlling the look angle [15]. In this method, the look angle is regarded as a control variable, and the guidance law is designed to maintain the look angle within the seeker's FOV limit, which is equivalent to deviated pure pursuit (DPP). The merits of this approach are as follows. The look-angle control directly utilizes the measurement, which does not require LOS reconstruction unlike in the case of PNG. Furthermore, the look-angle control is regarded as an attitude control loop, which has been

widely utilized in other control applications such as the orientation control of a spacecraft and the visual servoing problem. Kim et al. proposed a look-angle control guidance law based on multiple phases, which is similar to the PN-based IACG [16]. Ann et al. proposed an impact time and angle guidance (ITACG) law using the reference shaping method [17]. However, the pursuit-type guidance schemes show unstable behavior in the head-on configuration and therefore are not adequate for air-to-air engagement.

- Look-Angle Constrained Guidance (LCG): PPN + Look-Angle Control

  To deal with the shortcomings arising from the abovementioned two approaches, a composite guidance method consisting of different types of guidance laws with switching logic has been developed for FOV limit application. Manchester et al. proposed a modified circular navigation guidance law, where circular navigation is the main guidance to intercept a target and pursuit guidance was partially adopted to deal with the look angle saturation [18]. Sang and Tahk [19] proposed a switching guidance law consisting of two guidance commands: PPN-based impact time control guidance and deviated-pure pursuit (DPP) guidance. The concept of the switching guidance law is to change the guidance law depending on the switching condition. When the look angle reaches the FOV limit, the guidance law is switched to the DPP and then returned to the original guidance law when the returning condition is satisfied. In addition, the arc length of the switching guidance was obtained using a geometric approach. The calculated arc length can be incorporated to estimate the time-to-go, which gives the possibility of impact time control considering the FOV limit [20–25]. For air-to-air engagement, Lee suggested

an extended version of the switching logic [4, 26]. As shown in Fig. 1.2, the proposed guidance law consists of two guidance commands with the switching logic. The PN guidance law is primarily used, and the sliding mode control is used as an auxiliary control to keep the look angle at the boundary and to ensure that the FOV limit is not exceeded when the look angle reaches its FOV limit.

Table 1.1 summarizes the characteristics of the FOV-constrained guidance laws.

Table 1.1: Summary of FOV-Constrained Guidance Laws for Target Interception

	PNG	Pursuit-type	LCG
Strength	Good compatibility Performance and robustness	Guaranteed lock-on condition No requirement of LOS reconstruction Simple structure	Guaranteed performance and lock-on condition Good compatibility
Weakness	Parasite effect FOV limit consideration	Poor performance in head-on engagement	Discontinuous guidance command
Applied Engagement	Air-to-Surface Surface-to-Surface Air-to-Air	Surface-to-surface	Surface-to-Surface Air-to-Air (partial)

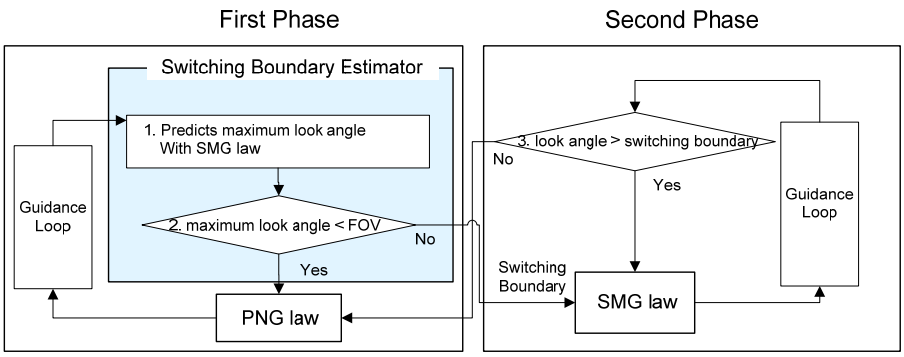

Figure 1.2: Description of Switching Guidance Law for Air-to-Air Engagement [26]

FOV-Constrained Impact Angle Control Guidance (FOV-IACG)

Recently, research on an impact-angle control guidance law considering the seeker's FOV has received considerable attention. Based on the switching framework proposed by Sang and Tahk [19], various guidance schemes have been proposed to fulfill the impact angle constraint together with the FOV limit, which include a two-stage guidance law [27–30], optimal guidance law [31, 32], biased proportional navigation guidance [33, 34], and nonlinear methods [35, 36]. Compared with the guidance laws for target interception, the FOV-IACG follows the following strategy: a turning maneuver is performed by DPP in the early phase of the engagement to achieve an impact-angle constraint, and homing guidance is performed by PPN in the terminal phase for the target interception with the desired impact angle. To intercept moving targets, Park et al. proposed a composite guidance law [29] as an extension of Ref. [28]. With the use of the composite structure with PN guidance, the guidance law enables the interception of a slow-moving target while satisfying the FOV constraint.

This approach has the advantages of a simple structure and satisfactory target interception performance even in the case of a change in the missile speed, which may be effective for ground-based missiles performing surface-to-surface engagement. In spite of its excellent performance, we still need to analyze the capture region for various initial conditions, particularly for several types of engagements.

1.2.2 Capturability Analysis of Guidance Laws

For capturability, a considerable amount of research has been performed, most of which has focused on the capturability of the PN family, such as linearized guidance [37], true proportional navigation (TPN) [38–43], and pure proportional navigation [44–47]. In particular, the capturability analysis was mainly interpreted as PPN and TPN. Although TPN has advantages over PPN in the tractability of mathematical analysis, PPN shows better capturability performance and is more suitable for implementation. In an early study on capturability analysis, Guelman analyzed the capture region of PPN by investigating the qualitative behavior of the trajectory [44]. Guelman investigated the solution in two particular cases where the navigation constant is one or two. Becker [48] obtained a solution as a uniformly convergent infinite product. In the analysis, the missile guided by PPN reaches the target for almost all the initial conditions along a straight line whose direction is determined by the initial conditions. Ghosh et al. [47] obtained the capture region of the augmented PPN guidance law for a maneuvering target, and the capture condition for retro-PN dealing with a high-speed target that was faster than the interceptor was proposed [49]. For TPN, the capturability was analyzed on the basis of the closed-form solution [38–43]. Guelman also derived the capture region of the true proportional navigation (TPN) against a non-maneuvering target in the initial condition space on the basis of its closed-form solution and proved that the capture region of the TPN is more restricted than that of PPN [38]. To deal with maneuvering targets, many researchers have performed the capturability analysis of TPN [39], realistic TPN [40], and geometric guidance [41–43].

However, the previous studies have several limitations with respect to their

application to the situation considered in this study. First, the previous research did not consider the effect of the FOV limit on the capture region. In addition, it is very difficult to perform a capturability analysis when considering additional physical constraints including the miss distance and the acceleration capability together with the FOV limit. The capture region expressed in the position space is crucial for determining a handover point between the midcourse and the terminal phases. In spite of its importance, capturability analysis has rarely been conducted in the position space because of the difficulty of finding the analytic solution of the relative motion. Instead, most of the capturability analyses have been performed using the linearized dynamic model [37].

1.3 Objectives and Contributions

1.3.1 Contributions

In this study, the capture region of FOV-constrained guidance laws was analyzed to clearly understand the behavior of the guidance laws. To achieve this goal, two types of FOV-constrained guidance laws were investigated on the basis of the guidance objectives: i) guidance laws for target interception and ii) impact-angle control guidance (IACG). For the guidance laws, the capture region was derived in terms of the initial position and the FOV limit. The main contribution of this study can be addressed in three folds:

Contribution 1: Derivation of the capture region of FOV-constrained guidance laws

As an attempt to analyze the FOV-constrained guidance laws, we derived the capture region of the existing FOV-constrained guidance laws. None of the reported research on capturability analysis considered both the initial position space and the FOV limit. To describe the effect of the FOV limit, the notion of capture region was newly defined in this study and was described in terms of the initial position, FOV limit, and the impact angle. Based on the definition, two types of FOV-constrained guidance laws were investigated considering the guidance objectives: i) guidance laws for target interception and ii) impact-angle control guidance. The capture regions associated with the two guidance types were derived. For the guidance law for target interception, PPN and LCG based on Lee [26] were considered, and the capture regions were obtained using the closed-form solution of DPP and PPN.

Moreover, the capture region of IACCG [29] was obtained in the general engagement geometry for FOV-IACG. Compared with the previous work [29] in which the achievable impact angle set was obtained for two particular geometries $(\lambda_0, \gamma_T) = (0, 0)$ and $(0, \pi)$, in this study, the derived capture region was established for the general configuration and could therefore be utilized for both surface-to-surface and air-to-air engagements. Moreover, the proposed capture region was obtained analytically by considering a switching condition at which the acceleration reached its maximum. Doing so did not require the use of a root-finding method unlike in previous works wherein the achievable impact angles were numerically obtained [29]. Note that the capture region could be utilized to determine the launch points or the predicted handover points in the midcourse guidance.

Contribution 2: Analysis of the characteristics of the capture region, particularly with respect to the limited FOV

The characteristics of the capture regions were analyzed by the means of a performance evaluation of the existing guidance laws. Thus far, the effect of the reduced FOV limit on the capture region has rarely been studied, particularly in the case of a narrow FOV limit. In this sense, the capture region of the PPN with respect to the FOV limit was investigated for the first time in this study. Compared with a previous study [44], in this study, the effect of the FOV limit on the capture region was found. The narrow FOV limit led to the reduced and divided capture regions according to the head-on and the tail-chase configurations.

Furthermore, the performance of the existing methods was compared by

showing the inclusive relationships between the obtained capture regions. For example, the capture region of LCG was extended in both the engagement geometries (tail-chase and head-on) as compared to PPN, which demonstrated that the LCG was superior to PPN from the perspective of target interception.

The qualitative behaviors and characteristics of the guidance laws were demonstrated on the basis of the capture region. The guidance laws had a relatively wide capture region in the tail-chase engagement, which reflected the favorable behavior of the guidance laws. Therefore, the analysis performed in this study can help a designer to understand the features of the FOV-constrained guidance laws and provide a guideline for the design of a guidance law considering the FOV limit.

Contribution 3: Design of improved FOV-IACG adequate for air-to-air engagement

To improve the existing method, a guidance law adequate for air-to-air engagement was formulated in this study. As an extension of Ref. [29], a modified guidance law was designed to improve the performance of IACCG. For compatibility with the existing method, a look-angle correction method was designed so that this angle could be automatically adjusted to satisfy the prescribed impact angle according to the engagement configuration. The capture region corresponding to the proposed method was also obtained and compared with the existing one.

1.4 Dissertation Outline

The organization of this dissertation is as follows:

In Chapter 1, the backgrounds, motivations, and a related research on FOV-constrained guidance laws and capturability analysis are described. The objectives and achievements of this study are also presented.

In Chapter 2, definitions about capture, lock-on, and capture region in the view of FOV limit are introduced as the mathematical preliminaries. The preliminary results on classical guidance laws, PPN and DPP, are described.

In Chapter 3, the derivation of capture region of guidance laws for target interception are described. As the representatives of the guidance category, capture reigons of PPN and LCG are derived according to head-on and tail-chase engagement geometries.

In Chapter 4, the derivation of capture region for FOV-IACGs is described. In Section 4.1, the capture region of IACCG is derived, where the necessary condition for achievable impact angle is analyzed. In Section 4.2, the guidance law is proposed, and the corresponding capture region is analyzed.

In Chapter 5, characteristics of the capture regions of guidance laws are discussed. First, the performance of the PPN and LCG are investigated and compared. The characteristics of FOV-IACGs are also investigated.

In Chapter 6, the derived capture regions of guidance laws are verified by numerical simulation for air-to-air engagement. The performances of the guidance laws including the method proposed in this study are demonstrated.

In Chapter 7, some concluding remarks and suggestions for further research are presented.

Chapter 2

Mathematical Preliminaries and Problem Formulation

This chapter is devoted to the problem formulation. First, the notion of the capturability and the engagement kinematics between a missile and a target is derived. Then, preliminary results of the guidance laws are provided. For this purpose, the basic equations of motion between two objects in a planar engagement geometry and fundamental assumptions are described as the mathematical preliminaries. Depending on mission objectives, the missile guidance law considered in this study is classified as two categories; i) guidance law for target interception and ii) the impact-angle control guidance law. Capture condition depending on the guidance type is defined. In Sec. 2.2, the definitions considered in the analysis are presented, where the notion of capture region are defined according to two types of guidance. The basic guidance laws consisting of the FOV contrained guidances are described in Sec. 2.3. Finally, problem statements are established in Sec. 2.4.

2.1 Two-dimensional Engagement Kinematics

The engagement geometry between a missile and a target is shown in Fig. 2.1. (V_T, γ_T) denotes the speed and the flight path angle of the target, respectively, (V_m, γ_M) are the speed and the flight path angle of the missile, respectively, and a_M is the acceleration of the missile which is perpendicular to the velocity vector. Throughout the study, the following assumptions are

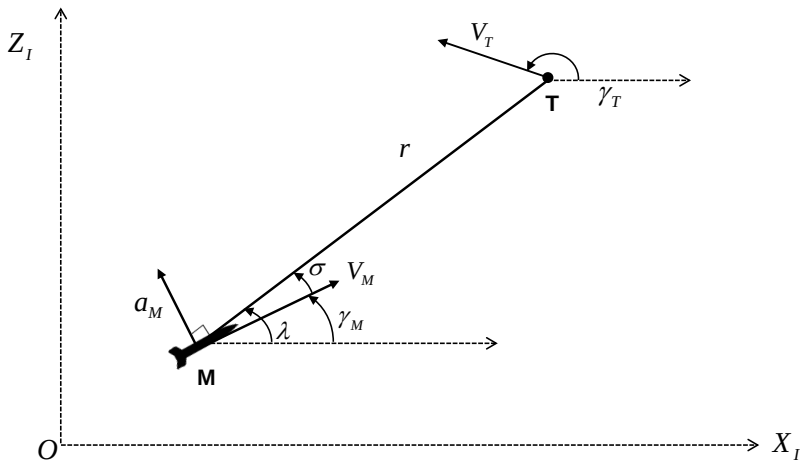

Figure 2.1: Planer Engagement Geometry

considered.

Assumption 2.1. The missile and the target are considered as point-mass models.

Assumption 2.2. The missile is faster than the target, i.e., $\eta = V_T/V_m < 1$, and the target is not maneuvering.

Assumption 2.3. The target is detected by a seeker if the image of the target is within the FOV of the seeker.

Assumption 2.4. The centerline of the seeker is aligned with the axial direction of the missile body, and the seeker's FOV has a symmetric configuration such that $FOV = [-\sigma_{\text{lim}}, \sigma_{\text{lim}}]$.

Assumption 2.5. The angle of attack (AOA) is small enough to be neglected.

Usually, in the formulation of a missile-target engagement problem, the initial distance r_0 is selected in regard to the maximum detection range and the hand-over point between the mid-course and terminal phases. From the Assumptions 2.4 and 2.5, the pitch angle of the missile coincides with the flight-path angle γ_m, and the look angle σ is defined by the rotational angle from the direction of missile velocity to the line-of-sight (LOS) angle λ as

$$\sigma = \lambda - \gamma_m \tag{2.1}$$

The nonlinear engagement kinematics can be represented as

$$\begin{aligned} \dot{r} &= V_T \cos(\gamma_T - \lambda) - V_m \cos\sigma \\ \dot{\lambda} &= \frac{V_T}{r} \sin(\gamma_T - \lambda) + \frac{V_m}{r} \sin\sigma \\ \dot{\gamma}_m &= \frac{a_m}{V_m} \end{aligned} \tag{2.2}$$

where r represents the distance between the missile and the target, γ_T denotes the flight-path angle of the target, and a_m is the acceleration of the missile perpendicular to the velocity vector. Using Eqs.(2.1) and (2.2), the differential equation of the look angle can be obtained as

$$\dot{\sigma} = \frac{V_T}{r} \sin(\gamma_T - \lambda) + \frac{V_m}{r} \sin\sigma - \frac{a_m}{V_m} \tag{2.3}$$

Note that the look angle is defined as an angle from the flight path angle to the LOS angle, which has the opposite sign of the lead angle [29].

2.2 Definitions

Before analyzing the capturability, intercept conditions of the missile-target is described in this section. Because most of the previous research has rarely investigated the capturability of the guidance laws considering the FOV limit, it is better to define the capture region in the view of the FOV limit. Section 2.2.1 describes the interception condition with the definition of the capture region of guidance laws for target interception in the view of FOV limit. In Sec. 2.2.2, impact angle constraint is additionally considered with hit-to-kill constraint and FOV limit to define the capture region of impact-angle control guidance laws.

2.2.1 Capture Region for Target Interception

First, the notion of the interception is mathematically described as follows.

Definition 2.1. Given an allowable miss distance R_{miss}, the target is said to be intercepted by the missile if the range becomes less than R_{miss} at the final time t_f, i.e., $r(t_f) < R_{\text{miss}}$.

Specifically, the air-to-air engagement requires R_{miss} within a meter for hit-to-kill performance. The ideal situation of the collision is that the missile pursues a target by entering a collision course and keeps zero LOS rate near the collision. By applying $\dot{\lambda} = 0$ in Eq. (2.2), the terminal LOS angle from the collision

geometry can be expressed as

$$\lambda_{f,TC} = \gamma_T + \sin^{-1}\left(\frac{V_M}{V_T}\sin\sigma_f\right) \qquad (\text{if } |\gamma_T - \gamma_m| < \pi/2) \tag{2.4a}$$

$$\lambda_{f,HO} = \pi + \gamma_T - \sin^{-1}\left(\frac{V_M}{V_T}\sin\sigma_f\right) \qquad (\text{if } |\gamma_T - \gamma_m| > \pi/2) \tag{2.4b}$$

where λ_f and σ_f denote the LOS angle and the look angle at the final time, respectively. Equations (2.4a) and (2.4b) correspond to the cases of tail-chase (TC) engagement and head-on (HO) engagement, respectively, and the terminal LOS angle, λ_f, is monotonic with respect to the terminal look angle, σ_f. Note from Eqs. (2.4a) and (2.4b) that the collision geometry is relatively constructed by the flight path angle of the target, γ_T. The domain of the terminal flight path angle can be expressed as

$$\Gamma_f = \Gamma_{f,TC} \cup \Gamma_{f,HO} \tag{2.5}$$

where

$$\begin{aligned} \Gamma_{f,TC} &= \left\{\gamma_f : \gamma_T - \frac{\pi}{2} \le \gamma_f < \gamma_T + \frac{1}{2}\pi\right\}, \\ \Gamma_{f,HO} &= \left\{\gamma_f : \gamma_T + \frac{\pi}{2} \le \gamma_f < \gamma_T + \frac{3}{2}\pi\right\} \end{aligned} \tag{2.6}$$

Likewise, the domain of the terminal LOS angle can be expressed as follows,

$$\Lambda_f = \Lambda_{f,TC} \cup \Lambda_{f,HO} \tag{2.7}$$

where

$$\begin{aligned} \Lambda_{f,TC} &= \left\{\gamma_f : \gamma_T - \frac{\pi}{2} \le \gamma_f < \gamma_T + \frac{1}{2}\pi\right\}, \\ \Lambda_{f,HO} &= \left\{\gamma_f : \gamma_T + \frac{\pi}{2} \le \gamma_f < \gamma_T + \frac{3}{2}\pi\right\} \end{aligned} \tag{2.8}$$

Meanwhile, the lock-on condition can be defined as follows.

Definition 2.2. The lock-on condition is said to be satisfied if the look angle is always within the FOV range of the seeker, i.e., $\sigma \in [\underline{\sigma}, \bar{\sigma}]$.

where $\underline{\sigma}$ and $\bar{\sigma}$ indicate the minimum and maximum look angles due to the FOV limit σ_{lim} from the center of the seeker's image plane, respectively, and $[\underline{\sigma}, \bar{\sigma}] = [-\sigma_{\text{lim}}, \sigma_{\text{lim}}]$ for the symmetric configuration. Note that the narrowness of the FOV with respect to the speed ratio $\eta = V_T/V_m$ must be considered, although its degree is mainly determined by the specification of the seeker. If the FOV is substantially narrow, then the collision geometry is confined, and the terminal LOS angle λ_f cannot be determined if $\frac{V_M}{V_T} \sin \sigma_f > 1$ from Eqs. (2.4a) and (2.4b). In this respect, let us define the relative narrowness of the FOV limit as follows.

Definition 2.3. The engagement is classified as **relatively narrow FOV** (RN-FOV) if the FOV limit satisfies the following relation [50].

$$\zeta_{\text{lim}} = \frac{V_T}{V_M \sin \sigma_{\text{lim}}} > 1 \tag{2.9}$$

Otherwise, the engagement is classified as **relatively wide** FOV (RW-FOV).

Similar to Eq. (2.9), let us define a parameter $\zeta = \eta / \sin \sigma$, which will be used in the next section. To accomplish interception and the lock-on condition, the initial position (r_0, λ_0) and look angle σ_0 should be properly selected as the initial condition. Combined with the lock-on condition, let us define two types of capture regions, a *partially capturable* region and a *capturable* region, in consideration of the FOV limit.

Definition 2.4. Given a guidance command a_c, the capture region of the guidance law is defined as

$$\mathcal{C} = \{(r_0, \lambda_0, \sigma_0) | \sigma(t) \in [\underline{\sigma}, \bar{\sigma}] \text{ for } \forall t \in [t_0, t_f], r(t_f) < R_{\text{miss}}\} \tag{2.10}$$

Moreover, a sub-region of $\mathcal{C}$ projected to the initial position space (r_0, λ_0) can be expressed as

$$proj_{\Sigma}\mathcal{C} = \mathcal{C}_{\sigma_0} \tag{2.11}$$

where Σ is a hyper-plane that represents the initial position space (r_0, λ_0). Using the notation, the ***capturable region*** is defined as $\mathcal{A}_{a_c} = \bigcap_{\sigma_0 \in [\underline{\sigma}, \bar{\sigma}]} \mathcal{C}_{\sigma_0}$. And $\mathcal{B}_{a_c} = \bigcup_{\sigma_0 \in [\underline{\sigma}, \bar{\sigma}]} \mathcal{C}_{\sigma_0}$ is defined as a ***partially capturable region*** of the a_c if there exists at least one initial look angle σ_0 such that the trajectory satisfies $\sigma(t) \in [\underline{\sigma}, \bar{\sigma}]$ for $\forall t \in [t_0, t_f]$ and $r(t_f) < R_{\text{miss}}$.

Remark 2.1. Note that the degree of the seeker's FOV is usually determined by the specification of the seeker. However, the collision condition can be influenced by the speed ratio even in wide FOV case. For example, a strapdown seeker having 20 degrees of FOV limit cannot maintain the lock-on condition at the intercept instant if $\gamma_{imp} = 90$ deg is required under the speed ratio $\eta = 2$. To deal with the situation, Definition 2.3 addresses the degree of the seeker's FOV relatively defined in relation to the speed ratio.

If the initial position of the missile is in the *capturable region*, then the guidance law initiated with any velocity direction satisfying the lock-on condition can intercept the target. When the missile is in the *partially capturable region*, then at least one velocity direction can achieve the interception. In this respect, the *partially capturable region* corresponds to the necessary condition, and the *capturable region* corresponds to the sufficient condition for intercepting the target while maintaining the lock-on condition.

2.2.2 Capture Region for Impact-Angle Control

Based on the defined domain, the definition of impact angle can be introduced. Let $\gamma_{imp} = \gamma_T - \gamma_f$ be the impact angle. The impact angle between the target and the missile can be defined with respect to the flight path angle of the target at the intercept instant as [51]

$$\gamma_{imp} = \gamma_T - \gamma_f \tag{2.12}$$

Figure 2.2 shows the geometric relationship between the terminal flight-path angle and impact angle. In the TC engagement, the missile approaches behind the target and finishes the interception. The impact angle is constructed as $-\pi/2 < \gamma_{imp} \leq \pi/2$, and the flight path angle should be made in first and fourth quadrants with respect to the target-central frame. Likewise, the missile approaches in front of the target as $-3\pi/2 < \gamma_{imp} \leq -\pi/2$, and the flight path angle should be in the second and third quadrants in HO engagement. The domain of Eq. (2.5) can be expressed as follows.

$$\mathcal{K} = \left\{ \gamma_{imp} : -\frac{3}{2}\pi < \gamma_{imp} \leq \frac{\pi}{2} \right\} \tag{2.13}$$

To achieve the desired impact angle, γ_{imp}, the terminal constraint of the flight path angle should be imposed as $\gamma_f = \gamma_T - \gamma_{imp}$. For example, the terminal flight path angle can be selected as $\gamma_f = \gamma_T + \pi$ for the exact head-on interception. Similar to Definition 2.4, the capture region of the guidance law for achieving specified impact angle is defined as follows.

Definition 2.5. Given a guidance command a_c, the capture region for the

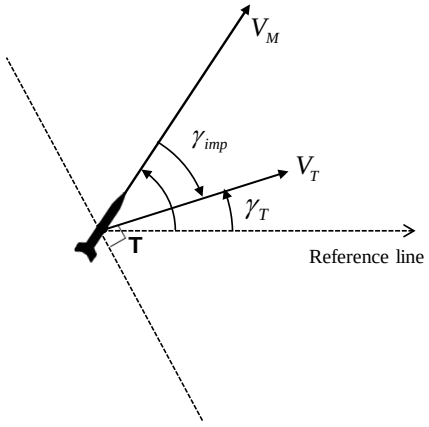

(a) Tail chase (TC)

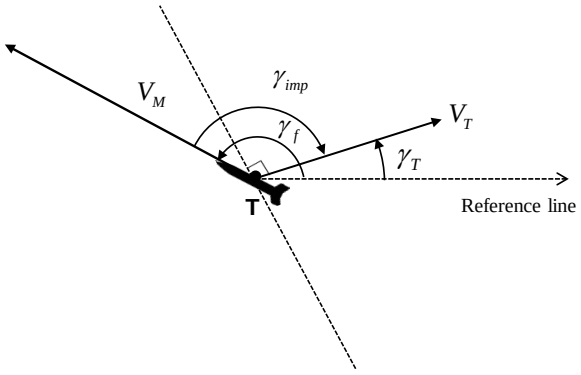

(b) Head on (HO)

Figure 2.2: Description of Impact Angle and Terminal Flight-Path Angle

impact-angle control is defined as

$$\mathcal{C}_{imp} = \{(r_0, \lambda_0, \sigma_0, \gamma_{imp}) | \sigma(t) \in [\underline{\sigma}, \bar{\sigma}] \text{ for } \forall t \in [t_0, t_f], \\ r(t_f) < R_{\text{miss}}, \gamma_{imp}(t_f) = \gamma_{imp,d}\} \tag{2.14}$$

Like Eq. (2.11), $\mathcal{C}_{imp}$ has several sub-regions. The characteristics of the regions will be discussed in Sec. 5.2.

2.3 Preliminaries of Guidance Laws for FOV Limit

In this section, characteristics of the guidance laws considering FOV limit are studied. In most of the previous studies, guidance command has a composite structure consisting of two guidance laws; homing guidance law and boundary guidance law. If the look angle is within the FOV limit during the maneuver, homing guidance command is governed to accomplish terminal constraints. In most relevant studies [19, 28, 29], PPN was used as a homing guidance law. By contrast, if the look angle reaches its upper or lower bound, then the boundary guidance command is generated to make the look angle converge to the desired look angle. Therefore, the trajectory under a FOV-constrained guidance law is characterized mainly by PPN guidance and deviated pursuit guidance. Let us explain the qualitative behavior of the two guidance laws.

Pure Proportional Navigation Guidance

Proportional navigation guidance has been widely used for modern missile systems, whose guidance command generated by PPN is proportional to the LOS rate. Among the PN family, PPN whose guidance command is perpendicular to the velocity vector of the missile has known as the representative of the

PNG. The guidance command of the PPN expressed as

$$a_{PPN} = NV_m\dot{\lambda} \tag{2.15}$$

where N denotes a navigation gain. Under PPN, the relationship between the look angle and LOS can be represented as

$$\dot{\lambda} = \dot{\gamma}_m + \dot{\sigma} = \frac{1}{1-N}\dot{\sigma} \tag{2.16}$$

Integrating Eq. (2.16) with respect to time yields

$$\lambda - \lambda_0 = -\frac{1}{N-1}\left(\sigma - \sigma_0\right) \tag{2.17}$$

Note from Eqs. (2.16) and (2.17) that the change in the look angle is proportional to that of the LOS. In order to succeed the interception by PPN, the change in the LOS should converge to zero by collision condition. Theorem 2.1 shows the necessary condition of the navigation gain for boundedness of the LOS rate.

Theorem 2.1. In the ideal environment, a missile pursuing a target by using PPN with $(N-1)V_m > V_T$ and $V_m > V_T$ will reach the target for all but a finite number of initial conditions. Moreover, the missile will arrive at the target along a straight line whose direction $\lambda = \lambda_{PPN}$ is determined by

$$V_T \sin(\gamma_T - \lambda_{PPN}) + V_m \sin\left(\sigma_0 + (1-N)\left(\lambda_{PPN} - \lambda_0\right)\right) = 0 \tag{2.18}$$

Moreover, the magnitude of LOS rate decreases if the following condition satisfies

$$\eta < 1/\sqrt{2}, \quad N > 2\left(1 + \eta/\sqrt{1-\eta^2}\right) > 2(1+\eta) \tag{2.19}$$

Detailed proof of the Theorem 2.1 can be found in Ref. [44]. Followed by Eq. (2.19), the guidance gain N usually takes a value between three and five.

Remark 2.2. Equation (2.18) determines the equilibrium LOS angle for a given initial condition corresponding to the stable collision course. The LOS converges monotonically to the equilibrium LOS λ_{PPN}, and the missile approaches the target.

Remark 2.3. When the velocity directions of the missile and the target are opposite and aligned with LOS, i.e., $V_r > 0, V_\lambda = 0$, where $V_r = V_T \cos(\gamma_T - \lambda) - V_m \cos\sigma$ and $V_\lambda = V_T \sin(\gamma_T - \lambda) + V_m \sin\sigma$, the missile cannot intercept the target. This exceptional case can be excluded by taking only the initial condition satisfying the lock-on condition.

In the meantime, closed-form trajectory of PPN can be obtained in the form of a uniformly convergent infinite product [48]. By substituting Eq. (2.17) into Eq. (2.2), the differential equation can be expressed as

$$\frac{dr}{r} = \frac{V_T \cos\theta - V_m \cos(\varphi_0 - (N-1)\theta)}{-V_T \sin\theta + V_m \sin(\varphi_0 - (N-1)\theta)} d\theta = F(\theta) d\theta \tag{2.20}$$

where $\theta = \lambda - \gamma_T$, and $\varphi_0 = \sigma_0 + (N-1)(\lambda_0 - \gamma_T)$. By Mittag-Leffler's expansion theorem [48], $F(\theta)$ can be expressed in the form of a uniformly convergent series of rational functions as

$$F(z) = F(0) + \sum_{\nu=1}^{\infty} \left(\frac{A_\nu}{z - \theta_\nu} + \frac{A_\nu}{\theta_\nu} \right) \tag{2.21}$$

where

$$\begin{aligned} F(0) &= \frac{\eta - \cos\varphi_0}{\sin\varphi_0} \\ A_\nu &= \frac{\cos(\varphi_0 - (N-1)\theta_\nu) - \eta\cos\theta_\nu}{(N-1)\cos(\varphi_0 - (N-1)\theta_\nu) + \eta\cos\theta_\nu} \end{aligned} \tag{2.22}$$

In Eqs. (2.21) and (2.22), θ_ν represents the zeros of the denominator $H(\theta) = \sin(\varphi_0 - (N-1)\theta) - \eta\sin\theta$, which has infinitely many simple zeros. Let θ_ν be

arranged in the order of increasing absolute value, i.e., $|\theta_1| < |\theta_2| < \cdots$, then the solution can then be expressed as

$$\begin{aligned}\frac{r}{r_0} &= \exp\left(F(0)(\theta-\theta_0) + \sum_{\nu=1}^{\infty}\left(A_\nu \ln\left|\frac{\theta-\theta_\nu}{\theta_0-\theta_\nu}\right| + \frac{A_\nu}{\theta_\nu}(\theta-\theta_\nu)\right)\right) \\ &\triangleq \Psi(\lambda, \lambda_0; \sigma_0)\end{aligned} \tag{2.23}$$

Guidance law at the Boundary: Deviated Pure Pursuit (DPP)

When the look angle reaches the FOV limit and is about to exceed the FOV, the best strategy for maintaining a lock-on condition is to perform a maneuver that keeps the look angle at the FOV limit value. This trajectory can be described by the DPP, where the look angle is kept constant. The guidance command generated by DPP can be expressed as

$$a_{DPP} = V_m \dot{\lambda} \tag{2.24}$$

Figure 2.3 shows the phase portrait of the deviated pursuit for the case of $\gamma_T = 180\text{deg}, \lambda_f = -10\text{deg}$, and 190deg. The deviated pursuit guidance has two equilibrium points, and the trajectory by DPP shows different patterns in the phase plane depending on the type of engagement geometry. The LOS rate for RN-FOV limit, $\zeta_{\text{lim}} > 1$, has the following relation.

$$\dot{\lambda} \propto \sin(\gamma_T - \lambda) + \frac{1}{\zeta} = \begin{cases} < 0 & \text{if } \lambda \in (\lambda^*_{TC}, \lambda^*_{HO}) \quad \text{(2.25a)} \\ > 0 & \text{if } \lambda \in \Lambda_f \setminus (\lambda^*_{TC}, \lambda^*_{HO}) \quad \text{(2.25b)} \end{cases}$$

The LOS angle monotonically converges to the stable equilibrium point λ^*_{TC}, as shown in Eqs. (2.25a) and (2.25b). By contrast, the LOS angle diverges from the unstable equilibrium point λ^*_{HO}. Considering physical constraints, the trajectory reaches the one corresponding to its limited maneuver due to the limited acceleration capability. The restriction of maneuverability can be expressed by

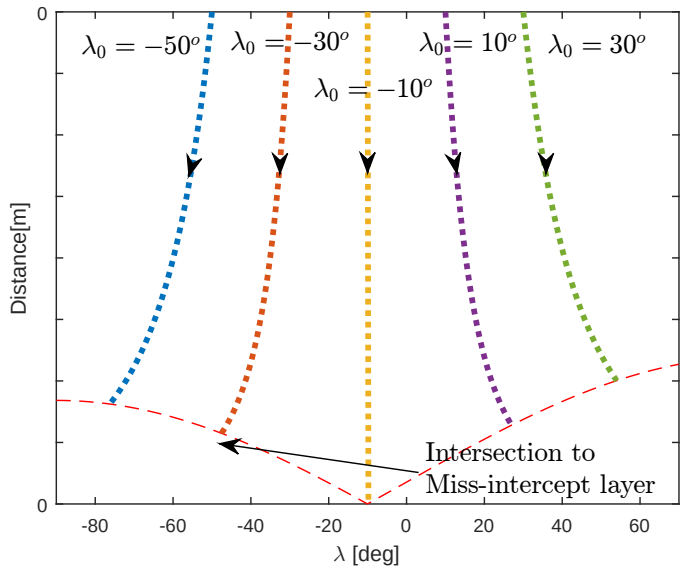

(a) Head-on Case

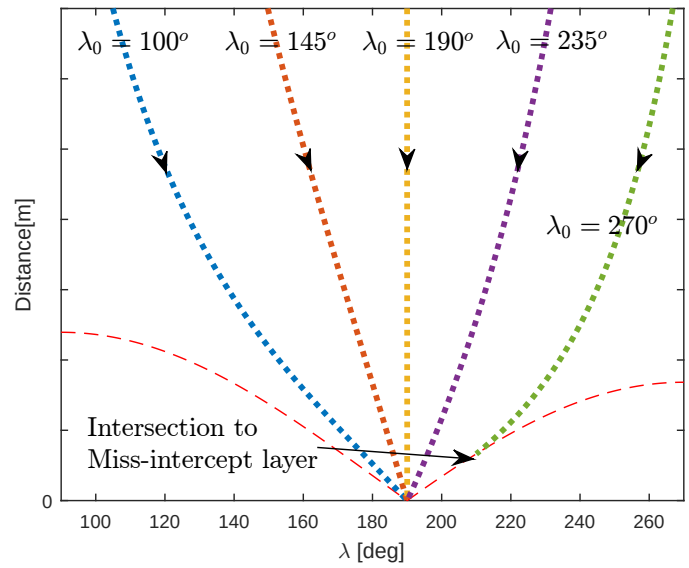

(b) Tail-chase Case

Figure 2.3: Phase Portrait of Deviated Pursuit Trajectory (RN-FOV, $\zeta_{\text{lim}} > 1$)

considering the relationship between the LOS rate and maximum turning rate as

$$\left|\dot{\lambda}\right| = \left|\frac{V_T}{r}\sin(\gamma_T - \lambda) + \frac{V_m}{r}\sin\sigma\right| \leq \dot{\gamma}_{\max} = \frac{a_{\max}}{V_m} \tag{2.26}$$

where $a_{\max}$ is the maximum normal acceleration. When Eq.(2.26) cannot hold during the maneuver, the missile misses the target because it cannot keep its seeker locked on the target after reaching the acceleration limit, especially at the end of homing phase. Because $r > 0$, the region in which the missile misses the target can be obtained from Eq. (2.26) as

$$r \leq |V_T \sin(\gamma_T - \lambda) + V_m \sin\sigma| \frac{V_m}{a_{\max}} \tag{2.27}$$

In Eq.(2.27), the boundary of the region can be defined as *miss-intercept layer*, because the LOS rate begins to exceed the maximum turning rate and the missile fails to maintain the lock-on condition. Considering the FOV range, let us introduce a region of miss-intercept as

$$\mathbf{M} = \left\{(r,\lambda)|r = |V_T \sin(\gamma_T - \lambda) + V_m \sin\sigma| \frac{V_m}{a_{\max}}, \sigma \in [\underline{\sigma}, \bar{\sigma}]\right\} \tag{2.28}$$

The missile within $\mathbf{M}$ may result in a missed intercept, which depends on the final look angle. The lower boundary of $\mathbf{M}$ contains the equilibrium interval $\mathcal{L}_{adm,HO}$ and $\mathcal{L}_{adm,TC}$, which represents stable homing for some initial conditions and will be defined in Section 2.4. When a miss-intercept occurs, the minimum distance between the missile and the target is defined as the *miss-intercept* distance.

Remark 2.4. In both the head-on and tail-chase geometries, the miss-intercept distance becomes larger if the initial LOS is farther from the equilibrium points. As shown in Fig. 2.3-(b), some trajectories whose initial LOS angles are away

from the equilibrium intervals may reach their *miss-intercept layer* even though the trajectories converge to the equilibrium point.

The solution based on the deviated pursuit can be obtained analytically. Let us assume that the look angle is $\sigma = \bar{\sigma}$ during the engagement without loss of generality. The trajectory of DPP can be expressed as follows [29, 52],

$$\frac{r}{r_0} = \frac{\eta \sin(\gamma_T - \lambda_0) + \sin\sigma}{\eta \sin(\gamma_T - \lambda) + \sin\sigma} \exp \int_{\lambda_0}^{\lambda} \frac{-\cot\sigma}{\zeta \sin(\gamma_T - \lambda) + 1} d\lambda \tag{2.29}$$

The integral of the trigonometric function has a closed-form solution depending on the value of $\zeta = \eta / \sin\sigma$, as follows,

$$\int_{\lambda_0}^{\lambda} \frac{\cot\sigma}{\zeta \sin(\gamma_T - \lambda) + 1} d\lambda = \begin{cases} -\frac{2\cot\sigma}{\sqrt{1-\zeta^2}} \left\{ \tan^{-1}\left(\frac{\tan\left(\frac{\gamma_T - \lambda}{2}\right) + \zeta}{\sqrt{1-\zeta^2}} \right) - \tan^{-1}\left(\frac{\tan\left(\frac{\gamma_T - \lambda_0}{2}\right) + \zeta}{\sqrt{1-\zeta^2}} \right) \right\} & \zeta^2 < 1 \\ -\frac{2\cot\sigma}{\sqrt{\zeta^2-1}} \left\{ \tanh^{-1}\left(\frac{\tan\left(\frac{\gamma_T - \lambda}{2}\right) + \zeta}{\sqrt{\zeta^2-1}} \right) - \tanh^{-1}\left(\frac{\tan\left(\frac{\gamma_T - \lambda_0}{2}\right) + \zeta}{\sqrt{\zeta^2-1}} \right) \right\} & \zeta^2 > 1 \end{cases} \tag{2.30}$$

Then, the trajectory of the deviated pursuit with RN-FOV ($\zeta_{\text{lim}} > 1$) can be expressed as

$$\begin{aligned} \frac{r}{r_0} &= \frac{\eta \sin(\gamma_T - \lambda_0) + \sin\sigma_d}{\eta \sin(\gamma_T - \lambda) + \sin\sigma_d} \\ &\quad \times \exp\left\{ -\frac{2\cot\sigma_d}{\sqrt{\zeta^2-1}} \left\{ \tanh^{-1}\left(\frac{\tan\left(\frac{\gamma_T - \lambda}{2}\right) + \zeta}{\sqrt{\zeta^2-1}} \right) - \tanh^{-1}\left(\frac{\tan\left(\frac{\gamma_T - \lambda_0}{2}\right) + \zeta}{\sqrt{\zeta^2-1}} \right) \right\} \right\} \\ &= \Phi(\lambda, \lambda_0; \sigma) \end{aligned} \tag{2.31}$$

where Φ is the transition function of the deviated pursuit from λ_0 to λ with parameter σ, and $(\bar{r}, \bar{\lambda})$ denotes the trajectory of the deviated pursuit obtained by $\sigma = \bar{\sigma}$. Appendix A contains the details of the derivation of Eq. (2.29). The transition function Φ in Eq. (2.31) can be factorized as $\Phi(\lambda, \lambda_0; \sigma_0) = \phi(\lambda; \sigma_0)/\phi(\lambda_0; \sigma_0)$, where $\phi(\lambda)$ can be expressed as

$$\phi(\lambda; \sigma_0) = \frac{\exp\left(-\frac{2\cot\sigma}{\sqrt{\zeta^2-1}} \tanh^{-1}\left(\frac{\tan\left(\frac{\gamma_T - \lambda}{2}\right) + \zeta}{\sqrt{\zeta^2-1}} \right) \right)}{\eta \sin(\gamma_T - \lambda) + \sin\sigma_0} \tag{2.32}$$

Note from Eq. (2.32) that ϕ has an one-to-one correspondence to r in the domains $[\gamma_T - \frac{3\pi}{2}, \lambda_{f,HO})$, $(\lambda_{f,HO}, \lambda_{f,TC})$, and $(\lambda_{f,TC}, \gamma + \frac{\pi}{2}]$. However, it is difficult to obtain the inverse mapping $\lambda = \phi^{-1}(r)$. Instead, let us define $\lambda(r_1)$ as the value of the LOS angle at $r = r_1$, which can be obtained by substituting r_1 into Eq. (2.31).

2.4 Problem Statement

Under the planar engagement, the RN-FOV case is mainly considered in this study. Due to the limited FOV, the range of admissible LOS angles at the final time in accordance with Definition 2.3 is confined to the local intervals as

$$\begin{aligned} &\mathcal{L}_{adm,HO} = \left[\lambda^*_{\bar{\sigma},HO}, \lambda^*_{\underline{\sigma},HO}\right] \\ &\lambda^*_{\bar{\sigma},HO} = \gamma_T + \pi - \sin^{-1}\left(\frac{1}{\zeta_{\lim}}\right), \quad \lambda^*_{\underline{\sigma},HO} = \gamma_T + \pi + \sin^{-1}\left(\frac{1}{\zeta_{\lim}}\right) \end{aligned} \tag{2.33}$$

and

$$\begin{aligned} &\mathcal{L}_{adm,TC} = \left[\lambda^*_{\underline{\sigma},TC}, \lambda^*_{\bar{\sigma},TC}\right] \\ &\lambda^*_{\underline{\sigma},TC} = \gamma_T - \sin^{-1}\left(\frac{1}{\zeta_{\lim}}\right), \quad \lambda^*_{\bar{\sigma},TC} = \gamma_T + \sin^{-1}\left(\frac{1}{\zeta_{\lim}}\right) \end{aligned} \tag{2.34}$$

where $\lambda^*_{\bar{\sigma},HO}$ and $\lambda^*_{\bar{\sigma},TC}$ are the equilibrium points when $\sigma_f = \bar{\sigma}$ in the head-on and tail-chase cases, respectively, and $\lambda^*_{\underline{\sigma},HO}$ and $\lambda^*_{\underline{\sigma},TC}$ are the equilibrium points when $\sigma_f = \underline{\sigma}$ in the head-on and tail-chase cases, respectively. Based on the interval, the capture regions of guidance laws will be derived according to the separated engagement geometries. The objective of the guidance law considered in this study is summarized as follows:

1. Missile should intercept the target, i.e., $r(t_f) \leq r_{\text{miss}}$.
2. Flight path angle of the missile at the final time should be made as $|\gamma_M(t_f) - \gamma_f| \leq \epsilon$.
3. During the engagement, the look angle must be within the FOV limit, i.e., $\sigma(t) \in [\sigma_{\min}, \sigma_{\max}]$ for all $t \in [t_0, t_f]$.

Chapter 3

Capture Region of Guidance Laws for Target Interception

This chapter is devoted to derive the capture region of guidance laws for target interception. The primary objective of the guidance laws considered in this chapter is to intercept the target while maintaining FOV limit during the entire engagement. Terminal guidance laws for this objective have been widely developed. In the capturability analysis, the capture region expressed in initial position space is usually obtained by performing multiple numerical simulations with various initial conditions, and its performance is evaluated by the phase portraits. The phase portrait analysis is limited, because it was performed for a limited region of state space using particular constant parameter values.

In this study, based on the interval by RN-FOV, Eqs. (2.33)-(2.34), the capture region is derived according to separated engagement geometries. First, the proportional navigation guidance law is investigated in regard to FOV limit in Sec. 3.1. Then, the look-angle constrained guidance law is introduced, and its capture region is derived in Sec 3.2.

3.1 Capture Region of PPN

In this section, the capture region of PPN is obtained for the situation in which the seeker's FOV limit is relatively narrow. First, capture condition of PPN satisfying the lock-on condition is investigated. Given the initial relative position (r_0, λ_0), the feasible range of the LOS satisfying the lock-on condition can be obtained by considering the FOV limit in Eq. (2.17) as follows

$$\lambda_0 - \frac{1}{N-1}(\bar{\sigma} - \sigma_0) \leq \lambda \leq \lambda_0 + \frac{1}{N-1}(\sigma_0 - \underline{\sigma}) \tag{3.1}$$

Note from Theorem 2.1 that λ monotonically approaches λ_{PPN} in Eq. (2.18). The necessary condition for the interception satisfying the lock-on condition can be presented as follows,

Condition 3.1. Suppose that the missile is guided by PPN with $N > 2(1+\eta)$. Given r_0, λ_0 and $\sigma_0 \in [\underline{\sigma}, \bar{\sigma}]$, the missile eventually intercepts the target while satisfying the lock-on condition if the terminal LOS, λ_{PPN}, lies within the feasible range of the LOS, i.e.,

$$\lambda_0 - \frac{1}{N-1}(\bar{\sigma} - \sigma_0) \leq \lambda_{PPN} \leq \lambda_0 + \frac{1}{N-1}(\sigma_0 - \underline{\sigma}) \tag{3.2}$$

where λ_{PPN} and the terminal look angle $\sigma_f \in [\underline{\sigma}, \bar{\sigma}]$ satisfy the following collision condition.

$$V_T \sin(\gamma_T - \lambda_{PPN}) + V_m \sin \sigma_f = 0 \tag{3.3}$$

In the following, the capture region for each engagement configuration will be discussed on the basis of Condition 3.1.

Capture Region of PPN in Head-on Engagement

First, consider the domain $\Lambda_{HO} = \{(r, \lambda) : \lambda \in [\gamma_T + \frac{\pi}{2}, \gamma_T + \frac{3\pi}{2}]\}$, for head-on engagement. Note from Condition 3.1 that λ_{PPN} by the collision course should be inside the admissible range $\mathcal{L}_{adm,HO}$ to satisfy the lock-on condition at the interception. Otherwise, the look angle at the final time cannot remain in the FOV range at the final phase. In this respect, the capture region can be obtained by inspecting the location of the equilibrium point of PPN according to the various initial conditions, especially for λ_0 and σ_0. Let $f(\sigma) = \lambda_0 - \frac{1}{N-1}(\sigma - \sigma_0)$ be the transition of λ by PPN and $g_H(\sigma) = \gamma_T + \pi - \sin^{-1}\left(\frac{V_m}{V_T}\sin\sigma\right)$ be the collision condition in the head-on engagement case. Considering the initial condition (λ_0,σ_0) as parameters, the equilibrium point of PPN σ_f can be obtained by solving $h_H(\sigma; \lambda_0, \sigma_0) = f(\sigma) - g_H(\sigma) = 0$. Note that the function h_H satisfies the following condition.

Proposition 3.1. *h_H is strictly decreasing function in $\sigma \in [\underline{\sigma}, \bar{\sigma}]$.*

Proof. h_H is continuously differentiable with respect to $\sigma \in [\underline{\sigma}, \bar{\sigma}]$. Taking partial derivative of h_H repeatedly with respect to σ yields

$$\frac{\partial h_H}{\partial \sigma} = -\frac{1}{N-1} + \frac{\frac{1}{\eta}\cos\sigma}{\sqrt{1 - \left(\frac{1}{\eta}\right)^2 \sin^2\sigma}} \tag{3.4}$$

Taking second partial derivative shows that $\frac{\partial h_H}{\partial \sigma}$ has an local minima at $\sigma = 0$. Since $N > 2(1+\eta) > 1+\eta$, $\frac{\partial h_H}{\partial \sigma}$ gives

$$\frac{\partial h_H}{\partial \sigma} > \frac{\partial h_H}{\partial \sigma}(0) = -\frac{1}{N-1} + \frac{1}{\eta} > 0 \tag{3.5}$$

Therefore, h_H is a strictly increasing function of σ in the FOV range. □

Using Proposition 3.1, Theorem 3.1 addresses the capture region of the PPN.

Theorem 3.1. Under Assumptions 2.1-2.5, consider a planar engagement between a target and a missile guided by PPN with $N > 2(1+\eta)$. The missile is equipped with an RN-FOV strapdown seeker satisfying $\zeta_{\lim} > 1$. Then, the capture region for head-on geometry can be expressed as

$$\mathcal{C}_{PPN,HO} = \left\{(r_0, \lambda_0, \sigma_0) : r_0 \geq \underline{R}_0, \lambda_0 \in [\bar{\lambda}_{PPN,HO}(\sigma_0), \underline{\lambda}_{PPN,HO}(\sigma_0)], \sigma_0 \in [\underline{\sigma}, \bar{\sigma}]\right\} \tag{3.6}$$

where

$$\begin{aligned} \underline{\lambda}_{PPN,HO}(\sigma_0) &= \gamma_T + \pi + \sin^{-1}\left(\frac{1}{\zeta_{\lim}}\right) + \frac{1}{N-1}(\underline{\sigma} - \sigma_0) \\ \bar{\lambda}_{PPN,HO}(\sigma_0) &= \gamma_T + \pi - \sin^{-1}\left(\frac{1}{\zeta_{\lim}}\right) + \frac{1}{N-1}(\bar{\sigma} - \sigma_0) \end{aligned} \tag{3.7}$$

Proof. Considering the initial condition (λ_0,σ_0) as parameters, the equilibrium point of PPN σ_f can be obtained by solving $h_H(\sigma; \lambda_0, \sigma_0) = f(\sigma) - g_H(\sigma) = 0$. By Proposition 3.1, it can be stated that the location of an equilibrium point is $\sigma_f \in (\underline{\sigma}, \bar{\sigma})$ by the intermediate value theorem if and only if $h_H(\underline{\sigma}) < 0$, and $h_H(\bar{\sigma}) > 0$. Using $\sin\bar{\sigma}/\eta = 1/\zeta_{\lim}$ and $\sin\underline{\sigma}/\eta = -1/\zeta_{\lim}$, h_H gives

$$h_H(\underline{\sigma}; \lambda_0, \sigma_0) = \lambda_0 - \frac{1}{N-1}(\underline{\sigma} - \sigma_0) - (\gamma_T + \pi) - \sin^{-1}\left(\frac{1}{\zeta_{\lim}}\right) < 0 \tag{3.8}$$

$$h_H(\bar{\sigma}; \lambda_0, \sigma_0) = \lambda_0 - \frac{1}{N-1}(\bar{\sigma} - \sigma_0) - (\gamma_T + \pi) + \sin^{-1}\left(\frac{1}{\zeta_{\lim}}\right) > 0 \tag{3.9}$$

Substituting $\underline{\lambda}_{PPN,HO}(\sigma_0)$ and $\bar{\lambda}_{PPN,HO}(\sigma_0)$ into Eqs. (3.8)-(3.9) yields

$$\bar{\lambda}_{PPN,HO}(\sigma_0) < \lambda_0 < \underline{\lambda}_{PPN,HO}(\sigma_0) \tag{3.10}$$

Moreover, $\sigma_f = \underline{\sigma}$ when $\lambda_0 = \underline{\lambda}_{PPN,HO}(\sigma_0)$, and $\sigma_f = \bar{\sigma}$ when $\lambda_0 = \bar{\lambda}_{PPN,HO}(\sigma_0)$.

□

Corollary 3.1 addresses the *capturable* and the *partially capturable regions* of PPN with respect to the lock-on condition.

Corollary 3.1. Under Assumptions 2.1-2.5, consider a planar engagement between a target and a missile guided by PPN with $N > 2(1+\eta)$. The missile is equipped with an RN-FOV strapdown seeker satisfying $\zeta_{\lim} > 1$. Then, $\mathcal{A}_{PPN,HO} = \{(r_0, \lambda_0) : r_0 \geq \underline{R}_0, \lambda_0 \in [\bar{\lambda}^c_{PPN,HO}, \underline{\lambda}^c_{PPN,HO}]\}$ is a *capturable region* of PPN in the head-on engagement case where

$$\begin{aligned} \underline{\lambda}^c_{PPN,HO} &= \gamma_T + \pi + \sin^{-1}\left(\frac{1}{\zeta_{\lim}}\right) - \frac{1}{N-1}(\bar{\sigma} - \underline{\sigma}) \\ \bar{\lambda}^c_{PPN,HO} &= \gamma_T + \pi - \sin^{-1}\left(\frac{1}{\zeta_{\lim}}\right) + \frac{1}{N-1}(\bar{\sigma} - \underline{\sigma}) \end{aligned} \tag{3.11}$$

Furthermore, $\mathcal{B}_{PPN,HO} = \{(r_0, \lambda_0) : r_0 \geq \underline{R}_0, \lambda_0 \in [\bar{\lambda}^{pc}_{PPN,HO}, \underline{\lambda}^{pc}_{PPN,HO}]\}$ is a *partially capturable region* of PPN in the head-on engagement case where

$$\begin{aligned} \underline{\lambda}^{pc}_{PPN,HO} &= \gamma_T + \pi + \sin^{-1}\left(\frac{1}{\zeta_{\lim}}\right) = \lambda^*_{\underline{\sigma},HO} \\ \bar{\lambda}^{pc}_{PPN,HO} &= \gamma_T + \pi - \sin^{-1}\left(\frac{1}{\zeta_{\lim}}\right) = \lambda^*_{\bar{\sigma},HO} \end{aligned} \tag{3.12}$$

Proof. See Appendix B.1. □

Capture Region of PPN in Tail-Chase Engagement

For a tail-chase engagement, the capturability is analyzed within the domain $\mathcal{D}_{TC} = \{(r, \lambda) : \lambda \in [\gamma_T - \frac{\pi}{2}, \gamma_T + \frac{\pi}{2}]\}$. Similar to the head-on case, the capture region of the PPN can be obtained based on Proposition 3.1. If the collision course is formed outside $\mathcal{L}_{adm,TC}$, the look angle cannot remain in the FOV range at the final phase. The capture region can be obtained by showing whether or not the locus of the collision condition is made within the FOV range. Let $g_T = \gamma_T + \sin^{-1}\left(\frac{V_m}{V_T}\sin\sigma\right)$ be the collision condition in the tail-chase engagement, and $h_T(\sigma; \lambda_0, \sigma_0) = f(\sigma) - g_T(\sigma) = 0$. Note that the function h_T satisfies the following condition.

Proposition 3.2. h_T is strictly decreasing function in $\sigma \in [\underline{\sigma}, \bar{\sigma}]$.

Proof. Proof of Proposition 3.3 is similar to the proof of Proposition 3.1. □

Theorem 3.2 addresses the capture region of PPN for the tail-chase engagement case.

Theorem 3.2. Under Assumptions 2.1-2.5, consider a planar engagement between a target and a missile guided by PPN with $N > 2(1+\eta)$. The missile is equipped with an RN-FOV strapdown seeker satisfying $\zeta_{\lim} > 1$. Then, the capture region for tail-chase geometry can be expressed as

$$\mathcal{C}_{PPN,TC} = \left\{(r_0, \lambda_0, \sigma_0) : r_0 \geq \underline{R}_0, \lambda_0 \in [\underline{\lambda}_{PPN,TC}(\sigma_0), \bar{\lambda}_{PPN,TC}(\sigma_0)], \sigma_0 \in [\underline{\sigma}, \bar{\sigma}]\right\} \tag{3.13}$$

where

$$\begin{aligned} \underline{\lambda}_{PPN,TC}(\sigma_0) &= \gamma_T - \sin^{-1}\left(\frac{1}{\zeta_{\lim}}\right) + \frac{1}{N-1}(\underline{\sigma} - \sigma_0) \\ \bar{\lambda}_{PPN,TC}(\sigma_0) &= \gamma_T + \sin^{-1}\left(\frac{1}{\zeta_{\lim}}\right) + \frac{1}{N-1}(\bar{\sigma} - \sigma_0) \end{aligned} \tag{3.14}$$

Proof. Similar to Theorem 3.1, it can be proved by determining whether the solution σ_f lies in the FOV limit. By Proposition 3.2, it can be stated that the location of an equilibrium point is $\sigma_f \in (\underline{\sigma}, \bar{\sigma})$ by the intermediate value theorem if and only if $h_T(\underline{\sigma}) > 0$, and $h_T(\bar{\sigma}) < 0$. Consequently, we have

$$h_T(\underline{\sigma}; \lambda_0, \sigma_0) = \lambda_0 - \frac{1}{N-1}(\underline{\sigma} - \sigma_0) - \gamma_T + \sin^{-1}\left(\frac{1}{\zeta_{\lim}}\right) > 0 \tag{3.15}$$

$$h_T(\bar{\sigma}; \lambda_0, \sigma_0) = \lambda_0 - \frac{1}{N-1}(\bar{\sigma} - \sigma_0) - \gamma_T - \sin^{-1}\left(\frac{1}{\zeta_{\lim}}\right) < 0 \tag{3.16}$$

□

Corollary 3.2 addresses the *capturable* and *partially capturable* regions of PPN in regard to the lock-on condition.

Corollary 3.2. Under Assumptions 2.1-2.5, consider a planar engagement between a target and a missile guided by PPN with $N > 2(1+\eta)$. The missile is equipped with an RN-FOV strapdown seeker satisfying $\zeta_{\lim} > 1$. Then, $\mathcal{A}_{PPN,TC} = \{(r_0, \lambda_0) : r_0 \geq \underline{R}_0, \lambda_0 \in \mathcal{L}_{adm,TC}\}$ is a *capturable region* of PPN for the tail-chase engagement case where $\mathcal{L}_{adm,TC}$ is obtained from Eq. (2.34). Furthermore, $\mathcal{B}_{PPN,TC} = \{(r_0, \lambda_0) : r_0 \geq \underline{R}_0, \lambda_0 \in [\underline{\lambda}^{pc}_{PPN,TC}, \bar{\lambda}^{pc}_{PPN,TC}]\}$ is a *partially capturable region* of PPN where $\underline{\lambda}^{pc}_{PPN,TC}$ and $\bar{\lambda}^{pc}_{PPN,TC}$ can be obtained as

$$\begin{aligned} \underline{\lambda}^{pc}_{PPN,TC} &= \gamma_T - \sin^{-1}\left(\frac{1}{\zeta_{\lim}}\right) - \frac{1}{N-1}(\bar{\sigma} - \underline{\sigma}) \\ \bar{\lambda}^{pc}_{PPN,TC} &= \gamma_T + \sin^{-1}\left(\frac{1}{\zeta_{\lim}}\right) + \frac{1}{N-1}(\bar{\sigma} - \underline{\sigma}) \end{aligned} \tag{3.17}$$

Proof. Proof of Corollary 3.2 is similar to that for the head-on engagement case. The details of the proof are shown in Appendix B.2. □

Figure 3.1 shows the capture region of PPN, $\mathcal{C}_{PPN} = \mathcal{C}_{PPN,TC} \cup \mathcal{C}_{PPN,HO}$. The capture region is expressed in terms of σ_0 and (r_0, λ_0) and divided according to two engagement configurations. Characteristics of the capture region will be discussed in Section 5.1.1.

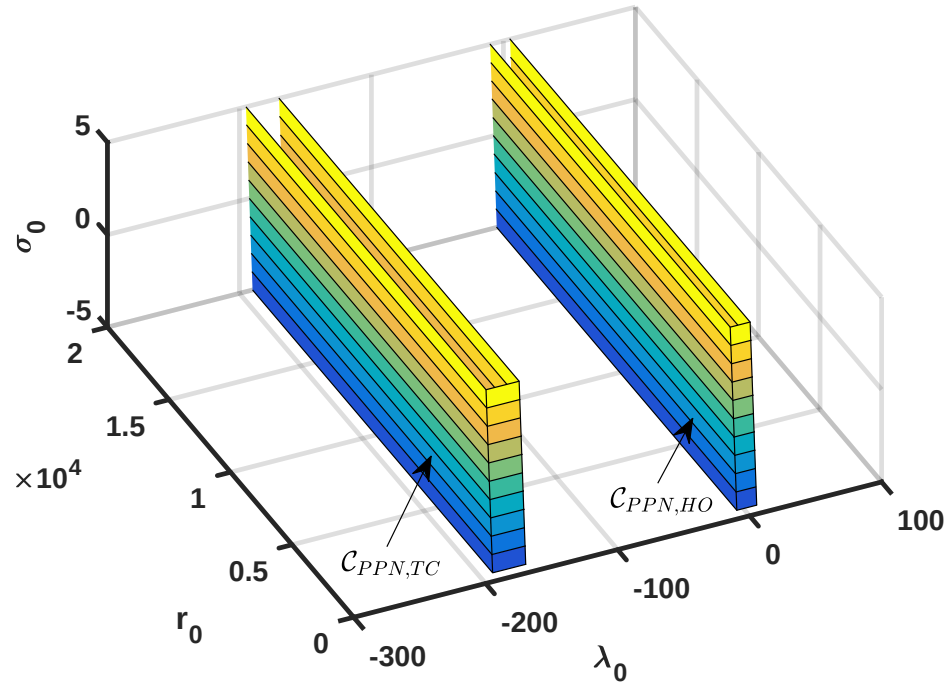

(a) Overall Region

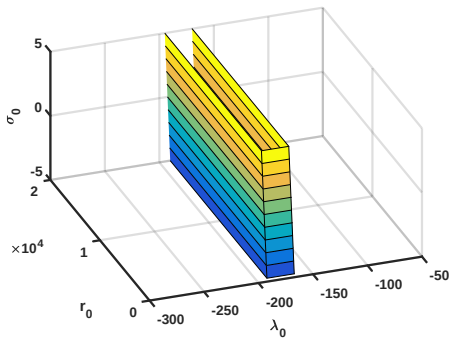

(b) Tail-chase

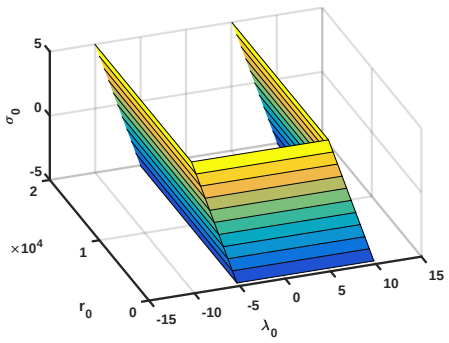

(c) Head-on

Figure 3.1: Capture Region of PPN

3.2 Capture Region of Look-angle Constrained Guidance Law (LCG)

3.2.1 Guidance Law

In this section, LCG consisting of PPN and look angle control is considered. The guidance strategy is summarized as follows:

Stage 1: PPN is performed to enter a collision course.

Stage 2: (If necessary) DPP is executed for the look angle not to exceed FOV limit.

In this strategy, PPN guidance is performed as long as the look angle is within the FOV limit, and the guidance law is switched to the look angle controller if the look angle reaches its limit. By holding the look angle at the limiting value, the missile continues the flying to intercept the target. The guidance command of LCG can be expressed as

$$a_{LCG} = \begin{cases} NV_m\dot{\lambda}, & \underline{\sigma} < \sigma < \bar{\sigma} \\ V_m\dot{\lambda} + kV_m(\sigma_c - \sigma), & \sigma = \bar{\sigma},\ \sigma = \underline{\sigma} \end{cases} \tag{3.18}$$

where N is the guidance gain, and k is the feedback gain of the look angle control. The LOS angle at which the guidance law is switched from PPN to look angle control can be obtained as

$$\lambda_{sw} = \lambda_0 - \frac{1}{N-1}\left(\sigma_{FOV} - \sigma_0\right) \tag{3.19}$$

where $\sigma_{FOV} = \bar{\sigma}$ or $\underline{\sigma}$. After the transition, the corresponding trajectory is followed by the pursuit trajectory. Note that the performance of LCG is same as that of PPN, if the look angle is always within FOV limit and the capture

region includes that of PPN. Therefore, the capture region can be extended especially when the engagement is ended by DPP. The necessary condition for the transition of the guidance logic is summarized in Condition 3.2.

Condition 3.2. For a given initial position (r_0, λ_0), switching of the guidance occurs when the switching LOS angle is between λ_0 and λ_{PPN}, i.e.,

$$\lambda_0 \leq \lambda_{sw} \leq \lambda_{PPN}, \quad \text{or} \quad \lambda_{PPN} \leq \lambda_{sw} \leq \lambda_0 \tag{3.20}$$

The switching position is located on the straight line $\lambda = \lambda_{sw}$. Moreover, the transition always occurs when the initial position of the missile lies outside the *partially capturable region* of PPN.

To successfully intercept the target by DPP, the miss distance resulting from DPP trajectory should be smaller than a specified value. Therefore, the capture region of LCG can be obtained using the trajectory of the DPP unlike PPN case. In the following, the capture region according to the two engagement geometries is analyzed based on this property.

3.2.2 Capture Region Derivation of LCG

Capture Region of LCG in Head-on Engagement

In the head-on engagement, PPN and DPP guidance commands constituting the LCG show different characteristics in the phase portraits. The trajectory of DPP diverges from its equilibrium point, whereas PPN converges to the collision course. For given σ_0, suppose that the initial position of the missile lies outside the cap of PPN such that $\lambda_0 < \bar{\lambda}_{PPN,HO}(\sigma_0)$. From Eqs. (2.17) and (2.25b), the LOS angle decreases with time, because $\dot{\lambda} < 0$ and $\sigma \to \bar{\sigma}$. Note

that the switching of the guidance command always occurs in the domain as shown in Condition 3.2. Substituting $\lambda_{sw} = \bar{\sigma}$ yields

$$\lambda_{sw}(r_{sw}) = \lambda_0(r_0) - \frac{1}{N-1}(\bar{\sigma} - \sigma_0) < \lambda^*_{\bar{\sigma},HO} \tag{3.21}$$

The switching position (r_{sw}, λ_{sw}) can be expressed as

$$r_{sw} = \Psi\left(\lambda_{sw}, \lambda_0; \sigma_0\right) r_0 \tag{3.22}$$

After switching the command, the trajectory by DPP gets away from the unstable equilibrium point as $r \to 0$. Likewise, the terminal look angle can be determined according to the location of initial LOS angle as

$$\sigma_f = \begin{cases} \bar{\sigma} & \text{if } \lambda_0 < \bar{\lambda}_{PPN,HO}\left(\sigma_0\right) \\ \in (\underline{\sigma}, \bar{\sigma}) & \text{if } \lambda_0 \in \left(\bar{\lambda}_{PPN,HO}\left(\sigma_0\right), \underline{\lambda}_{PPN,HO}\left(\sigma_0\right)\right) \\ \underline{\sigma} & \text{if } \lambda_0 > \underline{\lambda}_{PPN,HO}\left(\sigma_0\right) \end{cases} \tag{3.23}$$

Tendency of the LCG trajectory according to the initial position can be addressed as follows.

Proposition 3.3. Suppose that a missile is guided by LCG with $N > 2(1+\eta)$. The missile is equipped with an RN-FOV strapdown seeker satisfying $\zeta_{\text{lim}} > 1$. If the initial position satisfies $\lambda_0 < \bar{\lambda}_{PPN,HO}(\sigma_0)$, then every trajectory governed by LCG finally becomes the trajectory governed by the deviated pursuit with the $\bar{\sigma}$ command, $\bar{r} = \Phi(\bar{\lambda}, \lambda_{sw}; \bar{\sigma}) r_{sw}$. Furthermore, the switching occurs fast as the initial position is placed far away from the equilibrium point. ln case of $\lambda_0 > \underline{\lambda}_{PPN,HO}(\sigma_0)$, every trajectory governed by LCG finally becomes the trajectory governed by the deviated pursuit with the $\underline{\sigma}$ command, $\underline{r} = \Phi(\underline{\lambda}, \lambda_{sw}; \underline{\sigma}) r_{sw}$. Considering the maneuverability limit, the minimum miss

distance r_f for (r_0, λ_0) and corresponding terminal LOS λ_f satisfy the following relation.

$$r_f \frac{a_{\max}}{V_m} = \begin{cases} V_T \sin(\lambda - \gamma_T) - V_m \sin\bar{\sigma} & \text{if } \lambda_0 < \bar{\lambda}_{PPN,HO}(\sigma_0) \\ V_T \sin(\gamma_T - \lambda) + V_m \sin\underline{\sigma} & \text{if } \lambda_0 > \underline{\lambda}_{PPN,HO}(\sigma_0) \end{cases} \tag{3.24}$$

Proof. Without loss of generality, consider an initial condition $\lambda_0 < \bar{\lambda}_{PPN,HO}(\sigma_0)$. It can be shown that the terminal look angle satisfying collision condition by PPN gives $\sigma_{f,PPN} > \bar{\sigma}$ by solving $h_H(\bar{\sigma}) < 0$. Therefore, we have

$$\lambda_{PPN} = \lambda_0 - \frac{1}{N-1}(\sigma_{f,PPN} - \sigma_0) < \lambda_0 - \frac{1}{N-1}(\bar{\sigma} - \sigma_0) = \lambda_{sw} < \lambda_0 \tag{3.25}$$

Now, guidance transition occurs to DPP with $\sigma_f = \bar{\sigma}$. For the tendency of the switching locus, let $\lambda_1 = \int_{t_0}^{t_1} \dot{\lambda} dt$ and $\lambda_2 = \int_{t_0}^{t_1} \dot{\lambda} dt$ be the LOS angles starting from $\lambda_1(t_0) = \lambda_{01}$ and $\lambda_2(t_0) = \lambda_{02}$. If $\lambda_{01} < \lambda_{02} < \bar{\lambda}_{PPN,HO}(\sigma_0)$, PPN shows monotonic behavior as $\dot{\lambda} < 0$ and $\dot{r} < 0$. Note that $\partial\dot{r}/\partial\lambda$ and $\partial\dot{\lambda}/\partial\lambda$ initially satisfy the following condition.

$$\begin{aligned} \frac{\partial \dot{r}}{\partial \lambda_0} &= V_T \sin(\gamma_T - \lambda_0) < 0 \\ \frac{\partial \dot{\lambda}}{\partial \lambda_0} &= -\frac{V_T}{r}\cos(\gamma_T - \lambda_0) > 0 \end{aligned} \tag{3.26}$$

From the comparison principle, $|\dot{\lambda}|_{\lambda_{02}} > |\dot{\lambda}|_{\lambda_{01}}$ as $\lambda_{02} > \lambda_{01}$, and $|\dot{r}|_{\lambda_{02}} < |\dot{r}|_{\lambda_{01}}$. □

From Proposition 3.3, for the trajectories converted to DPP of $\bar{\sigma}$ to be successful, the intercept error should be within the allowable value, i.e., $r_f \leq R_{\text{miss}}$. Considering the allowable miss distance, the marginal trajectory that succeeds the engagement can be obtained by integrating the solution of DPP backward from the value value $(R_{\text{miss}}, \bar{\lambda}_{HO,f})$ at the final time as

$$r_{sw,HO} = \Phi\left(\bar{\lambda}_{sw,HO}, \bar{\lambda}_{HO,f}; \bar{\sigma}\right) R_{\text{miss}} \tag{3.27}$$

where $\bar{\lambda}_{HO,f}$ can be obtained by substituting $r = R_{\text{miss}}$ into Eq. (3.24) as

$$\bar{\lambda}_{HO,f} = \gamma_T + \pi - \sin^{-1}\left(\frac{R_{\text{miss}} a_{\max}}{V_m V_T} - \frac{V_m}{V_T}\sin\bar{\sigma}\right) \tag{3.28}$$

Note that the switching point also lies on the marginal trajectory, and therefore, the marginal trajectory can be regarded as a switching curve. Using Eqs. (3.21), (3.22), and (3.27), we have

$$r = \begin{cases} \Psi\left(\lambda, \lambda_{sw}(r_{sw}); \bar{\sigma}\right) \Phi\left(\lambda_{sw}(r_{sw}), \bar{\lambda}_{HO,f}; \bar{\sigma}\right) R_{\text{miss}} & (r_{sw} \le r \le r_0) \\ \Phi\left(\lambda, \bar{\lambda}_{HO,f}; \bar{\sigma}\right) R_{\text{miss}} & (R_{\text{miss}} \le r \le r_{sw}) \end{cases} \tag{3.29}$$

where r_{sw} and λ_{sw} satisfy the following relation at the switching time:

$$r_{sw} = \Phi\left(\lambda(r_{sw}), \bar{\lambda}_{HO,f}; \bar{\sigma}\right) R_{\text{miss}} \tag{3.30}$$

The upper equation in Eq. (3.29) shows the trajectory obtained by PPN before the switching time, and the lower equation shows the deviated pursuit trajectory. Note that λ_0 and $(r_{sw}, \lambda_{HO}(r_{sw}, \sigma_0))$ change according to the initial distance r_0, and therefore the locus of $(r_0, \lambda_0(r_0))$ can be the boundary of the capture region of LCG for σ_0. Similarly, another boundary $(\underline{r}_{HO}(\sigma_0), \underline{\lambda})$ can be also obtained by changing the initial look angle as $\sigma_0 = \underline{\sigma}$. In summary, the capture region of LCG in the head-on engagement case can be expressed as follows.

Theorem 3.3. Under Assumptions 2.1-2.5, consider a planar engagement between a target and a missile guided by LCG with $N > 2(1+\eta)$. The missile is equipped with an RN-FOV strapdown seeker satisfying $\zeta_{\text{lim}} > 1$. The capture

region of LCG in the head-on case can be expressed as

$$\mathcal{C}_{LCG,HO} = \{(r_0, \lambda_0, \sigma_0) : r_0 \geq \underline{R}_0, \lambda_0 \in [\bar{\lambda}_{HO}(r_0, \sigma_0), \underline{\lambda}_{HO}(r_0, \sigma_0)], \sigma_0 \in [\underline{\sigma}, \bar{\sigma}]\} \tag{3.31}$$

where $\bar{\lambda}_{HO}(r_0, \sigma_0)$ and $\underline{\lambda}_{HO}(r_0, \sigma_0)$ can be implicitly expressed as

$$r_0 = \Psi\left(\bar{\lambda}_{HO}(r_0, \sigma_0), \bar{\lambda}_{sw}(r_{sw}); \bar{\sigma}\right) \Phi\left(\bar{\lambda}_{sw}(r_{sw}), \bar{\lambda}^{pc}_{HO,f}; \bar{\sigma}\right) R_{\text{miss}} \tag{3.32a}$$

$$r_0 = \Psi\left(\underline{\lambda}_{HO}(r_0, \sigma_0), \underline{\lambda}_{sw}(r_{sw}); \underline{\sigma}\right) \Phi\left(\underline{\lambda}_{sw}(r_{sw}), \underline{\lambda}^{pc}_{HO,f}; \bar{\sigma}\right) R_{\text{miss}} \tag{3.32b}$$

$$\bar{\lambda}_{HO}(r_0, \sigma_0) = \bar{\lambda}_{sw}(r_{sw}) + \frac{1}{1-N}(\sigma_0 - \bar{\sigma}) \tag{3.32c}$$

$$\underline{\lambda}^{c}_{HO}(r_0, \sigma_0) = \underline{\lambda}_{sw}(r_{sw}) + \frac{1}{1-N}(\sigma_0 - \underline{\sigma}) \tag{3.32d}$$

Note that Ψ is the transition function of PPN obtained from Eq.(2.22). $(r_{sw}, \bar{\lambda}_{sw})$ and $(\underline{r}_{sw}, \underline{\lambda}_{sw})$ lying on the marginal trajectories (3.27) can be expressed as

$$\begin{aligned} r_{sw} &= \Phi\left(\bar{\lambda}_{sw}(r_{sw}), \bar{\lambda}^{pc}_{HO,f}; \bar{\sigma}\right) R_{\text{miss}} \\ r_{sw} &= \Phi\left(\underline{\lambda}_{sw}(r_{sw}), \underline{\lambda}^{pc}_{HO,f}; \underline{\sigma}\right) R_{\text{miss}} \end{aligned} \tag{3.33}$$

$$\bar{\lambda}_{HO,f} = \gamma_T + \pi - \sin^{-1}\left(\frac{R_{\text{miss}} a_{\max}}{V_m V_T} - \frac{V_m}{V_T}\sin\bar{\sigma}\right) \tag{3.34a}$$

$$\underline{\lambda}_{HO,f} = \gamma_T + \pi - \sin^{-1}\left(\frac{-R_{\text{miss}} a_{\max}}{V_m V_T} - \frac{V_m}{V_T}\sin\underline{\sigma}\right) \tag{3.34b}$$

Proof. Interception is achieved by PPN if $\lambda_0 \in [\bar{\lambda}_{PPN,HO}(\sigma_0), \underline{\lambda}_{PPN,HO}(\sigma_0)]$. Suppose that $\bar{\lambda}_{HO}(r_0, \lambda_0) \leq \lambda_0 < \bar{\lambda}_{PPN,HO}(\sigma_0)$ without loss of generality. From Proposition 3.3, the transition occurs at $\lambda_{sw} = \lambda_0 + \frac{1}{1-N}(\bar{\sigma} - \sigma_0)$. Let $\Delta\lambda_0 = \frac{1}{1-N}(\bar{\sigma} - \sigma_0)$, then the switching position satisfies

$$\bar{\lambda}_{sw} = \bar{\lambda}_{HO}(\sigma_0) + \Delta\lambda_0 \leq \lambda_{sw} < \lambda^*_{\bar{\sigma},HO} \tag{3.35}$$

$$r_{sw} = \Psi(\lambda_{sw}, \lambda_0) r_0 < \Psi(\bar{\lambda}_{HO}(\sigma_0) + \Delta\lambda_0, \bar{\lambda}_{HO}(\sigma_0)) r_0 = \bar{r}_{sw,HO} \tag{3.36}$$

Since $r_{sw} < \bar{r}_{sw,HO}$ and $\dot{\lambda} < 0$, there exists $\bar{\lambda}_1 < \bar{\lambda}_{sw}$ such that

$$\Phi(\bar{\lambda}_1, \bar{\lambda}_{sw})\bar{r}_{sw,HO} = r_{sw} \tag{3.37}$$

From the comparison principle, there exists λ_2 satisfying the following inequalities.

$$\begin{aligned} \bar{\lambda}_1 \leq \lambda_{sw} < \lambda^*_{\bar{\sigma},HO} \qquad & \text{at } r = r_{sw} \\ \bar{\lambda}_{HO,f} \leq \lambda_2 < \lambda^*_{\bar{\sigma},HO} \qquad & \text{at } r = R_{miss} \end{aligned} \tag{3.38}$$

where $|\dot{\gamma}(\lambda_2, R_{miss})| \leq \left|\frac{a_{max}}{V_m}\right|$. Therefore, DPP trajectory by LCG reaches the miss distance within the acceleration limit. □

Capture Region of LCG in Tail-chase Engagement

In the tail-chase engagement, the trajectories by PPN and look angle control both show stable phase portraits. Therefore, in contrast to the head-on engagement case, the capture region of LCG can be extended by taking advantage of the DPP trajectory in the homing phase. For given σ_0, suppose that the initial position is outside the capture region of PPN, $\bar{\lambda}_{PPN,TC}(\sigma_0) < \lambda_0$. In this domain, the LOS decreases with respect to time because $\dot{\lambda} < 0$ from Eq. (2.25b), and the look angle $\sigma \to \bar{\sigma}$ by PPN as the missile approaches the target with guidance transition at $\lambda = \lambda_{sw}$. If guidance switching occurs, $\lambda_{sw}(r_{sw})$ at the switching instance $r = r_{sw}$ has

$$\bar{\lambda}_{\underline{\sigma},TC} \leq \lambda_{sw} = \lambda_0 - \frac{1}{N-1}(\bar{\sigma} - \sigma_0) \tag{3.39}$$

After switching the guidance command, the DPP trajectory $\bar{\sigma}$ converges to the equilibrium point $\bar{\lambda}_{\underline{\sigma},TC}$. In this regard, the *"worst"* solution giving the maximum miss distance for the initial position can be addressed as follows.

Proposition 3.4. Suppose that a missile is guided by LCG with $N > 2(1+\eta)$. The missile is equipped with an RN-FOV strapdown seeker satisfying $\zeta_{\lim} > 1$. If the initial position satisfies $\lambda_0 < \underline{\lambda}_{PPN,TC}(\sigma_0)$, then every trajectory governed by LCG finally becomes the trajectory governed by the deviated pursuit with $\underline{\sigma}$ command. Furthermore, if $\sigma_0 = \underline{\sigma}$, the trajectory $(\underline{r}, \underline{\lambda})$ gives the maximum miss distance, $\underline{r} = \Phi(\underline{\lambda}, \lambda_0; \underline{\sigma}) r_0$. In case of $\lambda_0 > \bar{\lambda}_{PPN,TC}(\sigma_0)$, every trajectory governed by LCG finally becomes the trajectory governed by the deviated pursuit with $\bar{\sigma}$ command. Furthermore, if $\sigma_0 = \bar{\sigma}$, the trajectory $(\bar{r}, \bar{\lambda})$ gives the maximum miss distance, $\bar{r} = \Phi(\bar{\lambda}, \lambda_0; \bar{\sigma}) r_0$. Considering the maneuverability limit, the minimum miss distance r_f for (r_0, λ_0) and the corresponding terminal LOS λ_f satisfy the following relation.

$$r_f \frac{a_{\max}}{V_m} = \begin{cases} V_T \sin(\gamma_T - \lambda) + V_m \sin \underline{\sigma} & \text{if } \lambda_0 < \underline{\lambda}_{PPN,TC} \\ V_T \sin(\lambda - \gamma_T) - V_m \sin \bar{\sigma} & \text{if } \lambda_0 > \bar{\lambda}_{PPN,TC} \end{cases} \tag{3.40}$$

In this regard, The DPP trajectory that maintains $\sigma_0 = \bar{\sigma}$ and eventually reaches the *miss-intercept layer* at $r_f = R_{\text{miss}}$ is the switching trajectory. In a similar manner to the head-on engagement, the trajectory can be obtained by integrating the solution backward from the value $(R_{\text{miss}}, \bar{\lambda}^c_{TC,f})$ at the final time as

$$\bar{r}_{TC} = \Phi(\bar{\lambda}^c_{TC}, \bar{\lambda}^c_{TC,f}; \bar{\sigma}) R_{\text{miss}} \tag{3.41}$$

$$\bar{\lambda}_{TC,f} = \gamma_T + \sin^{-1}\left(\frac{R_{\text{miss}} a_{\max}}{V_m V_T} - \frac{V_m}{V_T} \sin \bar{\sigma} \right) \tag{3.42}$$

In order for the engagement to be successful, the trajectory by PPN should enter the switching layer obtained from Eq. (3.41). The lower bound of the LOS angle at the switching time, $(r_{sw}, \lambda_{sw}(r_{sw}))$, can be obtained as

$$\lambda_{sw}(r_{sw}) = \lambda_0(r_0) - \frac{1}{N-1}(\bar{\sigma} - \sigma_0) \tag{3.43}$$

Now, the trajectory can be expressed as

$$r = \begin{cases} \Psi\left(\lambda, \lambda_{sw}(r_{sw}); \bar{\sigma}\right) \Phi\left(\lambda_{sw}(r_{sw}), \bar{\lambda}_{TC,f}; \bar{\sigma}\right) R_{\text{miss}} & (r_{sw} \leq r \leq r_0) \\ \Phi\left(\lambda, \bar{\lambda}_{TC,f}; \bar{\sigma}\right) R_{\text{miss}} & (R_{\text{miss}} \leq r \leq r_{sw}) \end{cases} \tag{3.44}$$

where the switching point (r_{sw}, λ_{sw}) can be expressed as follows,

$$r_{sw} = \Phi\left(\lambda(r_{sw}), \bar{\lambda}_{TC,f}; \bar{\sigma}\right) R_{\text{miss}} \tag{3.45}$$

Note that λ_0 and $(r_{sw}, \bar{\lambda}_{TC}(r_{sw}))$ are determined by the initial distance r_0. The boundary of the capture region of LCG can be expressed from the locus of $(r_0, \lambda_0(r_0))$. In summary, the capture region of LCG can be obtained in the tail-chase engagement case as follows.

Theorem 3.4. Under Assumptions 2.1-2.5, consider a planar engagement between a target and a missile that is guided by LCG with $N > 2(1+\eta)$. The missile is equipped with an RN-FOV strapdown seeker satisfying $\zeta_{\text{lim}} > 1$. The capture region of LCG can be obtained in the tail-chase engagement case as

$$\mathcal{C}_{LCG,TC} = \{(r_0, \lambda_0, \sigma_0) : r_0 \geq \underline{R}_0, \lambda_0 \in [\underline{\lambda}_{TC}(r_0, \sigma_0), \bar{\lambda}_{TC}(r_0, \sigma_0)], \sigma_0 \in [\underline{\sigma}, \bar{\sigma}]\} \tag{3.46}$$

where $(r_0, \underline{\lambda}_{TC}(r_0, \sigma_0))$ and $(r_0, \bar{\lambda}_{TC}(r_0, \sigma_0))$ can be expressed as

$$\begin{aligned} r_0 &= \Psi\left(\underline{\lambda}_{TC}(r_0, \sigma_0), \underline{\lambda}_{sw}(r_{sw}); \underline{\sigma}\right) \Phi\left(\underline{\lambda}_{sw}(r_{sw}), \underline{\lambda}_{TC,f}; \underline{\sigma}\right) R_{\text{miss}} \\ r_0 &= \Psi\left(\bar{\lambda}_{TC}(r_0, \sigma_0), \bar{\lambda}_{sw}(r_{sw}); \bar{\sigma}\right) \Phi\left(\bar{\lambda}_{sw}(\bar{r}_{sw}), \bar{\lambda}_{TC,f}; \underline{\sigma}\right) R_{\text{miss}} \\ \underline{\lambda}_{TC}(r_0, \sigma_0) &= \underline{\lambda}_{sw}(r_{sw}) + \frac{1}{1-N}(\sigma_0 - \underline{\sigma}) \\ \bar{\lambda}_{TC}(r_0, \sigma_0) &= \bar{\lambda}_{sw}(r_{sw}) + \frac{1}{1-N}(\sigma_0 - \bar{\sigma}) \end{aligned} \tag{3.47}$$

where the switching points $(r_{sw}, \underline{\lambda}_{sw})$ and $(r_{sw}, \bar{\lambda}_{sw})$ can be obtained as follows:

$$\begin{aligned} r_0 &= \Phi(\underline{\lambda}_{TC}(r_0), \underline{\lambda}_{TC,f}; \underline{\sigma}) R_{\text{miss}} \\ r_0 &= \Phi(\bar{\lambda}_{TC}(r_0), \bar{\lambda}_{TC,f}; \bar{\sigma}) R_{\text{miss}} \end{aligned} \tag{3.48}$$

$$\begin{aligned} \underline{\lambda}_{TC,f} &= \gamma_T + \sin^{-1}\left(\frac{-R_{\text{miss}} a_{\max}}{V_m V_T} - \frac{V_m}{V_T}\sin\underline{\sigma}\right) \\ \bar{\lambda}_{TC,f} &= \gamma_T + \sin^{-1}\left(\frac{R_{\text{miss}} a_{\max}}{V_m V_T} - \frac{V_m}{V_T}\sin\bar{\sigma}\right) \end{aligned} \tag{3.49}$$

Proof. Interception is achieved by PPN if $\lambda_0 \in [\underline{\lambda}_{PPN,TC}(\sigma_0), \bar{\lambda}_{PPN,TC}(\sigma_0)]$. Suppose that $\bar{\lambda}_{TC}(r_0, \lambda_0) \geq \lambda_0 > \bar{\lambda}_{PPN,TC}(\sigma_0)$ without loss of generality. From Proposition 3.4, the transition occurs at $\lambda_{sw} = \lambda_0 + \frac{1}{1-N}(\bar{\sigma} - \sigma_0)$. Let $\Delta\lambda_0 = \frac{1}{1-N}(\bar{\sigma} - \sigma_0)$, then switching position satisfies

$$\bar{\lambda}_{sw} = \bar{\lambda}_{TC}(\sigma_0) + \Delta\lambda_0 \geq \lambda_{sw} > \lambda^*_{\bar{\sigma},TC} \tag{3.50}$$

$$r_{sw} = \Psi(\lambda_{sw}, \lambda_0) r_0 < \Psi(\bar{\lambda}_{TC}(\sigma_0) + \Delta\lambda_0, \bar{\lambda}_{TC}(\sigma_0)) r_0 = \bar{r}_{sw,TC} \tag{3.51}$$

Since $r_{sw} < \bar{r}_{sw,TC}$ and $\dot{\lambda} < 0$, there exists $\bar{\lambda}_1 > \bar{\lambda}_{sw}$ such that

$$\Phi(\bar{\lambda}_1, \bar{\lambda}_{sw}) \bar{r}_{sw,TC} = r_{sw} \tag{3.52}$$

From the comparison principle, there exists λ_2 satisfying the following inequalities.

$$\begin{aligned} \bar{\lambda}_1 \geq \lambda_{sw} > \lambda^*_{\bar{\sigma},TC} \qquad & \text{at } r = r_{sw} \\ \bar{\lambda}_{TC,f} \geq \lambda_2 > \lambda^*_{\bar{\sigma},TC} \qquad & \text{at } r = R_{miss} \end{aligned} \tag{3.53}$$

where $|\dot{\gamma}(\lambda_2, R_{miss})| \leq \left|\frac{a_{max}}{V_m}\right|$. Therefore, DPP trajectory by LCG reaches the miss distance within the acceleration limit. □

In similar way to PPN, the *capturable* and the *partially capturable* regions expressed as the initial condition for interception with regard to the FOV limit

can be addressed. Figure 3.2 shows the design procedure for $\mathcal{C}_{LCG}$, and Fig. 3.3 shows the capture region of LCG. Discussions of the corresponding capture regions will be provided in Section 5.1.3.

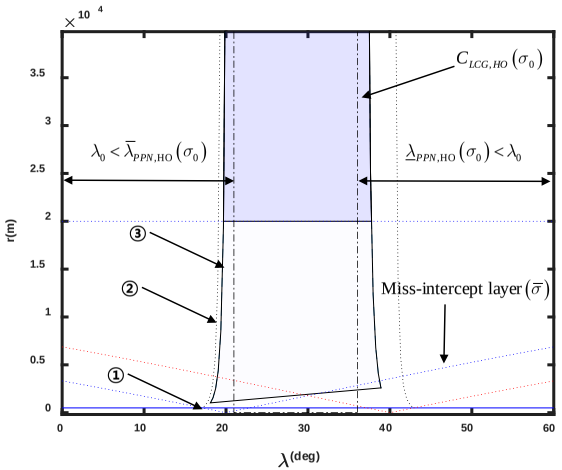

Step 1

Step 1.1 - $\lambda_0 < \bar{\lambda}_{PPN,\mathrm{HO}}(\sigma_0)$

① **Allowable miss intercept position :** by Eq. (3.24)

$$\bar{\lambda}_{HO,t} = \gamma_T - \pi - \sin^{-1}\left(\frac{R_{miss}a_{\max}}{V_m V_T} - \frac{V_m}{V_T}\sin\bar{\sigma}\right) \qquad \text{Eq. (3.34a)}$$

↓

② **Marginal Trajectory : Backward integration from (3.32a)**

$$r_{sw,HO} = \Phi\left(\bar{\lambda}_{sw,HO}, \bar{\lambda}_{HO,f}; \bar{\sigma}_0\right) R_{\mathrm{miss}} \qquad \text{Eq. (3.27)}$$

↓

③ **Locus of initial position : Backward integration from (3.25)**

$$\bar{\lambda}_{HO}(r_0,\sigma_0) = \bar{\lambda}_{sw}(r_{sw}) + \frac{1}{1-N}(\sigma_0 - \bar{\sigma}) \qquad \text{Eq. (3.32c)}$$

$$r_0 = \Phi\left(\bar{\lambda}_{HO}(r_0,\sigma_0), \bar{\lambda}_{sw,HO}(r_{sw}); \bar{\sigma}\right) r_{sw,HO} \qquad \text{Eq. (3.32a)}$$

Step 1.2 - $\underline{\lambda}_{PPN,\mathrm{HO}}(\sigma_0) < \lambda_0$ **Same procedure as Step 1.1**

$$\underline{\lambda}_{HO}(r_0,\sigma_0) = \underline{\lambda}_{sw}(r_{sw}) + \frac{1}{1-N}(\sigma_0 - \underline{\sigma}) \qquad \text{Eq. (3.32d)}$$

$$r_0 = \Phi\left(\bar{\lambda}_{HO}(r_0,\sigma_0), \bar{\lambda}_{sw,HO}(r_{sw}); \bar{\sigma}\right) r_{sw,HO} \qquad \text{Eq. (3.32b)}$$

Step 2

$$C_{LCG,\sigma_0} = \left\{(r_0,\lambda_0) : r_0 \geq R_0, \lambda_0 \in \left[\bar{\lambda}_{HO}(r_0,\sigma_0), \underline{\lambda}_{HO}(r_0,\sigma_0)\right] \cup \left[\underline{\lambda}_{TC}(r_0,\sigma_0), \bar{\lambda}_{TC}(r_0,\sigma_0)\right]\right\}$$

$$C_{LCG} = \bigcup_{\sigma_0 \in [\underline{\sigma}, \bar{\sigma}]} C_{LCG,\sigma_0}$$

Figure 3.2: Procedure of C_{LCG}

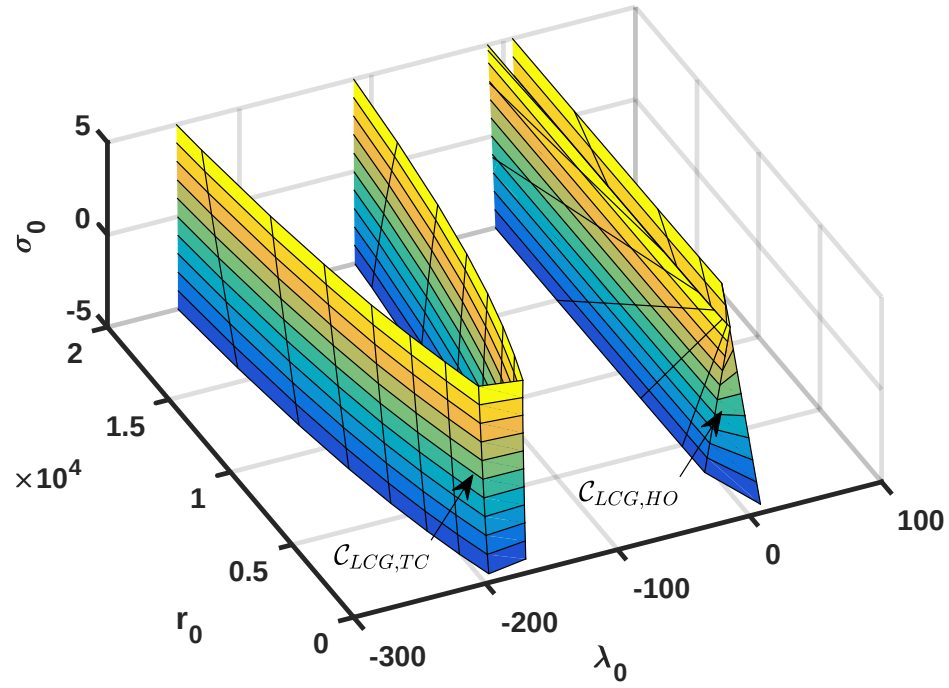

(a) Overall Region

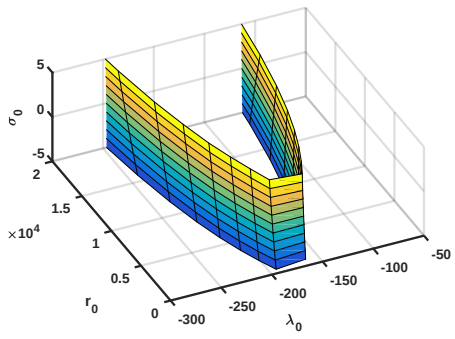

(b) Tail-chase

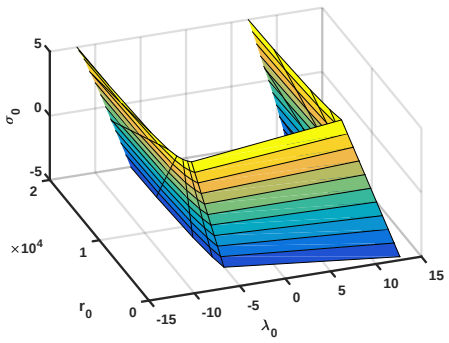

(c) Head-on

Figure 3.3: Capture Region of LCG

Chapter 4

Capture Region of FOV-constrained Impact-Angle Control Guidance

This chapter deals with the derivation of capture region for FOV-IACGs. FOV-IACG has been widely studied [27–32, 36, 53], but most of the design was to intercept stationary target or slowly moving target for the seeker with wide FOV limit. To investigate the achievable impact angle, the capture region with achievable impact angle [31] was constructed by multiple numerical simulations with various initial conditions. Especially for a particular scenario, i.e., $\lambda_0 = 0$, $\gamma_T = 0$ and π for surface-to-surface engagement, the region of achievable impact angle was investigated in Refs. [27–29].

In this study, a capture region of the impact angle control composite guidance (IACCG) is derived in Section 4.1. The necessary condition for achievable impact angle in RN-FOV case is provided, and the capture region is obtained by using DPP trajectory and switching condition. In Section 4.2, modified IACCG is proposed to improve the existing method. The corresponding capture region is provided.

4.1 Capture Region of Impact Angle Control Composite Guidance Law (IACCG)

4.1.1 Existing Guidance Law

In this section, IACCG [29] is briefly described. The composite guidance law has the following strategy.

Stage 1: Look angle control is initiated for trajectory shaping maneuver.

Stage 2: PPN is switched to enter a desired collision course.

Figure 4.1 shows the concept of IACCG. A trajectory shaping maneuver is performed while maintaining the FOV limit (phase 1), and the guidance command is switched to PPN guidance to intercept the target with the desired impact angle in the homing phase (phase 2). To focus on the RN-FOV case, the following assumption is considered as

Assumption 4.1. Considering RN-FOV limit, the look angle command is prespecified as its maximum/minimum values, i.e.,

$$\sigma_c = \pm\sigma_{\lim} \tag{4.1}$$

Note that look angle control is performed first to achieve a switching condition for impact angle control, unlike LCG. The switching condition can be derived by considering the terminal condition from the PPN. By selecting navigation gain as discussed in Theorem 2.1, the missile enter a desired collision course. The terminal LOS angle corresponding to the terminal impact angle can be calculated as follows,

$$\lambda_f = \tan^{-1}\left(\frac{\sin\gamma_f - \eta\sin\gamma_T}{\cos\gamma_f - \eta\cos\gamma_T}\right) \tag{4.2}$$

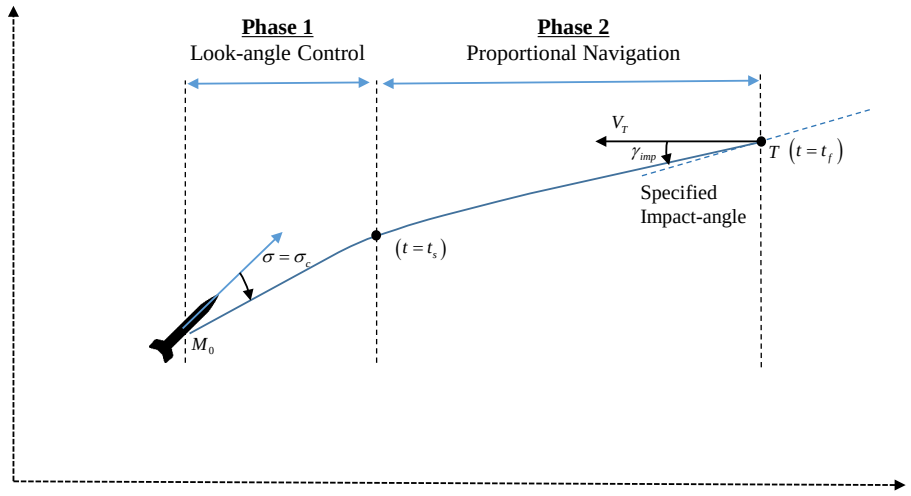

Figure 4.1: Concept of the IACCG Scheme

Using Eqs. (4.2) and (2.17), a relation between the terminal flight path angle, navigation gain, and initial conditions can be obtained as follows,

$$\frac{\sin\gamma_f - \eta\sin\gamma_T}{\cos\gamma_f - \eta\cos\gamma_T} = \tan\left(\lambda_0 + \frac{\gamma_f - \gamma_0}{N}\right) \tag{4.3}$$

By substituting $\lambda_s = \lambda_0$ and $\sigma_0 = \sigma_d$, switching criteria can be expressed in terms of LOS as follows,

$$\lambda_s = \left(\frac{N}{N-1}\right)\left(\tan^{-1}\left(\frac{\sin\gamma_f - \eta\sin\gamma_T}{\cos\gamma_f - \eta\cos\gamma_T}\right) - \frac{\gamma_f + \sigma_d}{N}\right) \tag{4.4}$$

When the switching condition satisfies, PPN command is generated to enter the desired collision course. Finally, the guidance law can be expressed in the form of switching framework as

$$a_{cmd} = \begin{cases} V_M\dot{\lambda} + kV_M(\sigma_c - \sigma), & |\lambda - \lambda_f| > |\lambda_s - \lambda_f| \\ NV_M\dot{\lambda}, & |\lambda - \lambda_f| \leq |\lambda_s - \lambda_f| \end{cases} \tag{4.5}$$

where σ_c denotes a look-angle command, and (k, N) are the feedback gain and navigation constant, respectively. After the switching, the missile is guided by PPN to intercept the target while satisfying the impact angle condition. In this study, the capture region with the achievable impact angle is investigated for generalized initial configuration.

4.1.2 Capture Region Derivation of IACCG

Necessary Condition of Achievable Impact Angle

Let us investigate the achievable impact set for the RN-FOV. For the parameter $\zeta_{\lim} > 1$, the FOV limit satisfies the following inequalities.

$$\sin\sigma_{\lim} < \eta, \quad \tan\sigma_{\lim} < \frac{\eta}{\sqrt{1-\eta^2}} \tag{4.6}$$

Note from Eq. (4.6) that the tangent of the FOV limit is less than the upper bound, which reduces the achievable look angle set for the collision condition. The look angle set can be expressed as

$$\tan\sigma_f \in [-\tan\sigma_{\lim}\ \tan\sigma_{\lim}] \tag{4.7}$$

The impact angle set associated with the reduced achievable look angle can be obtained based on the confined look angle. Considering the collision condition, the LOS angle is confined as follows,

$$\Lambda_f|_{\zeta_{\lim}>1} = \{\lambda_f | \lambda_f \in [\lambda^*_{\bar{\sigma},HO}, \lambda^*_{\underline{\sigma},HO}] \cup [\lambda^*_{\underline{\sigma},TC}, \lambda^*_{\bar{\sigma},TC}]\} \tag{4.8}$$

where

$$\begin{aligned}
&\lambda^*_{TC,\min} = \gamma_T - \sin^{-1}\left(\frac{1}{\zeta_{\lim}}\right), \lambda^*_{TC,\max} = \gamma_T + \sin^{-1}\left(\frac{1}{\zeta_{\lim}}\right) \\
&\lambda^*_{HO,\min} = \pi + \gamma_T - \sin^{-1}\left(\frac{1}{\zeta_{\lim}}\right), \lambda^*_{HO,\max} = \pi + \gamma_T + \sin^{-1}\left(\frac{1}{\zeta_{\lim}}\right)
\end{aligned} \tag{4.9}$$

And, the terminal flight path is also confined as follows,

$$\Gamma_f|_{\zeta_{\lim}>1} = \{\gamma_f | \gamma_f \in [\gamma^*_{TC,\min}, \gamma^*_{TC,\max}] \cup [\gamma^*_{HO,\min}, \gamma^*_{HO,\max}]\} \tag{4.10}$$

where

$$\begin{aligned}
&\gamma^*_{TC,\min} = \gamma_T - \sin^{-1}\left(\frac{1}{\zeta_{\lim}}\right) + \sigma_{\lim}\,,\ \gamma^*_{TC,\max} = \gamma_T + \sin^{-1}\left(\frac{1}{\zeta_{\lim}}\right) - \sigma_{\lim} \\
&\gamma^*_{HO,\min} = \pi + \gamma_T - \sin^{-1}\left(\frac{1}{\zeta_{\lim}}\right) - \sigma_{\lim}\,,\ \gamma^*_{HO,\max} = \pi + \gamma_T + \sin^{-1}\left(\frac{1}{\zeta_{\lim}}\right) + \sigma_{\lim}
\end{aligned} \tag{4.11}$$

Using $\gamma_{imp} = \gamma_T - \gamma_f$, the achievable impact angle is confined when associated with the FOV range as follows,

$$\mathcal{K}|_{\zeta_{\lim}>1} = \mathcal{K}_{TC} \cup \mathcal{K}_{HO} \tag{4.12}$$

where $\mathcal{K}_{TC}$ and $\mathcal{K}_{HO}$ satisfy

$$\begin{aligned}
\mathcal{K}_{TC} &= \left\{\gamma_{imp} | \gamma_{imp} \in \left[-\sin^{-1}\left(\frac{1}{\zeta_{\lim}}\right) + \sigma_{\lim}, \sin^{-1}\left(\frac{1}{\zeta_{\lim}}\right) - \sigma_{\lim}\right]\right\} \\
\mathcal{K}_{HO} &= \left\{\gamma_{imp} | \gamma_{imp} \in \left[-\pi - \sin^{-1}\left(\frac{1}{\zeta_{\lim}}\right) - \sigma_{\lim}, -\pi + \sin^{-1}\left(\frac{1}{\zeta_{\lim}}\right) + \sigma_{\lim}\right]\right\}
\end{aligned} \tag{4.13}$$

Note that the region of the achievable impact angle consists of two separated regions, which indicates that some collision geometries cannot be achieved due to the FOV reduction.

Capture Region Derivation

Let us derive a capture region of the composite guidance. Suppose that the desired flight path angle is selected, $\gamma_f \in \Gamma_n$, Considering symmetric configuration of the seeker, let us assume that the desired look angle is selected as $\sigma_d = -\sigma_{\lim}$ by Assumption 4.1. In order to achieve the desired collision course by PPN, the missile should start the engagement from the switching criteria obtained in Eq. (4.4). Therefore, a capture condition for IACCG can be addressed as follows.

Condition 4.1. The locus of switching criteria (r_s, λ_s) of Eq. (4.4) corresponds to a boundary of the capture region.

Depending on the initial position at the switching locus, the acceleration command at the initial instant may exceed its maximum capability. Note from Eq. (2.2) that the LOS rate is proportional to $1/r$, and therefore a minimum distance $\underline{r}_s$ at which the saturation occurs can be determined as the allowable switching distance. By substituting $\lambda = \lambda_s$ and $\sigma = \sigma_d$, the switching criteria with regard to the physical constraint can be obtained as follows.

Proposition 4.1. Considering the limited acceleration $-a_{\lim} \leq NV_M\dot{\lambda}_M \leq a_{\lim}$, the locus of the switching criteria is represented as

$$(r_s, \lambda_s) \in \Omega_s = \{(r, \lambda) | \lambda = \lambda_s, r \geq \underline{r}_s(\lambda_s)\} \tag{4.14}$$

where

$$\underline{r}_s(\lambda_s) = -\frac{NV_M}{a_{\lim}} \left(V_T \sin(\gamma_T - \lambda_s) + V_M \sin\sigma_d\right) \tag{4.15}$$

Proof. Consider a missile with an initial position (r_0, λ_0) in Ω_l, which is guided by PPN. Using $N > 2(1+\eta)$, the guidance command monotonically converges to zero during the engagement. The maximum magnitude of the command occurs at the initial position, i.e.,

$$a_{cmd}|_{\lambda=\lambda_s} \leq a_{cmd} < 0 \tag{4.16}$$

The guidance command of PPN can be rewritten using Eq. (2.2) as

$$a_{cmd} = NV_M\dot{\lambda} = \frac{NV_M}{r} \left\{V_T \sin(\gamma_T - \lambda) + V_M \sin\sigma\right\} \tag{4.17}$$

Substituting $\lambda = \lambda_s$, $\sigma = \sigma_d$, and Eq. (4.15) into Eq. (4.17) gives

$$a_{cmd}|_{\lambda=\lambda_s} = \frac{NV_M}{r} \left\{V_T \sin(\gamma_T - \lambda_s) + V_M \sin\sigma_d\right\} = -a_{\lim}\frac{\underline{r}_s(\lambda_s)}{r} \tag{4.18}$$

Because $r \geq \underline{r}_s(\lambda_s) > 0$, the command converges to zero and is bounded by $a_{\lim}$ as follows,

$$0 < |a_{cmd}| \leq a_{\lim} \tag{4.19}$$

By generating the converging acceleration, the missile enters a stable collision course that satisfies a terminal flight path angle $\gamma_M(t_f) \to \gamma_f$. Therefore, the guidance command is generated within its acceleration limit, and the engagement succeeds in intercepting the target with a terminal flight path angle γ_f. □

By Proposition 4.1, the acceleration saturation can be avoided by choosing r_s to be larger than the minimum distance $\underline{r}_s$. Meanwhile, DPP trajectory should reach the switching criteria Ω_s in phase 1 of Fig. 4.1 to accomplish the objective. For that, the following condition should be satisfied.

Condition 4.2. In phase 1, the initial position of the missile should be placed as

$$\lambda^*_{\underline{\sigma},TC} \leq \lambda_s \leq \lambda_0 \leq \lambda^*_{\underline{\sigma},HO} \tag{4.20}$$

Proof. The LOS angle at the switching instance λ_s can be expressed using Eq. (2.17), as follows,

$$\lambda_s = \lambda_f + \frac{1}{N-1}(\sigma_f + \sigma_{\lim}) \tag{4.21}$$

By substituting Eq. (4.21) into Eq. (4.8), $\lambda_s \in [\lambda^*_{\underline{\sigma},TC}, \lambda^*_{\underline{\sigma},HO}]$ because

$$\begin{aligned} \lambda^*_{\underline{\sigma},TC} \leq \lambda_s \leq \lambda^*_{\bar{\sigma},TC} + \frac{2}{N-1}\sigma_{\lim} \\ \lambda^*_{\bar{\sigma},HO} + \frac{2}{N-1}\sigma_{\lim} \leq \lambda_s \leq \lambda^*_{\underline{\sigma},HO} \end{aligned} \tag{4.22}$$

In the interval, $\dot{\lambda} < 0$ and $\lambda \to \lambda^*_{\underline{\sigma},TC}$. Therefore, switching occurs only if $\lambda_s \leq \lambda_0$. □

When the initial position satisfies Condition 4. 2, then DPP trajectory $r = \Phi(\lambda, \lambda_0; \sigma_d)\, r_0$ reaches the switching criteria. To check if the Condition 4.1 holds, propagating of the DPP trajectory from λ_0 to λ_s gives

$$r_s = \Phi(\lambda_s, \lambda_0; \sigma_d)\, r_0 \geq \underline{r}_s \tag{4.23}$$

Finally, the capture region of IACCG can be obtained as follows.

Theorem 4.1. Consider a planar engagement between a target and a missile guided by IACCG with $N > 2(1+\eta)$. The missile is equipped with an RN-FOV strapdown seeker satisfying $\zeta_{\lim} > 1$. Then, the capture region can be expressed as

$$\mathcal{C}_{IACCG} = \left\{ (r_0, \lambda_0, \sigma_0, \gamma_f) | r_0 \geq R_0,\, \lambda_s \leq \lambda_0 \leq \underline{\lambda}_0,\, \sigma_0 = \underline{\sigma},\, \gamma_f \in \Gamma|_{\zeta_{\lim}>1} \right\} \tag{4.24}$$

where $(r_0, \underline{\lambda}_0)$ satisfies

$$\underline{r}_s(\lambda_s) = \Phi(\lambda_s, \underline{\lambda}_0) r_0 \tag{4.25}$$

Proof. For any $(r_0, \lambda_0) \in \mathcal{C}_{IACCG,\gamma_f}$, the initial LOS angle satisfies

$$\lambda_s < \lambda_0 \leq \underline{\lambda_0} < \lambda^*_{\underline{\sigma},HO} \tag{4.26}$$

Since $\dot{\lambda} < 0$ and $\dot{r} < 0$ when $\lambda_0 \leq \underline{\lambda_0} < \lambda^*_{\underline{\sigma},HO}$, transition function shows

$$\Phi(\lambda_1, \lambda_0; \underline{\sigma}) < 1 \tag{4.27}$$

for $\lambda_1 < \lambda_0 < \lambda^*_{\underline{\sigma},HO}$. Then, trajectory by DPP becomes

$$\underline{r}_1 = \Phi(\lambda_0, \underline{\lambda}_0; \underline{\sigma}) r_0 \leq r_0 \tag{4.28}$$

Multiplying $\Phi(\lambda_s, \lambda_0; \underline{\sigma})$ into (4.28) yields

$$r_s = \Phi(\lambda_s, \lambda_0) r_0 \geq \Phi(\lambda_s, \lambda_0) \underline{r}_1 = \Phi(\lambda_s, \lambda_0) \Phi(\lambda_0, \underline{\lambda}_0; \underline{\sigma}) r_0 = \Phi(\lambda_s, \underline{\lambda}_0; \underline{\sigma}) r_0 \tag{4.29}$$

Since $(r_0, \underline{\lambda}_0)$ lies on the marginal boundary, the right-hand side (RHS) of Eq. (4.29) is equivalent to

$$RHS = \Phi(\lambda_s, \underline{\lambda}_0; \underline{\sigma}) r_0 = \underline{r}_s \tag{4.30}$$

By Proposition 4.1, the guidance command switches to PPN within its limit and renders the missile to desired collision course. □

Figure 4.2 shows the design procedure for $\mathcal{C}_{IACCG}$.

4.2 Capture Region of Modified Impact Angle Control Composite Guidance Law (MIACCG)

4.2.1 Proposed Guidance Law

In the IACCG, the look angle command is predetermined as $\sigma_c = -\sigma_{\max}$ by Assumption 4.1. If a missile does not start from the initial position in the stage 1, the missile cannot reach the switching condition and fails to intercept the target with desired impact angle. To achieve the performance of the guidance scheme using the composite framework, look-angle command should be properly corrected. Suppose that the desired look angle is a design parameter within the FOV limit such that $-\sigma_{\lim} < \sigma_c < \sigma_{lim}$. Two equilibrium points (λ_1^*, λ_2^*) and λ_s are function of σ_c.

$$\lambda_1^*(\sigma_c) = \gamma_T + \sin^{-1}\left(\frac{V_m}{V_T}\sin\sigma_c\right) \tag{4.31}$$

$$\lambda_2^*(\sigma_c) = \gamma_T + \pi - \sin^{-1}\left(\frac{V_m}{V_T}\sin\sigma_c\right) \tag{4.32}$$

$$\lambda_s(\sigma_c) = \left(\frac{N}{N-1}\right)\left(\tan^{-1}\left(\frac{\sin\gamma_f - \eta\sin\gamma_T}{\cos\gamma_f - \eta\cos\gamma_T}\right) - \frac{\gamma_f}{N}\right) - \frac{\sigma_c}{N-1} \tag{4.33}$$

Note that λ_1^* in Eq. (4.31) is a stable equilibrium point located in the tail-chase engagement, and λ_2^* in Eq. (4.32) is an unstable equilibrium point in the head-on engagement. Based on the characteristics of DPP, let us modify look angle command.

Tail-chase Engagement

In this case, the trajectory in the stage 1 has stable phase characteristics such that LOS angle converges to the equilibrium point λ_1^*. To finish the engagement with PPN (stage 2), the LOS angle at the switching time should be

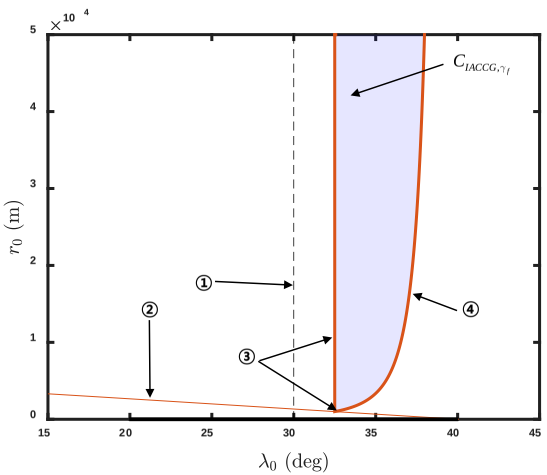

Step 1

Step 1.1 - $\gamma_f \in \Gamma_f\big|_{\zeta_{\lim}>1}$

① **Desired collision course :** by Eq. (3.24)

$$\lambda_s = \tan^{-1}\left(\frac{\sin\gamma_f - \eta\sin\gamma_T}{\cos\gamma_f - \eta\cos\gamma_T}\right) \qquad \text{Eq. (4.2)}$$

② **Limited acceleration layer at switching instant :** $\left(-a_{\lim} = NV_m\dot{\lambda}\right)$

$$r = -\frac{NV_m}{a_{\lim}}\left(V_T\sin\left(\gamma_T - \lambda\right) + V_m\sin\underline{\sigma}\right) \qquad \text{Eq. (4.17)}$$

③ **Switching criteria :** $\left(r_s,\lambda_s\right) \in \Omega_s = \left\{\left(r,\lambda\right) : \lambda = \lambda_s, r \geq \underline{r}_s\left(\lambda_s\right)\right\}$

$$\lambda_s = \left(\frac{N}{N-1}\right)\left(\lambda_f - \frac{\gamma_f + \underline{\sigma}}{N}\right) \qquad \text{Eq. (4.4)}$$

$$\underline{r}_s\left(\lambda_s\right) = -\frac{NV_m}{a_{\lim}}\left(V_T\sin\left(\gamma_T - \lambda_s\right) + V_m\sin\underline{\sigma}\right) \qquad \text{Eq. (4.15)}$$

④ **Marginal trajectory of IACCG : Backward integration from (4.15)**

$$r = \Phi\left(\lambda, \lambda_s; \underline{\sigma}\right)\underline{r}_s$$

Step 2

Capture region of IACCG

$$\mathcal{C}_{IACCG} = \left\{\left(r_0,\lambda_0,\sigma_0,\gamma_f\right) \mid r_0 \geq R_0, \lambda_s \leq \lambda_0 \leq \underline{\lambda}_0, \sigma_0 = \underline{\sigma}, \gamma_f \in \Gamma\big|_{\zeta_{\lim}>1}\right\}$$

Figure 4.2: Procedure of $\mathcal{C}_{IACCG}$

between λ_1^* and λ_0. The switching condition in the tail-chase engagement can be represented as

$$\lambda_0 \in \Omega_0^{TC}(\sigma_c) = \{\lambda_0 : \lambda_0 \leq \lambda_s \leq \lambda_1^* \quad \text{or} \quad \lambda_1^* \leq \lambda_s \leq \lambda_0\} \tag{4.34}$$

If the above condition does not hold, then the desired look angle σ_c should be corrected. Suppose that $\lambda_0 \leq \lambda_1^* < \lambda_s$. Then, the condition of Eq. (4.34) is satisfied if the look angle is corrected such that $\lambda_1^* - \lambda_s \geq 0$ as

$$\lambda_1^* - \lambda_s = \left(\frac{N}{N-1}\lambda_f - \frac{\gamma_f}{N}\right) - \gamma_T - \left(\frac{\sigma_c}{N-1} + \sin^{-1}\left(\frac{V_m}{V_T}\sin\sigma_c\right)\right) \tag{4.35}$$

From Eq. (4.35), $\frac{\partial}{\partial\sigma_c}(\lambda_1^* - \lambda_s) < 0$, and therefore σ_c is corrected to be decreased until the condition satisfies. The proposed algorithm of the look-angle modification logic in tail-chase engagement is summarized in Algorithm 1.

Head-on Engagement

In the head-on engagement, the characteristics of the trajectory in the stage 1 is unstable, and LOS angle gets away from the equilibrium point λ_2^*. To successfully finish the interception while achieving impact angle γ_f, guidance phase should be switched to the phase 2. The switching condition in the head-on engagement can be represented as

$$\lambda_0 \in \Omega_0^{HO}(\sigma_c) = \{\lambda_0 : \lambda_2^* \leq \lambda_0 \leq \lambda_s \quad \text{or} \quad \lambda_s \leq \lambda_0 \leq \lambda_2^*\} \tag{4.36}$$

Suppose that $\lambda_s \leq \lambda_2^* \leq \lambda_0$. Then, the LOS should increase to make λ_2^* greater than λ_0. Taking partial derivative of λ_2^* and λ_s with respect to σ_c yields

$$\frac{\partial\lambda_2^*}{\partial\sigma_c} < \frac{\partial\lambda_s}{\partial\sigma_c} < 0 \tag{4.37}$$

Algorithm 1 Modification of Look-Angle Command (Tail-chase Engagement)

procedure LOOK-ANGLE COMMAND CORRECTION

  Initialize :$\sigma_{c,old} = \sigma_0$

  while (1) **do**

    $\lambda_1^* = \gamma_f + \sin^{-1}(\frac{V_m}{V_T}\sin\sigma_{c,old})$

    $\lambda_{s,\sigma_{c,old}} = \left(\frac{N}{N-1}\right)\left(\lambda_f - \frac{\gamma_f+\sigma_{c,old}}{N}\right)$

    if $(\lambda_{s,\sigma_{c,old}} - \lambda_0)(\lambda_{s,\sigma_{c,old}} - \lambda_1^*) \geq 0$ **then**

      $\sigma_{c,old} = \sigma_{c,old} - ksign(\lambda_f - \lambda_s)$

    end if

    $\lambda_f =$ obtained from Eq. (4.2)

    $\lambda_s = \lambda_{s,\sigma_{c,old}}$

    Return (σ_c, λ_s)

  end while

end procedure

Therefore, σ_c is corrected to be decreased to satisfy the condition of Eq. 4.36. The look-angle modification logic in the head-on engagement is summarized in Algorithm 2.

Algorithm 2 Modification of Look-Angle Command (Head-on Engagement)

procedure LOOK-ANGLE COMMAND CORRECTION
    Initialize :$\sigma_{c,old} = \sigma_0$
    while (1) **do**
        $\lambda_2^* = \gamma_T + \pi - \sin^{-1}(\frac{V_m}{V_T}\sin\sigma_{c,old})$
        $\lambda_{s,\sigma_{c,old}} = \left(\frac{N}{N-1}\right)\left(\lambda_f - \frac{\gamma_f+\sigma_{c,old}}{N}\right)$
        if $(\lambda_{s,\sigma_{c,old}} - \lambda_0)(\lambda_{s,\sigma_{c,old}} - \lambda_2^*) \leq 0$ **then**
            $\sigma_{c,old} = \sigma_{c,old} - ksign(\lambda_0 - \lambda_2^*)$
        end if
        $\lambda_f =$ obtained from Eq. (4.2)
        $\lambda_s = \lambda_{s,\sigma_{c,old}}$
        Return (σ_c, λ_s)
    end while
end procedure

4.2.2 Capture Region Derivation of Proposed Guidance Law

In this section, capture region of the proposed method is derived. The additional assumption is introduced as

Assumption 4.2. The initial look angle converges to σ_c enough to neglect the transient performance.

Upon Assumption 4.2, capture region of the guidance law is investigated at $\sigma = \sigma_c$. Since the proposed method shares the same guidance structure as IACCG, the boundaries of the capture region has the similar form as that of IACCG. Only the difference is that the boundaries are function of σ_c in the proposed guidance law. By substituting $\sigma_d = \sigma_c$ into $\underline{r}_s(\sigma_c)$ of Eq. (4.15), switching locus $(r_s(\sigma_c), \lambda_s(\sigma_c))$ for a specified $\gamma_f \in \Gamma_n$ can be determined from Eq. (4.33). Likewise, another boundary associated with σ_c can be obtained by integrating backward from the switching locus at the minimum distance $\underline{r}_s(\sigma_c)$, that is

$$r = \Phi\left(\lambda_0, \lambda_s; \sigma_c\right) \underline{r}_s \tag{4.38}$$

Considering the two boundaries, the capture region $\mathcal{C}_{\gamma_f,\sigma_c}$ can be obtained as

$$\mathcal{C}_{\gamma_f,\sigma_c} = \left\{(r_0, \lambda_0) | \underline{r}_s(\lambda_s) \leq \Phi(\lambda_s, \lambda_0) r_0,\ \lambda_0 \in \Omega_0^{TC}(\sigma_c) \cup \Omega_0^{HO}(\sigma_c)\right\} \tag{4.39}$$

Considering allowable range, $\sigma_c \in [\underline{\sigma}, \bar{\sigma}]$, the capture region for achieving a specified impact angle, $\mathcal{C}_{\gamma_f}$, can be expressed as

$$\mathcal{C}_{MIACCG,\gamma_f} = \bigcup_{\sigma_c \in [\underline{\sigma}, \bar{\sigma}]} \mathcal{C}_{\gamma_f,\sigma_c} \tag{4.40}$$

Finally, the capture region of the proposed guidance law can be obtained as

$$\begin{aligned} \mathcal{C}_{MIACCG} = \Big\{ & (r_0, \lambda_0, \sigma_c, \gamma_f) | \gamma_f \in \Gamma|_{\zeta_{\lim}>1}, \underline{r}_s(\lambda_s) \leq \Phi(\lambda_s, \lambda_0) r_0, \\ & \lambda_0 \in \Omega_0^{TC}(\sigma_c) \cup \Omega_0^{HO}(\sigma_c), \sigma_c \in [\underline{\sigma}, \bar{\sigma}] \Big\} \end{aligned} \tag{4.41}$$

Figure 4.3 shows the capture region of the proposed guidance law. Compared to IACCG, capture region is expended both in the tail-chase and head-on engagement geometries. The properties of the capture region will be analyzed in Section 5.2.2.

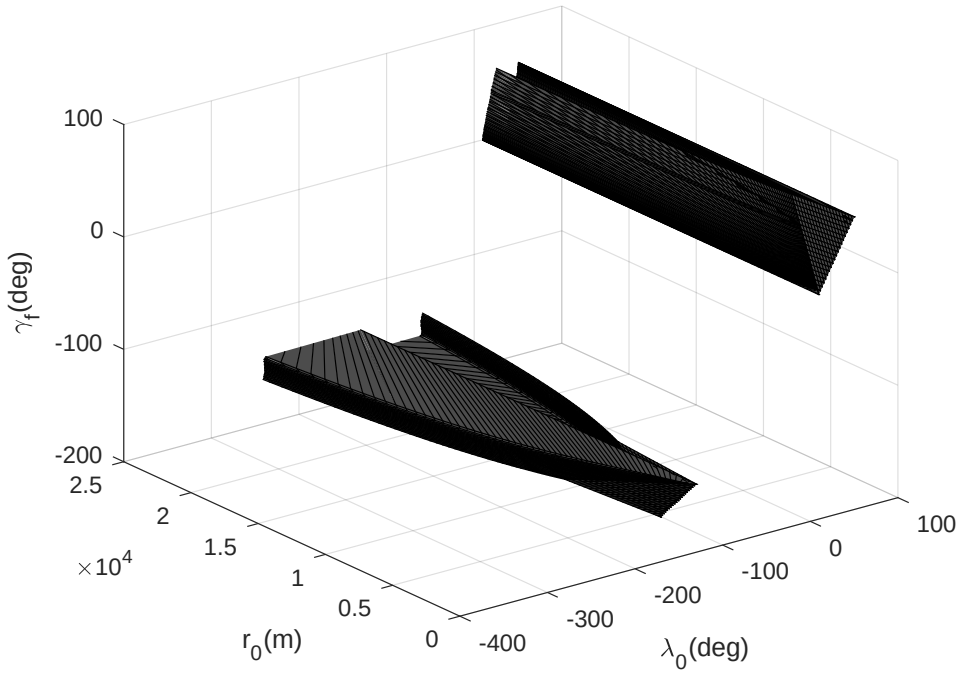

Figure 4.3: Capture Region of MIACCG

Chapter 5

Capture Region Analysis

This chapter is devoted to the analysis of the capture regions. In Section 5.1, the characteristics of the guidance law for target interception are investigated. RN-FOV arises the capture regions divided into head-on and tail-chases regions. In this regard, the qualitative behaviors of PPN is discussed by the corresponding capture region in Section 5.1.1. By the comparative study, the effect of the look angle control in LCG is discussed in Section 5.1.2. Then, the guaranteed capture zone of the guidance laws for handover point under the RN-FOV situation is suggested in Section 5.1.3.

In Section 5.2, the characteristics of FOV-IACG are investigated. Properties of the capture region of IACCG are analyzed in Section 5.2.1 by the several sub-regions: capture region for achieving speficifed impact angle, achievable impact angles according to initial configurations (λ_0, and r_0). The comparative study with guidance laws for target interception is also performed to evaluate the guidance laws. Then, the capture region of the proposed method, modified IACCG, is discussed by comparing with the existing method in Section 5.2.2.

5.1 Characteristics of Capture Regions for Target Interception

In this section, the properties of guidance laws for target interception are described. In Sec. 3.1 and 3.2, the capture regions of PPN and LCG are obtained for the situation in which the seeker's FOV limit is relatively narrow. Based on the capture regions, the effect of the guidance parameters on the performance of the guidance laws are investigated. In Sec. 5.1.1, characteristics of PPN is investigated based on the capture region. Capture region of PPN is analyzed depending on head-on and tail-chase engagement geometries, and the effect of the reduced FOV limit on the capture region are discussed. In Sec. 5.1.2, the characteristics of LCG is discussed by comparison with PPN. For application of air-to-air engagement, the necessary and sufficient condition of each capture region is discussed in Sec. 5.1.3. For the necessary condition, the *partially capturable region* is obtained. The sufficient condition expressed in the *capturable region* to successfully intercept the target without violating the look angle constraint is also presented using PPN and LCG.

5.1.1 Characteristics of PPN

In this section, characteristics of PPN is analyzed based on its capture region. The capture region is expressed in terms of λ_0, r_0, and σ_0, but it would be better to understand the properties of the PPN by investigating the region in two-dimensional space. $C_{\sigma_0,PPN}$.

Comparison of Capture Region in HO and TC Engagements

This section analyzes qualitative behavior of PPN depending on engagement geometries based on the capture region. Figure 5.1 shows the capture region of PPN. Compared to HO engagement case, the capture region in TC engagement is made much wider.

In the HO engagement, the initial range of $\mathcal{C}_{\sigma_0,PPN,HO}$ should satisfy the following condition.

$$[\bar{\lambda}_{PPN,HO}(\sigma_0), \underline{\lambda}_{PPN,HO}(\sigma_0)] \subset \mathcal{L}_{adm,HO} \tag{5.1}$$

Equation (5.1) implies that the $\mathcal{L}_{adm,HO}$ is the necessary condition to achieve the interception by PPN under RN-FOV limit. To intercept the target while maintaining the lock-on condition, at least the initial LOS angle should be in $\mathcal{L}_{adm,HO}$. Otherwise, the missile will fail to lock on the target through the seeker at the final time. Equation (5.1) also represents the qualitative behavior of PPN in the HO engagement. The missile tends to enter a collision course by forming the terminal LOS away from the direction of the target. The region can be made much narrower as the FOV is reduced. Figure 5.1(a) illustrates the behavior of PPN. If the initial position of the missile is placed in the capture region, then the collision course λ_f is formed in $\mathcal{L}_{adm,HO}$. The trajectory monotonically converges to the desired collision course.

On the other hand, in the TC engagement case, the initial range of $\mathcal{C}_{\sigma_0,PPN,HO}$ should satisfy the following condition.

$$\mathcal{L}_{adm,TC} \subset [\underline{\lambda}_{PPN,TC}(\sigma_0), \bar{\lambda}_{PPN,TC}(\sigma_0)] \tag{5.2}$$

Equation (5.2) implicates that $\mathcal{L}_{adm,TC}$ is invariant, i.e., $\lambda_0 \in \mathcal{L}_{adm,TC} \Rightarrow \lambda_f \in \mathcal{L}_{adm,TC}$. This implies that the missile can always intercept the target only if it

enters $\mathcal{L}_{adm,TC}$. Therefore, $\mathcal{L}_{adm,TC}$ is the sufficient condition for interception by PPN in the TC engagement under RN-FOV limit. For interpretation of qualitative behavior, suppose that the initial position of the missile is located at $\lambda_0 \in (\lambda^*_{\bar{\sigma},TC}, \gamma_T + \frac{\pi}{2}]$. PPN drives collision geometry formed in a direction inside the admissible range as the missile approaches the target. In this respect, the capture region of TC case is relatively wider than that of the HO case.

Effect of FOV on Capture Region

This section demonstrates how the degree of FOV limit affects the capture region. Suppose that initial look angle is within the FOV limit, the corresponding capture region $\mathcal{C}_{\sigma_0,PPN}$ can be shown in Fig. 5.1(a). As the FOV limit is reduced, the transition of λ is much restricted, and the capture region is very narrow. Figure 5.2 shows the relationship between the FOV limit and $\mathcal{C}_{\sigma_0,PPN}$. For the RN-FOV case, $\sigma_{\lim} < \sin^{-1}\eta$, the capture regions in both engagement cases becomes narrow as FOV limit is reduced. It is also observed that $\mathcal{C}_{\sigma_0,PPN,TC}$ is much wider and changes more, and two capture regions are connected and cover the entire range of λ space, i.e., $\lambda_0 \in \Lambda_f$. Therefore, the missile always intercepts a target while maintaining the lock-on condition for every initial position. It can also interpret the result in Ref. [44], where a missile guided by PPN can intercept a target for almost every initial position when the FOV limit is not considered.

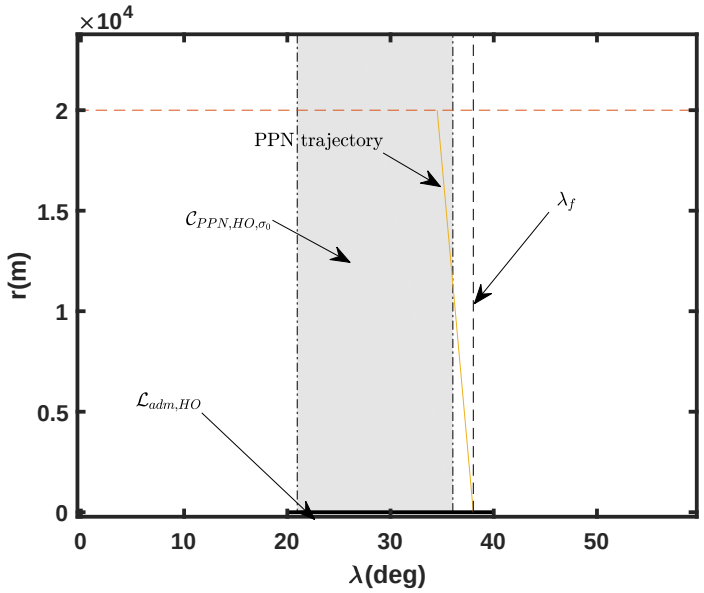

(a) $\mathcal{C}_{PPN,HO,\sigma_0}$ (Head-on Case)

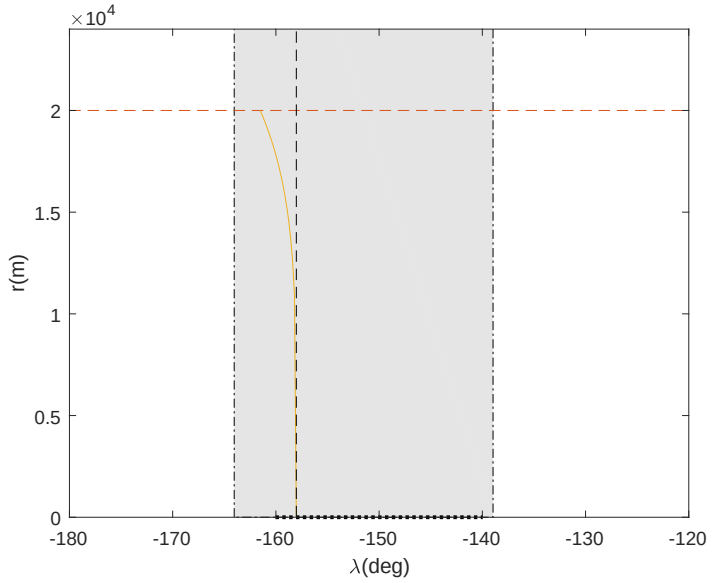

(b) $\mathcal{C}_{PPN,TC\sigma_0}$ (Tail-chase Case, $\sigma_0 = 1$ deg)

Figure 5.1: Capture Region of PPN $\mathcal{C}_{PPN,\sigma_0}$, ($\sigma_0 = 1$ deg)

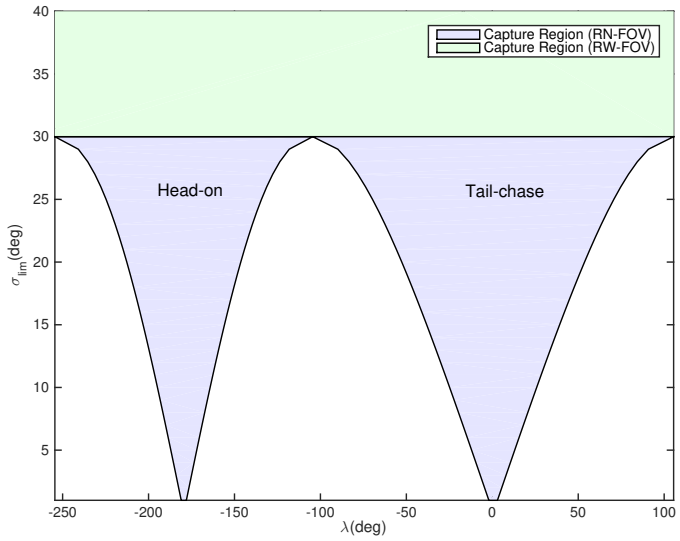

Figure 5.2: Effect of FOV Limit on Capture Region of PPN (Blue-Shaded Area: RN-FOV Limit, Green-Shaded Area: RW-FOV Limit)

5.1.2 Characteristics of LCG

Comparison with PPN

This section is devoted to investigate how look-angle control logic in LCG improves the performance of interception in perspective of capture region. Figure 5.3 shows the capture regions of PPN and LCG, and Fig. 5.4 shows the relationship with initial look angle and the capture region. Unlike PPN, the capture region of LCG has dependency on r_0, but the patterns of which are different according to HO/TC engagements. In the HO engagement, $|\bar{\lambda}_{LCG,HO}(r_0) - \underline{\lambda}_{LCG,HO}(r_0)|$ becomes narrower as r_0 increases. In the perspective of inclusive relation, we have

$$[\bar{\lambda}_{PPN,HO}(\sigma_0), \underline{\lambda}_{PPN,HO}(\sigma_0)] \subset [\bar{\lambda}_{LCG,HO}(r_0, \sigma_0), \underline{\lambda}^{c}_{LCG,HO}(r_0, \sigma_0)] \tag{5.3}$$

Equation (5.3) holds regardless of the initial distance r_0. Note that there is less significant difference between the capture region of LCG and that of PPN as shown in Fig. 5.4(a). If a small miss-intercept distance is allowable for hit-to-kill performance, then the capture region of LCG will be almost identical to those of PPN. Because the endgame using the pursuit is not favorable in this engagement, the capture region is slightly extended by the deviated pursuit composing the boundaries with respect to an allowable miss distance.

Compared to the head-on engagement case, the capture region of LCG is substantially extended in the tail-chase engagement case. Because the boundary composed of the deviated pursuit has an attractive phase portrait in the geometry, the guidance command of LCG can intercept the target even after switching the guidance command. As a result, the guaranteed initial LOS angles of LCG are further extended than those of PPN as shown in Fig. 5.4(b).

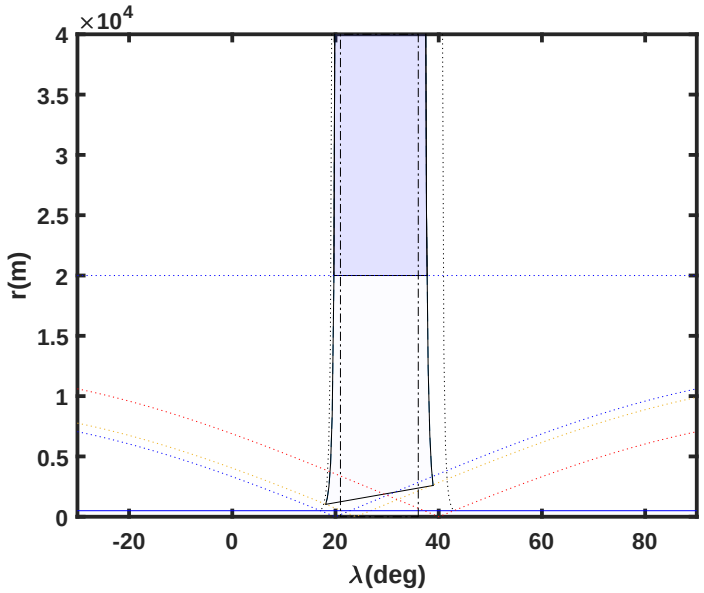

(a) $\mathcal{C}_{LCG,HO,\sigma_0}$ (Head-on Case, $\sigma_0 = 1$ deg)

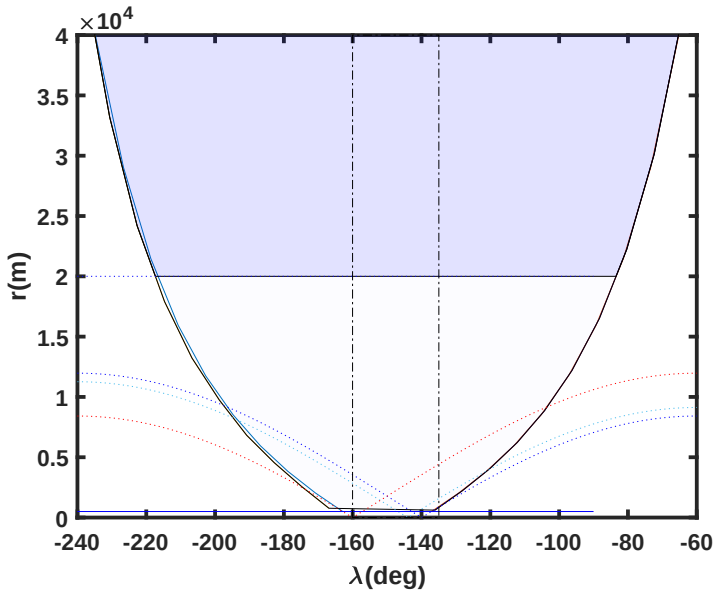

(b) $\mathcal{C}_{LCG,TC,\sigma_0}$ (Tail-chase Case, $\sigma_0 = 1$ deg)

Figure 5.3: Capture Region of LCG $\mathcal{C}_{LCG,\sigma_0}$, ($\sigma_0 = 1$ deg, $\gamma_T = -180$ deg)

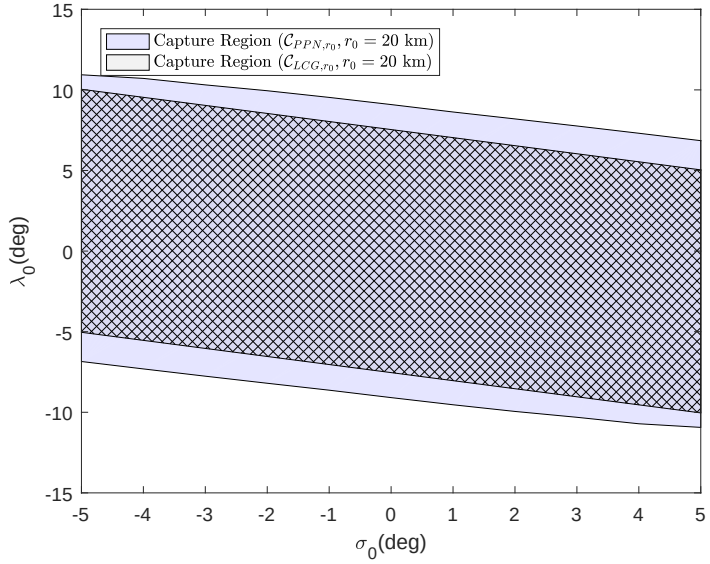

(a) Head-on

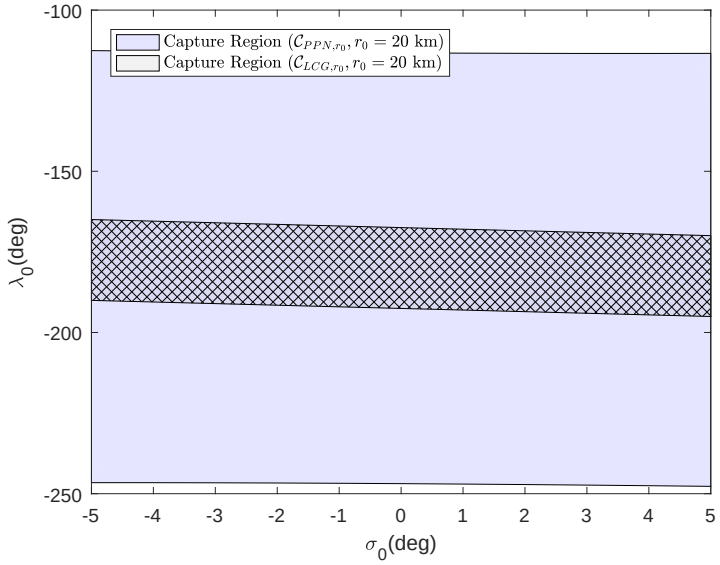

(b) Tail-chase

Figure 5.4: Relationship with σ_0 and $\mathcal{C}_{LCG,r_0}$ ($\sigma_0 = 1$ deg, $\gamma_T = -180$ deg)

5.1.3 Necessary and Sufficient Position for Target Interception

In this section, the guaranteed initial positions for target interception in the perspective of FOV limit is discussed. Considering the hand-over sequence between the midcourse and terminal phases, the midcourse guidance drives the missile to a suitable hand-over position at which the look angle may not be specified. To increase the intercept probability, the necessary and sufficient condition for guaranteed capture zone is required.

Figure 5.5 shows the *capturable* and *partially capturable regions* of PPN in LOS coordinate. The *capturable region* and the *partially capturable region* are significantly reduced for the case in which the allowable look angle is limited. LOS ranges of *capturable region* and *partially capturable region* has the following inclusive relations.

$$[\bar{\lambda}^{c}_{PPN,HO}, \underline{\lambda}^{c}_{PPN,HO}] \subset \mathcal{L}_{adm,HO} = [\bar{\lambda}^{pc}_{PPN,HO}, \underline{\lambda}^{pc}_{PPN,HO}] \tag{5.4}$$

From Eq. (5.4), phase portrait of PPN in the HO engagement situation can be interpreted as follows. LOS range of the *partially capturable region* coincides with $\mathcal{L}_{adm,HO}$, which implies that at least the initial LOS angle should be in $\mathcal{L}_{adm,HO}$ to intercept the target while maintaining the lock-on condition. Otherwise, the missile will fail to lock on the target through the seeker at the final time. In addition, the initial LOS range of the *capturable region* is smaller than the admissible range, which implies that the missile tends to enter a collision course by forming the terminal LOS away from the direction of the target. The region can be made much narrower as the FOV is reduced.

The capturable region and *partially capturable region* of the PPN for the tail-chase engagement are also confined similar to the head-on chase. Note that

the *capturable region* of the tail-chase engagement is larger than that of the head-on engagement case. LOS ranges of *capturable region* and the *partially capturable region* have

$$[\underline{\lambda}^{c}_{PPN,TC}, \bar{\lambda}^{c}_{PPN,TC}] = \mathcal{L}_{adm,TC} \subset [\underline{\lambda}^{pc}_{PPN,TC}, \bar{\lambda}^{pc}_{PPN,TC}] \tag{5.5}$$

From Eq. (5.5), phase portrait of PPN shows stable characteristics. In the *capturable region*, $\mathcal{L}_{adm,TC}$ is invariant, i.e., $\lambda_0 \in \mathcal{L}_{adm,TC} \Rightarrow \lambda_f \in \mathcal{L}_{adm,TC}$. This implies that the missile can always intercept the target only if it enters $\mathcal{L}_{adm,TC}$ with the lock-on condition at the end of the mid-course phase. In addition, the trajectory initiated from a position in the *partially capturable region* tends to enter the range of admissible LOS angles, i.e., $\mathcal{L}_{adm,TC} \subset [\underline{\lambda}^{pc}_{PPN,TC}, \bar{\lambda}^{pc}_{PPN,TC}]$, because the LOS kinematics exhibits a stable phase portrait in the tail-chase engagement case.

Figures 5.6 and 5.7 shows the *capturable* and *partially capturable regions* of LCG in LOS coordinate and cartesian coordinate, respectively. Similar to PPN, necessary and sufficient position for interception can be obtained from LCG. Following statements address *capturable* and *partially capturable region* of LCG

Corollary 5.1. Under Assumptions 2.1-2.5, consider a planar engagement between a target and a missile guided by LCG with $N > 2(1+\eta)$. The missile is equipped with an RN-FOV strapdown seeker satisfying $\zeta_{\text{lim}} > 1$. Using LCG, $\mathcal{B}_{LCG,HO} = \{(r_0, \lambda_0) : r_0 \geq \underline{R}_0, \lambda_0 \in [\bar{\lambda}^{pc}_{HO}(r_0), \underline{\lambda}^{pc}_{HO}(r_0)]\}$ is the *partially capturable region* of LCG in the head-on engagement case, where $\bar{\lambda}^{pc}_{HO}(r_0)$ and $\underline{\lambda}^{pc}_{HO}(r_0)$ represent the boundaries of the *partially capturable region* of LCG as

$$\begin{aligned} r_0 &= \Phi\left(\bar{\lambda}^{pc}_{HO}(r_0), \bar{\lambda}^{pc}_{HO,f}; \bar{\sigma}\right) R_{\text{miss}} \\ r_0 &= \Phi\left(\underline{\lambda}^{pc}_{HO}(r_0), \underline{\lambda}^{pc}_{HO,f}; \underline{\sigma}\right) R_{\text{miss}} \end{aligned} \tag{5.6}$$

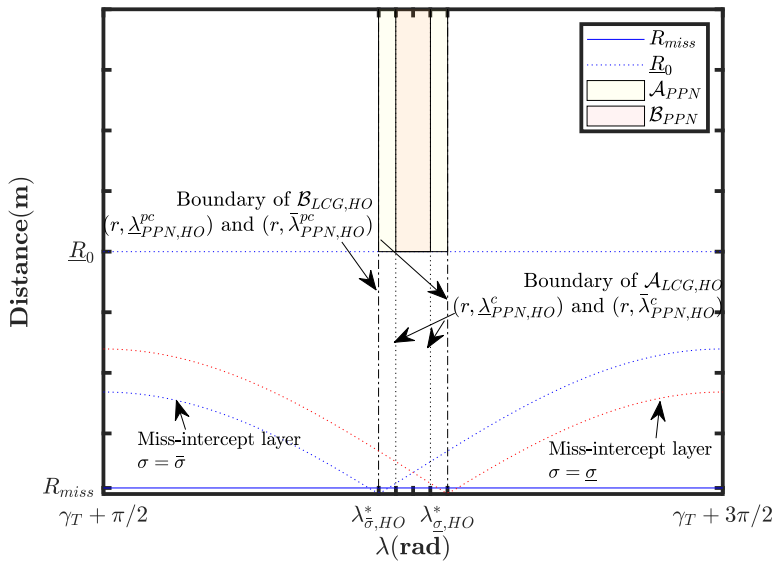

(a) Head-on

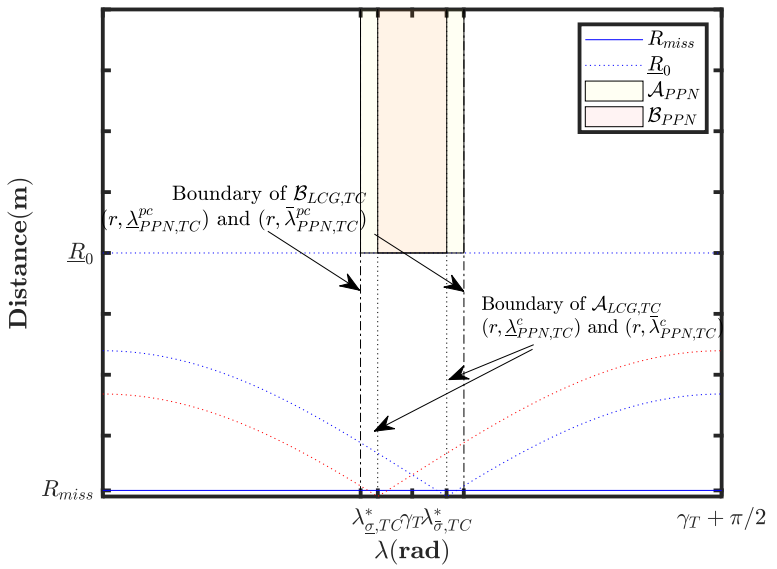

(b) Tail-chase

Figure 5.5: Capture Regions of PPN (Red-Shaded Area: *Capturable Region* of PPN, Yellow-Shaded Area: *Partially Capturable Region* of PPN)

where Φ is the transition function of the deviated pursuit, and the LOS angle at the interception time can be obtained as follows,

$$\begin{aligned}\bar{\lambda}^{pc}_{HO,f} &= \gamma_T - \pi - \sin^{-1}\left(\frac{R_{\text{miss}}a_{\max}}{V_m V_T} - \frac{V_m}{V_T}\sin\bar{\sigma}\right)\\ \underline{\lambda}^{pc}_{HO,f} &= \gamma_T - \pi - \sin^{-1}\left(\frac{-R_{\text{miss}}a_{\max}}{V_m V_T} - \frac{V_m}{V_T}\sin\underline{\sigma}\right)\end{aligned} \tag{5.7}$$

Moreover, $\mathcal{A}_{LCG,HO} = \{(r_0,\lambda_0) : r_0 \geq \underline{R}_0, \lambda_0 \in [\bar{\lambda}^c_{HO}(r_0), \underline{\lambda}^c_{HO}(r_0)]\}$ is the *capturable region* of LCG in the head-on engagement case. $\bar{\lambda}^c_{HO}(r_0)$ and $\underline{\lambda}^c_{HO}(r_0)$ can be obtained as

$$\begin{aligned} r_0 &= \Psi\left(\bar{\lambda}^c_{HO}(r_0), \bar{\lambda}^{pc}_{HO}(\bar{r}_1);\bar{\sigma}\right)\Phi\left(\bar{\lambda}^{pc}_{HO}(r_1), \bar{\lambda}^{pc}_{HO,f};\bar{\sigma}\right)R_{\text{miss}}\\ r_0 &= \Psi\left(\underline{\lambda}^c_{HO}(r_0), \underline{\lambda}^{pc}_{HO}(\underline{r}_1);\underline{\sigma}\right)\Phi\left(\underline{\lambda}^{pc}_{HO}(r_1), \underline{\lambda}^{pc}_{HO,f};\bar{\sigma}\right)R_{\text{miss}}\\ \bar{\lambda}^c_{HO}(r_0) &= \bar{\lambda}^{pc}_{HO}(\bar{r}_1) + \frac{1}{1-N}(\underline{\sigma}-\bar{\sigma})\\ \underline{\lambda}^c_{HO}(r_0) &= \underline{\lambda}^{pc}_{HO}(\underline{r}_1) + \frac{1}{1-N}(\bar{\sigma}-\underline{\sigma})\end{aligned} \tag{5.8}$$

where Ψ is the transition function of PPN obtained from Eq.(2.22). Note that $(\bar{r}_1, \bar{\lambda}^{pc}_{HO})$ and $(\underline{r}_1, \underline{\lambda}^{pc}_{HO})$ at the switching time lie on the boundary trajectories of the *partially capturable* region of LCG obtained from Eq.(5.6).

Proof. See Appendix C.1. □

Corollary 5.2. Under Assumptions 2.1-2.5, consider a planar engagement between a target and a missile that is guided by LCG with $N > 2(1+\eta)$. The missile is equipped with an RN-FOV strapdown seeker satisfying $\zeta_{\text{lim}} > 1$. Using LCG, $\mathcal{A}_{LCG,TC} = \{(r_0,\lambda_0) : r_0 \geq \underline{R}_0, \lambda_0 \in [\underline{\lambda}^c_{TC}(r_0), \bar{\lambda}^c_{TC}(r_0)]\}$ is the *capturable region* of LCG in the tail-chase engagement case, where $(r_0, \underline{\lambda}^c_{TC})$, and $(r_0, \bar{\lambda}^c_{TC})$ can be expressed as

$$\begin{aligned} r_0 &= \Phi(\underline{\lambda}^c_{TC}(r_0), \underline{\lambda}^c_{TC,f};\underline{\sigma})R_{\text{miss}}\\ r_0 &= \Phi(\bar{\lambda}^c_{TC}(r_0), \bar{\lambda}^c_{TC,f};\bar{\sigma})R_{\text{miss}}\end{aligned} \tag{5.9}$$

where the LOS angle at the final time can be obtained as follows,

$$\begin{aligned}\underline{\lambda}^{c}_{TC,f} &= \gamma_T + \sin^{-1}\left(\frac{-R_{\text{miss}}a_{\max}}{V_m V_T} - \frac{V_m}{V_T}\sin\underline{\sigma}\right)\\ \bar{\lambda}^{c}_{TC,f} &= \gamma_T + \sin^{-1}\left(\frac{R_{\text{miss}}a_{\max}}{V_m V_T} - \frac{V_m}{V_T}\sin\bar{\sigma}\right)\end{aligned} \tag{5.10}$$

Moreover, $\mathcal{B}_{LCG,HO} = \{(r_0, \lambda_0) : r_0 \geq \underline{R}_0, \lambda_0 \in [\underline{\lambda}^{pc}_{TC}(r_0), \bar{\lambda}^{pc}_{TC}(r_0)]\}$ is the *partially capturable region* of LCG in the tail-chase engagement case. $\underline{\lambda}^{pc}_{TC}$ and $\bar{\lambda}^{pc}_{TC}$ can be obtained as

$$\begin{aligned} r_0 &= \Psi\left(\underline{\lambda}^{pc}_{TC}(r_0), \underline{\lambda}^{c}_{TC}(\underline{r}_2); \underline{\sigma}\right)\Phi\left(\underline{\lambda}^{c}_{TC}(\underline{r}_2), \underline{\lambda}^{c}_{TC,f}; \underline{\sigma}\right) R_{\text{miss}}\\ r_0 &= \Psi\left(\bar{\lambda}^{pc}_{TC}(r_0), \bar{\lambda}^{c}_{TC}(\bar{r}_2); \bar{\sigma}\right)\Phi\left(\bar{\lambda}^{c}_{TC}(\bar{r}_2), \bar{\lambda}^{c}_{TC,f}; \underline{\sigma}\right) R_{\text{miss}}\\ \underline{\lambda}^{pc}_{TC}(r_0) &= \underline{\lambda}^{c}_{TC}(\underline{r}_2) + \frac{1}{1-N}(\bar{\sigma} - \underline{\sigma})\\ \bar{\lambda}^{pc}_{TC}(r_0) &= \bar{\lambda}^{c}_{TC}(\bar{r}_2) + \frac{1}{1-N}(\underline{\sigma} - \bar{\sigma})\end{aligned} \tag{5.11}$$

where Ψ is the transition function of PPN obtained from Eq.(2.22), and Φ is the transition function of the deviated pursuit. Note that $(\bar{r}_2, \bar{\lambda}^{pc}_{TC})$ and $(\underline{r}_2, \underline{\lambda}^{pc}_{TC})$ at the switching time lie on the boundary trajectories of the *partially capturable* region of LCG obtained from Eq.(5.9).

Proof. See Appendix C.2 □

Similar to PPN, the necessary condition for the capture by LCG is $\mathcal{B}_{LCG,HO}$. If the initial position of the missile is outside $\mathcal{B}_{LCG,HO}$, then the missile cannot execute the pursuit maneuver to maintain the FOV limit and finally misses the target. If the initial look angle is within the FOV limit when the initial position is in $\mathcal{A}_{LCG,HO}$, then the missile always succeeds in target interception, which means that $\mathcal{A}_{LCG,HO}$ is the sufficient condition for interception.

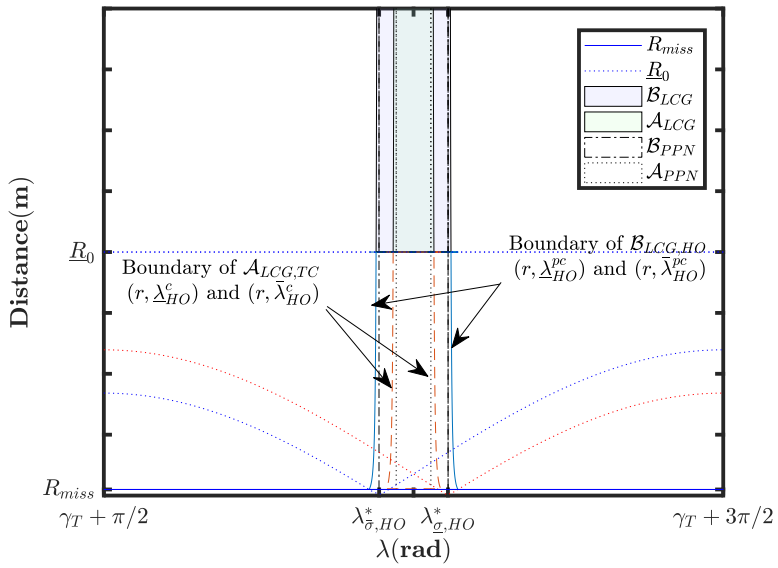

(a) Head-on (LOS coordinates)

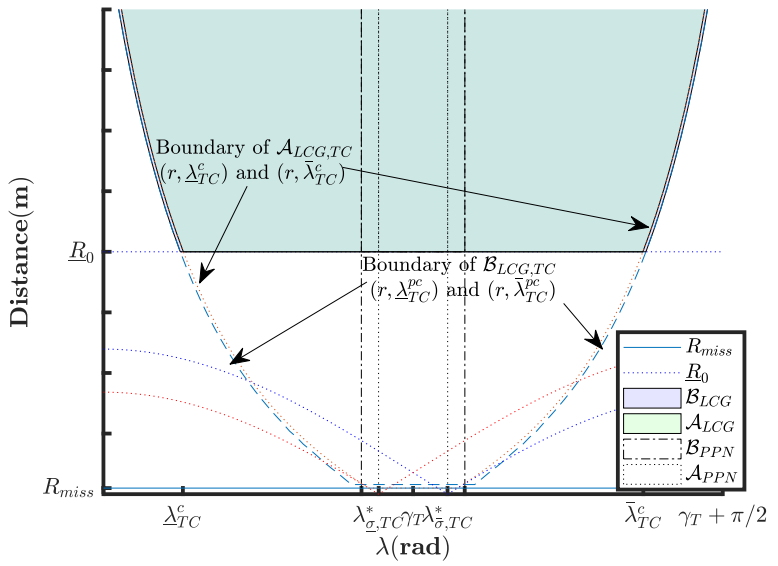

(b) Tail-chase (LOS coordinates)

Figure 5.6: Capture Region of LCG (Blue Area: *Partially Capturable Region*, Green Area: *Capturable Region*)

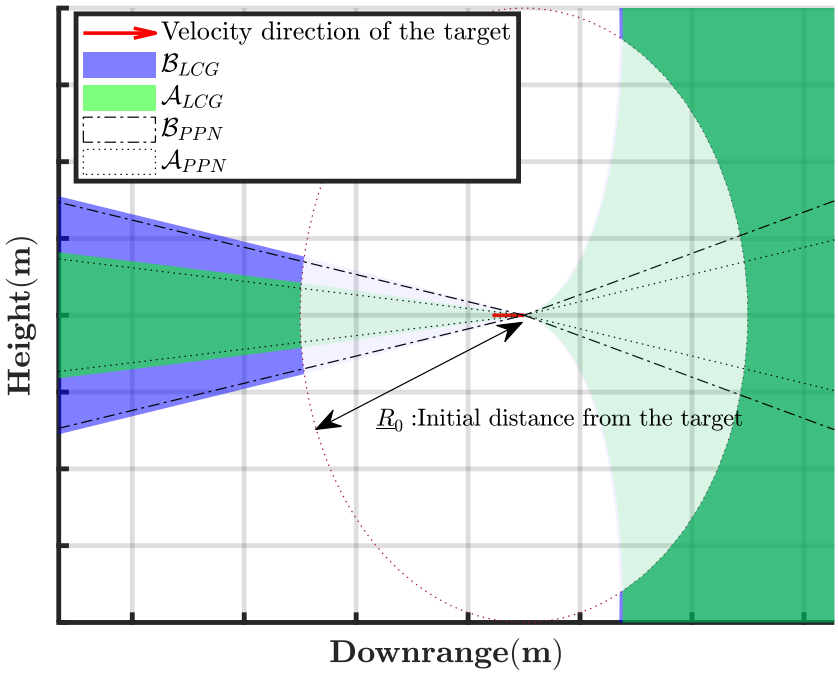

Figure 5.7: Capture Region of LCG in Cartesian Coordinate (Blue Area: *Partially Capturable Region*, Green Area: *Capturable Region*)

5.2 Characteristics of Capture Regions for FOV-IACG

In this section, the characteristics of the capture region are analyzed according to the FOV limit. The capture region $\mathcal{C}$ is expressed in $(r_0, \lambda_0) - \gamma_f$ space, and the characteristics of the capture region are explained by the subsets of the capture region.

5.2.1 Characteristics of IACCG

Capture Region for Achieving Specified Impact Angle

Figure 5.8 shows $\mathcal{C}_{\gamma_f}$ for the RN-FOV case. Compared to the wide FOV case, very narrow $\mathcal{C}_{\gamma_f}$ is constructed as shown in Figs. 5.8(a) and 5.8(b). In Fig. 5.8(a), the gray-shaded area corresponds to the candidate area for the capture region, which can be made by changing the impact angle in the achievable set $\mathcal{K}|_{\zeta_{\text{lim}}>1}$. Similar to PPN and LCG, the capture region is also made narrower in the head-on case than the tail-chase case. Figure 5.9 shows the effect of FOV limit on the capture region. As FOV decreases, $\mathcal{C}_f$ is made closer to desired collision course λ_f and become narrower. This reflects the performance of IACCG in that i) PPN executes much restricted transition for the collision condition, and ii) DPP with increased ζ_{lim} involves the sharp boundary of the IACCG. Figure 5.9(b) shows the variation of the capture region according to the FOV limit. As the FOV limit is strictly restricted, the capture region is made very small.

Achievable Impact Angle with Respect to λ_0

The initial LOS angle corresponding to the achievable impact angle can be determined for a given initial distance. If the initial distance is set to $r_0 = R$,

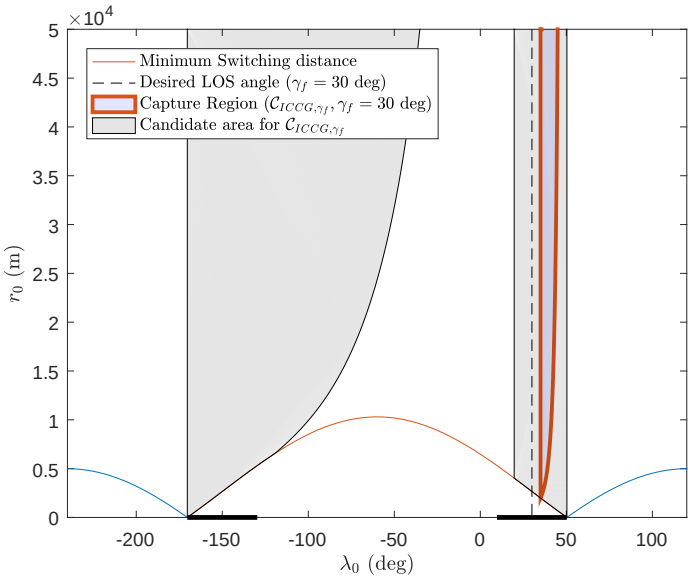

(a) $\mathcal{C}_{\gamma_f}$ (Narrow FOV Limit, $\gamma_f = 30$ deg)

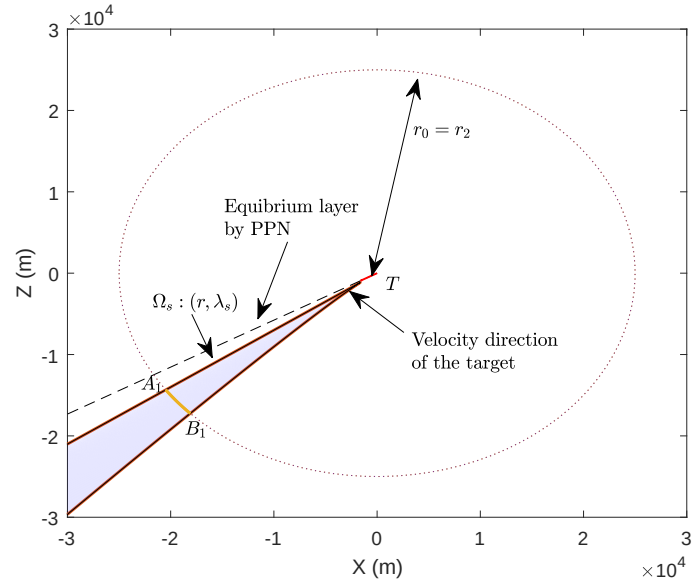

(b) $\mathcal{C}_{\gamma_f}$ (Narrow FOV Limit, $\gamma_f = 30$ deg, Cartesian Coordinate)

Figure 5.8: Capture Region of IACCG for Achieving the Specified Impact Angle with RN-FOV Limit, ($\gamma_T = -150$ deg, $\zeta_{\text{lim}} > 1$)

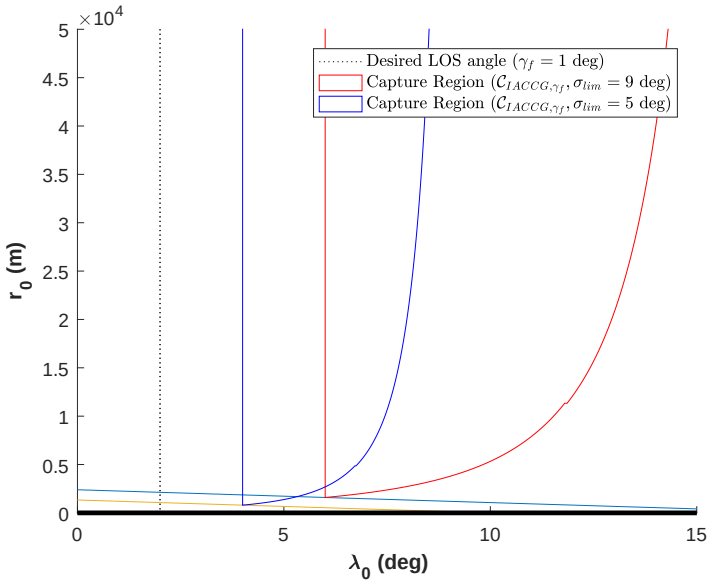

(a) $\mathcal{C}_{\gamma_f}$, with Different FOV Limits $\sigma_{\text{lim}} = 5$ and 9 deg)

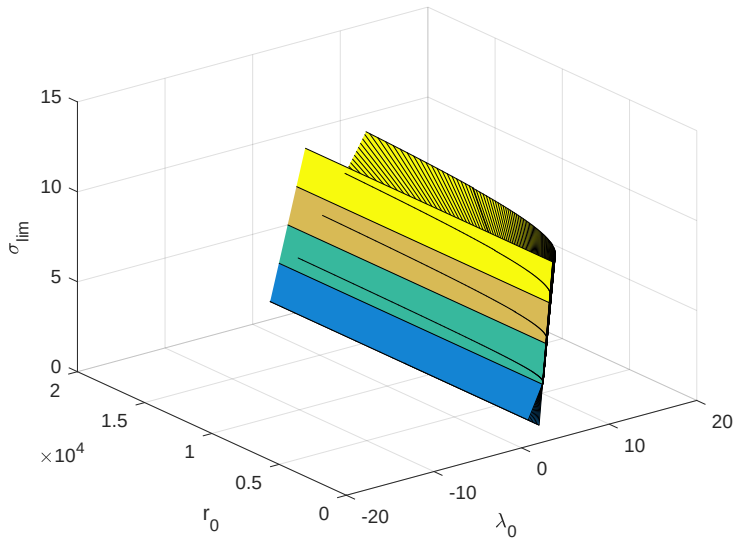

(b) $\mathcal{C}_2$, ($\lambda_0 = 0$ deg, $\zeta_{\text{lim}} > 1$; Narrow FOV Limit)

Figure 5.9: Effect of FOV Limit on $\mathcal{C}_{IACCG,\gamma_f}$

then the capture region $\mathcal{C}_1 \subset \mathcal{C}$ can be obtained as follows,

$$\mathcal{C}_1 = proj_{R_0}\mathcal{C} = \mathcal{C}|_{r_0=R} \tag{5.12}$$

where $R_0 \subset \mathcal{P}$ is the hyperplane that satisfies $r_0 = R$.

Figure 5.10 shows the relation between the LOS angle and the terminal flight path angle for the RN-FOV limit. Using $\mathcal{C}_1$, the range of the initial LOS angles for each terminal flight path angle can be obtained. For example, $\overline{P_1Q_1}$ corresponds to the range of the initial LOS angles for achieving $\gamma_f = 30$ deg. The range $\overline{P_1Q_1}$ is obtained by substituting $r_0 = 20,000$m and $\gamma_f = 30$ deg. Figure 5.10 shows $\mathcal{C}_1$, where the capture range is narrow because of the FOV reduction. Additionally, the capture region is separated into two disconnected regions that correspond to the different engagement geometries, because the set of achievable terminal flight path angles is divided by two sets. This means that there exist un-achievable impact angles due to the narrow FOV limit. Note that the achievable range of flight path angle is wide in the head-on engagement geometry. On the other hand, it is observed that the range $\overline{PQ}$ in the head-on engagement is relatively narrow compared to the tail-chase engagement due to the stable property of the DPP trajectory in the tail-chase engagement. The capture region $\mathcal{C}_1$ can be utilized for the guidance strategy in the mid-course phase. To achieve the terminal flight path angle γ_f, the missile should enter a proper initial position at the end of the midcourse phase. Using $\mathcal{C}_1$, a handover point between the midcourse phase and homing phase can be predetermined.

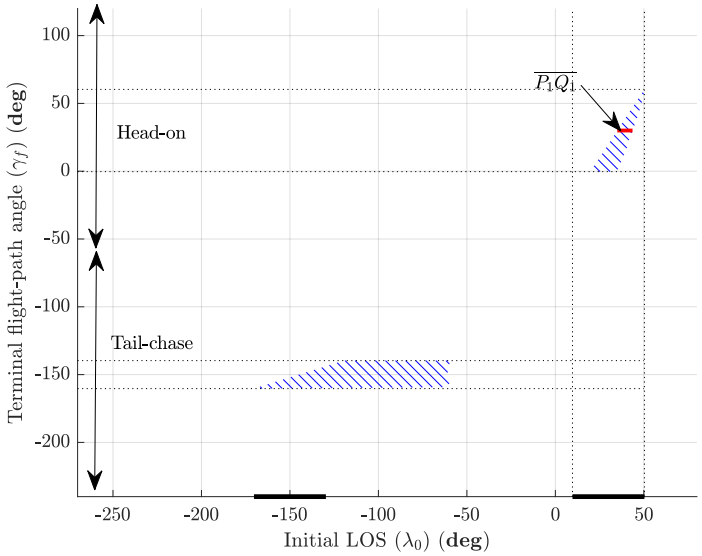

Figure 5.10: Achievable Terminal Flight-Path Angle with Respect to λ_0

Achievable Impact Angle with Respect to Distance

If the engagement begins in a particular configuration, for example, $\lambda_0 = c$, $c =$ constant, then the capture region $\mathcal{C}_2 \subset \mathcal{C}$ can be obtained as follows:

$$\mathcal{C}_2 = \mathcal{C}|_{\lambda_0 = c} \tag{5.13}$$

Using the capture region $\mathcal{C}_2$, the relation between the achievable impact angle and the initial distance can be analyzed. Figure 5.11 shows $\mathcal{C}_2$ for $\lambda_0 = \gamma_T + \pi$. The upper bound $\gamma_f(\lambda_s)$ is constructed from switching criteria of the capture region, which is constant regardless of the initial distance. The lower bound corresponds to the minimum distance for achieving $\gamma_f \in \Gamma_f$. Note also that the λ_s and $\underline{r}_s(\lambda_s)$ can be obtained from Eqs. (4.4) and (B.4), and the minimum distance for achieving $\gamma_f \in \Gamma_f$ can be obtained by integrating Eq. (2.2) backward from λ_s to λ_0 at $\underline{r}_s$ as follows,

$$\underline{r}_0|_{\gamma_f} = \Phi_1(\lambda_0, \lambda_s)\underline{r}_s(\lambda_s) \tag{5.14}$$

Due to the restricted terminal flight path angle, i.e., $\gamma_f \in \Gamma_{n,HO}$, $\underline{r}_0|_{\gamma_f}$ is only valid under $\gamma_f \in [\gamma^*_{HO,\min}, \gamma_f(\lambda_s)]$. Therefore, the bound at $\gamma_f = \gamma^*_{HO,\min}$ can be expressed as $r_0 \geq \underline{r}_0|_{\gamma_f = \gamma^*_{HO,\min}}$. If $r_0 > \underline{r}_0|_{\gamma_f = \gamma^*_{HO,\min}}$, then the achievable range of the terminal flight path angle is bounded by $[\gamma^*_{HO,min}, \underline{\gamma}_{f,PPN}]$, and the missile cannot accomplish the impact angle interception under $\gamma_f < \gamma^*_{HO,\min}$, although the missile is launched far enough away from the target.

Figure 5.11(a) also illustrates $\mathcal{C}_2$ with different acceleration limit. Note that $\mathcal{C}_2$ is made narrower as $\underline{r}_0|_{\gamma_f}$. As shown in 5.11(b), increasing acceleration capacity decreases $\underline{r}_0|_{\gamma_f}$ and widen the capture region.

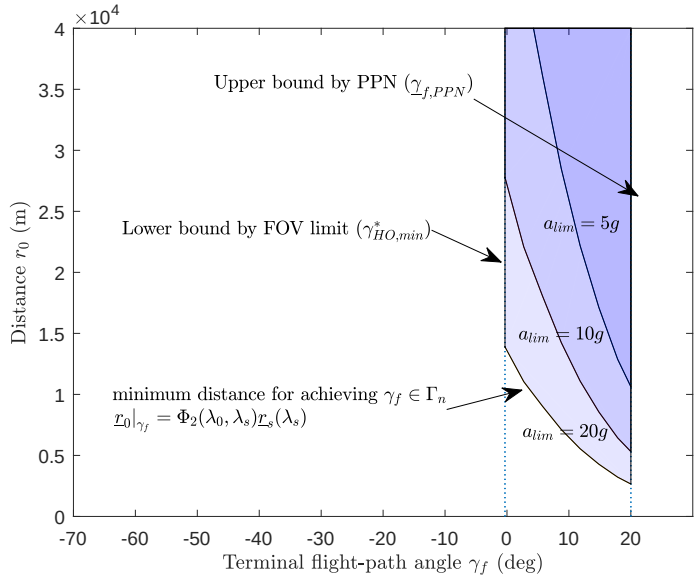

(a) $\mathcal{C}_2$, ($\lambda_0 = 30$ deg, $\zeta_{\text{lim}} > 1$; Narrow FOV Limit)

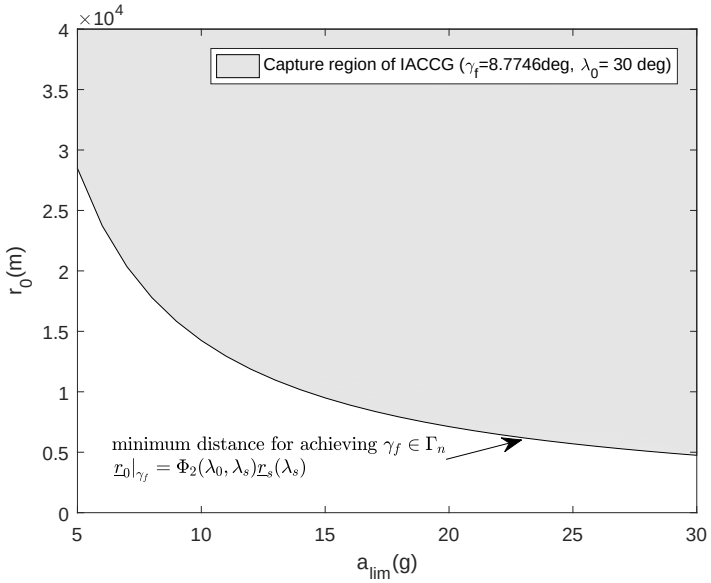

(b) $\mathcal{C}_{2,\gamma_f}$, ($\lambda_0 = 30$ deg, $\zeta_{\text{lim}} > 1$; Narrow FOV Limit)

Figure 5.11: Effects of η on DPP and Capture Region

Comparison of Guidance Laws for Target Interception

In this subsection, the capture region of IACCG is compared with the case of PPN and LCG. $\mathcal{C}_{PPN,\sigma_0}$ and $\mathcal{C}_{LCG,\sigma_0}$ are considered as the comparative capture regions, where the parameters of each capture region are selected as $\sigma_0 = -\sigma_{\lim} = -5deg$, $V_T = 500m/s$, $V_M = 1,000m/s$, and $N = 3$. Figure 5.12 shows the capture regions of the guidance laws represented in LOS coordinates. In the head-on situation, the capture region of IACCG is made much narrower and has the following inclusive relations.

$$\mathcal{C}_{IACCG,HO,\gamma_f} \subset \mathcal{C}_{PPN,HO,\sigma_0} \subset \mathcal{C}_{LCG,HO,\sigma_0} \tag{5.15}$$

Under the RN-FOV condition, the turning maneuver guided by DPP shows unstable characteristics in the head-on configuration, which makes the capture region very narrow for IACCG. Compared to the primary purpose for PPN and LCG, the impact angle control additionally requires a desired collision configuration at the instant of interception. Therefore, Eq. (5.15) implies that the impact angle control is usually difficult to achieve.

Figure 5.12(b) shows the capture regions in the tail-chase configuration. To enter a desired collision course, IACCG exploits the stable characteristics of DPP, and much wider range of capture region is made. The capture region of IACCG has the relation with LCG as

$$\mathcal{C}_{IACCG,TC,\gamma_f} \subset \mathcal{C}_{LCG,TC,\sigma_0} \tag{5.16}$$

In summary, LCG has widest capture region and is suitable if the mission focuses on the primary objective. If the mission requires a specified collision geometry, the missile should start the engagement in the capture region for the impact angle control during the terminal phase.

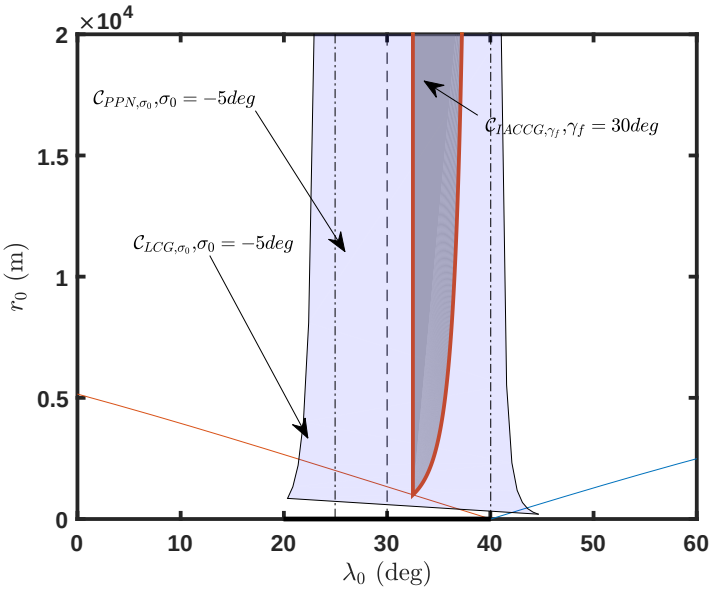

(a) $\mathcal{C}_{\gamma_f}$, with different FOV Limits$\sigma_{\text{lim}} = 5$ and 9 deg)

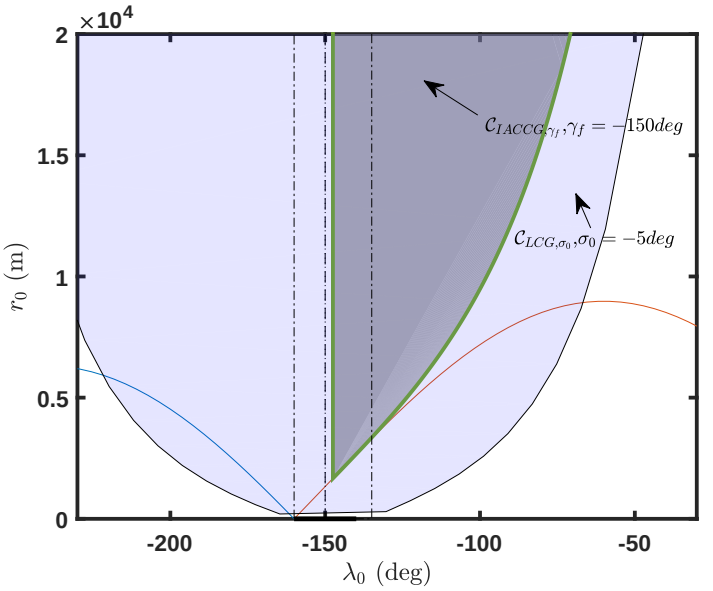

(b) $\mathcal{C}_2$, ($\lambda_0 = 0$ deg, $\zeta_{\text{lim}} > 1$; Narrow FOV Limit)

Figure 5.12: Effect of FOV Limit on $\mathcal{C}_{IACCG,\gamma_f}$

5.2.2 Characteristics of MIACCG

This section investigates how the proposed guidance law, MIACCG, improves the performance over the existing method. For this purpose, the capture region of MIACCG is compared with that of IACCG. For sufficient condition of the achievable impact angle set, subregion $\mathcal{C}_{MIACCG,1}$ is obtained, and its property is discussed. To investigate the capture region in terms of the initial position space, $\mathcal{C}_{MIACCG,\gamma_f}$ is analyzed.

Achievable Impact Angle with Respect to λ_0

Figure 5.13 shows the achievable terminal flight-path angle depending on the initial LOS angles. Compared to IACCG, the achievable angle set is wider in both the tail-chase and head-on cases. For example, the achievable range $\overline{P_2Q_2}$ and $\overline{P_1Q_1}$ of the IACCG has the following relation.

$$\overline{P_1Q_1} \subset \overline{P_2Q_2} \tag{5.17}$$

Note that the length of $\overline{PQ}$ represents the range of initial LOS angles which is sufficient to achieve the specific impact angle. This implies that the proposed guidance law improves interception performance by the proper correction of the look-angle command. Note also that the range of achievable impact angle set is constant, and the initial LOS angle set associated with the achievable impact angle is extended compared to IACCG. The initial LOS angles in the tail-chase case are much wider than those in the head-on case, which reflects the favorable phase portrait of the DPP in the tail-chase case.

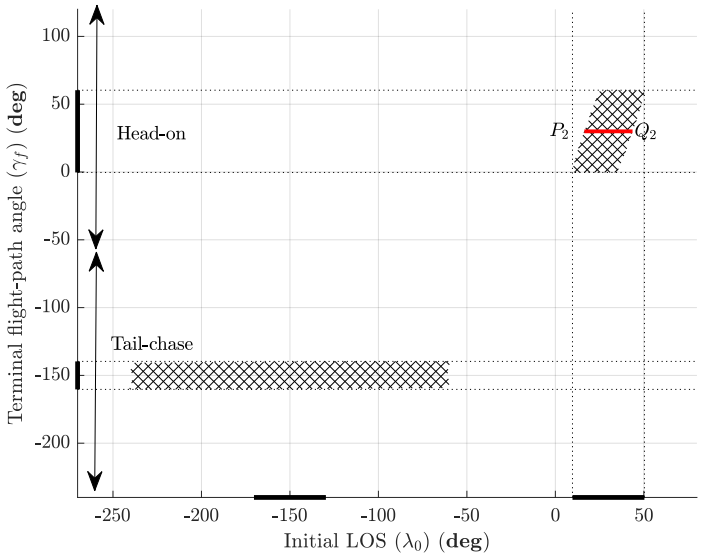

Figure 5.13: Comparison of Capture Regions of Composite Guidance with Wide/Narrow FOV Limit

Capture Region for Achieving Specified Impact Angle

In this section, property of $\mathcal{C}_{MIACCG,\gamma_f}$ is discussed. Figure 5.14 shows the capture region of the MIACCG. As shown in Fig. 5.14(a), the inclusion relation between $\mathcal{C}_{MIACCG,\gamma_f}$ and $\mathcal{C}_{IACCG,\gamma_f}$ has the following relation.

$$\mathcal{C}_{IACCG,\gamma_f} \subset \mathcal{C}_{MIACCG,\gamma_f} \tag{5.18}$$

Note from Eq. (4.40) that $\mathcal{C}_{MIACCG,\gamma_f}$ is obtained by integrating $\mathcal{C}_{MIACCG,\gamma_f,\sigma_c}$ for all $\sigma_c \in [\underline{\sigma}, \bar{\sigma}]$, and therefore $\mathcal{C}_{IACCG,\gamma_f}$ is the particular case of $\mathcal{C}_{MIACCG,\gamma_f,\sigma_c}$ when $\sigma_c = \sigma_{min}$. As shown in Fig. 5.14(b), the capture region is extended as the FOV limit increases. Compared to the result in Fig. 5.9(b), the effect of the FOV limit on the capture region is significant.

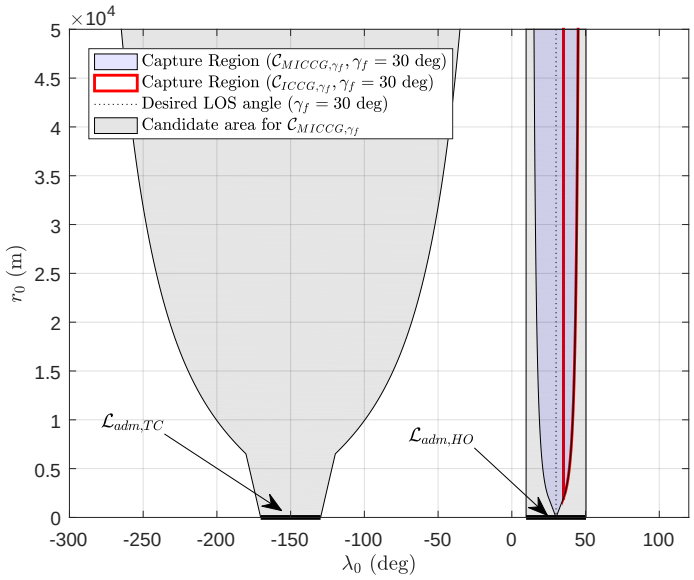

(a) $\mathcal{C}_{\gamma_f}$ (Narrow FOV Limit, $\gamma_f = 30$ deg)

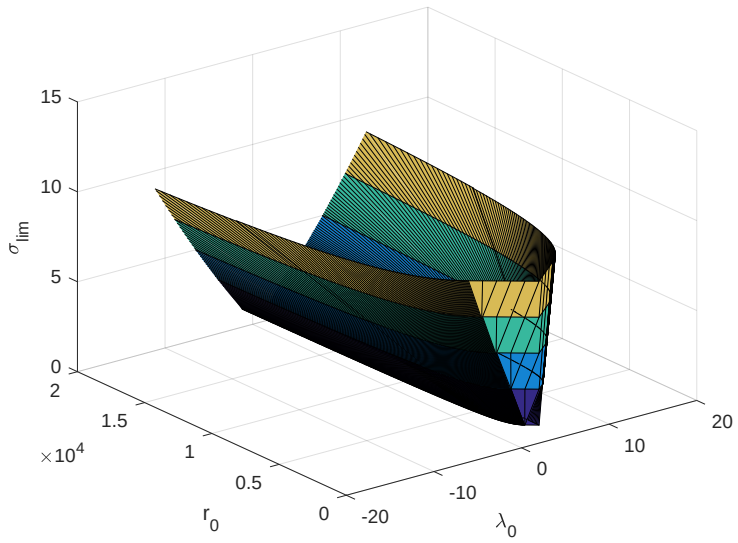

(b) $\mathcal{C}_1$, ($r_0 = 5,000m$, $\zeta_{\text{lim}} > 1$; Narrow FOV Limit)

Figure 5.14: Comparison of Capture Regions of Composite Guidance with Wide/Narrow FOV Limit

Chapter 6

Numerical Simulation

6.1 Simulation Setup

Numerical simulations are performed to demonstrate the performance of guidance laws upon the capture regions proposed in this study. Throughout the simulation, air-to-air engagement scenario is considered, where a missile is required to intercept a high-speed moving target. A three-degree-of-freedom point-mass model of a missile and a target is used in the simulations. Simulation parameters for the engagements are summarized in Table 6.1.

Table 6.1: Simulation Parameters

Description	Variable	Value	Unit
Speed of the target	V_T	500	[m/s]
Speed of the missile	V_M	$1,000$	[m/s]
FOV limit	σ_{lim}	5	[deg]
Maximum acceleration	$a_{m,max}$	20	[g's]
Navigation gain	N	3	[-]

In the first simulation, the performance of PPN and LCG analyzed in Chap.

Table 6.2: Simulation Cases for Scenario 1: Target Interception

Guidance Scheme	LCG		PPN	
Case	Case 1	Case 2	Case 3	Case 4
Initial look angle	$\sigma = \bar{\sigma}$	0	$\sigma = \bar{\sigma}$	0

3 is evaluated for target interception. To investigate the capture regions, two engagement geometries are considered. In head-on engagement geometry, the simulation is performed in two initial positions; $\mathcal{A}_{LCG}$ (Scenario 1-1), and $\mathcal{D}/\mathcal{B}_{LCG}$ (Scenario 1-2). In tail-chase geometry, the simulation is performed under the *partially capturable region of PPN* and *partially capturable region of LCG*, i.e., $\mathcal{B}_{PPN}$ (Scenario 1-3), and $\mathcal{B}_{LCG}$ (Scenario 1-4). In each simulation scenario, four different initial look angle are considered to compare the capture regions of LCG and PPN, which are summarized in Table 6.2.

In the second simulation, the performance of IACCG is demonstrated for target interception with desired impact angle, which are analyzed in Chapter 4. For air-to-air engagement, the capture region associated with achievable impact angle is evaluated by changing the desired impact angles upon the initial position. Then, the performance of IACCG is compared with that of LCG. Simulation cases are summarized in Table 6.3.

In the last simulation, the performance of IACCG is compared with proposed method to demonstrate the effectiveness of the proposed method. Simulation cases for the scenario 3 are summarized in Table 6.4.

Table 6.3: Simulation Cases for Scenario 2: Performance of IACCG

Scenario 2-1 $\lambda_0 = 30deg$				
Case	2-1	2-2	2-3	2-4
Distance (r_0)	$10,000m$		$20,000m$	
Impact angle (γ_{imp}, deg)	-160	-170	-160	-170
Scenario 2-2 $r_0 = 20,000m$				
Case	2-5	2-6	2-7	2-8
Guidance	LCG		PPN	
LOS angle (λ_0, deg)	24.5	35	24.5	35

Table 6.4: Simulation Cases for Scenario 3: Performance of MIACCG

Scenario 3 $r_0 = 20,000m$				
Case	3-1	3-2	3-3	3-4
Guidance	MIACCG		IACCG	
LOS angle (λ_0)	$29deg$	$34deg$	$29deg$	$34deg$

6.2 Simulation Results

6.2.1 Performance of PPN and LCG

Head-on Engagement

Figure 6.1 shows the simulation results of the LCG and PPN. When the initial position of the missile lies between the *capturable region of LCG* and the *partially capturable region of PPN* (Scenario 1-1), interception using PPN is guaranteed according to the initial look angle. When the initial look angle is $\sigma_0 = 0$, the missile successfully completes the interception while maintaining the lock-on condition as shown in Fig. 6.1-(a). Under these conditions, LCG does not switch the guidance command during the maneuver, and the performance of the LCG is the same as that of PPN.

As shown in Case 3, the LOS angle guided by PPN converges to a final LOS angle lying outside the admissible range $\mathcal{L}_{HO,adm}$ when the initial look angle $\sigma_0 = \bar{\sigma}$. Consequently, the missile guided by PPN fails to maintain the lock-on condition in the final homing phase. In the case of LCG, command switching occurs during the maneuver. LOS λ_{sw} at the switching time is close to its equilibrium value $\lambda_{\underline{\lambda},HO}$, which makes the miss distance within the allowable value.

For the case in which the initial position is located outside the *partially capturable region* (Scenario 1-2), PPN allows the missile to enter a collision course by forming the equilibrium LOS angle away from the admissible range. Thus, the missile cannot maintain the lock-on condition during the maneuver, even though the interception is fulfilled. Using LCG, switching the guidance command occurs for all initial conditions. Because the switching points are far

away from the equilibrium point $\lambda_{\underline{\lambda},HO}$, the LOS angle by the deviated pursuit diverges quickly from the equilibrium, which results in a large miss distance. In summary, neither guidance scheme can succeed in interception as shown in Fig. 6.2. The results of the numerical simulations are summarized in Table 6.5.

Table 6.5: Miss Distance and Terminal Look Angle (Simulation 1, Head-on Engagement)

Case	Guidance	Scenario 1-1: $\mathcal{A}_{LCG}$			Scenario 1-2: $\mathcal{D}_{HO}/\mathcal{B}_{LCG}$		
	scheme	r_f/R_{miss}	$\lvert\sigma_f/\sigma_{\text{lim}}\rvert$	$\lambda_f(^o)$	r_f/R_{miss}	$\lvert\sigma_f/\sigma_{\text{lim}}\rvert$	$\lambda_f(^o)$
1	LCG	0.027	0.9847	10.21	4.99	0.855	27.09
2	LCG	0.001	0.8489	6.6338	4.99	0.659	26.33
3	PPN	0.016	1.0577	10.17	0.001	3.208	17.08
4	PPN	0.001	0.8489	6.6338	0.001	2.409	16.85

Tail-chase Engagement

Simulation results for the tail-chase engagement cases are shown in Fig. 6.3. Two cases of the simulation are considered in which the initial condition lies in the *partially capturable region of PPN* (Scenario 1-3) and the *partially capturable region of LCG* (Scenario 1-4). Because both guidance commands consisting of LCG have a stable phase portrait in the tail-chase engagement, homing guidance can be finished in a stable manner. In Scenario 1-3, the initial condition $\sigma_0 = \bar{\sigma}$ (Case 3) can intercept the target with respect to the FOV limit. At the initial position with the initial look angle, the terminal LOS is determined to be within the admissible range $\mathcal{L}_{adm,TC}$, and the missile monotonically converges

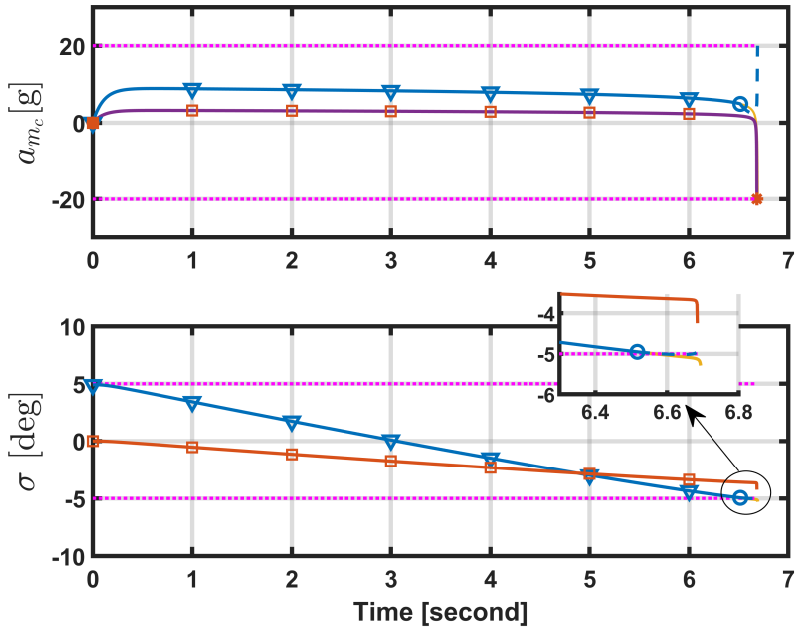

(a) Responses of Acceleration and Look angle (Scenario 1-1)

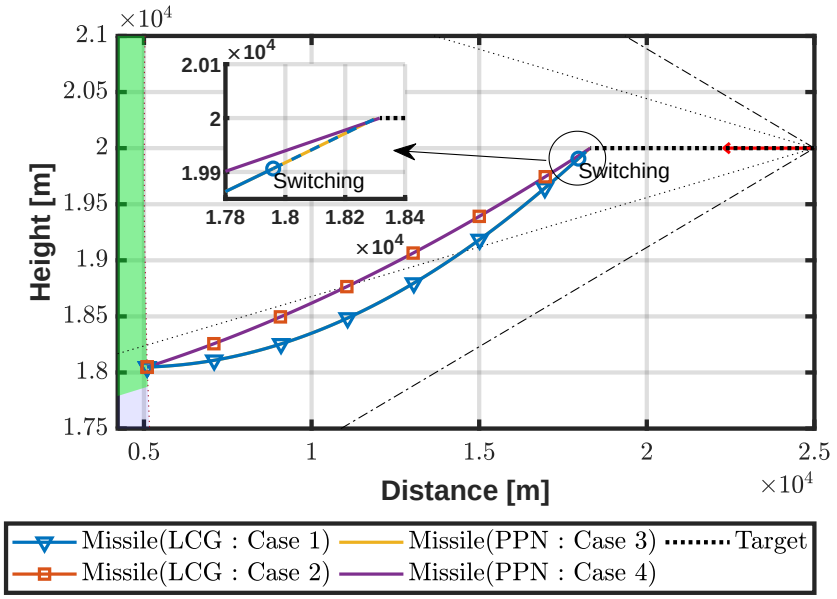

(b) Trajectories (Scenario 1-1)

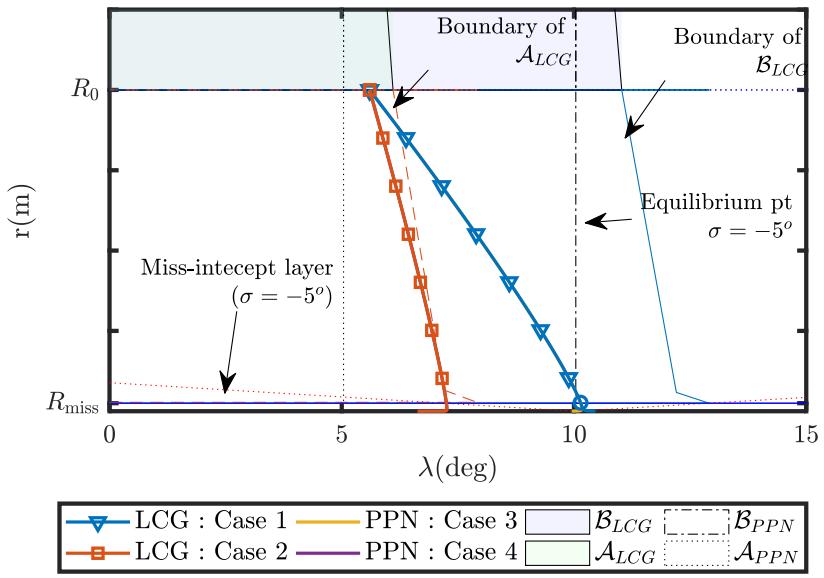

(c) Relative Trajectory of the Missile in LOS Coordinate (Scenario 1-1)

Figure 6.1: Simulation Results (Head-on Engagement, Scenario 1-1: Inside the *Capturable Region of LCG*)

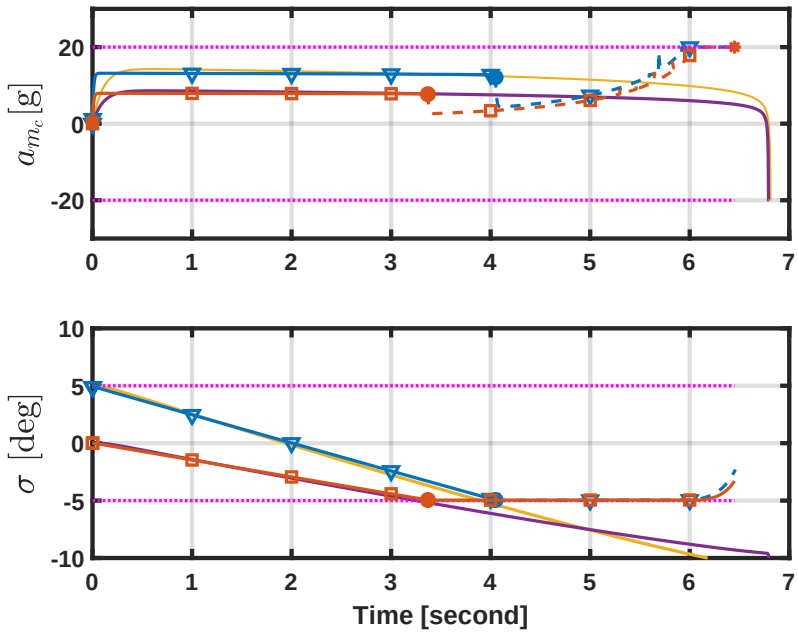

(a) Responses of Acceleration and Look angle (Scenario 1-2)

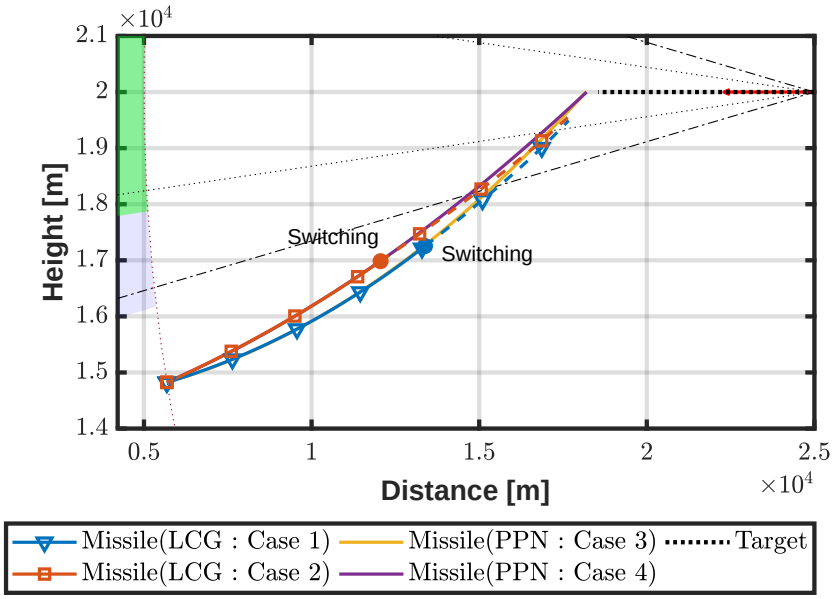

(b) Trajectories (Scenario 1-2)

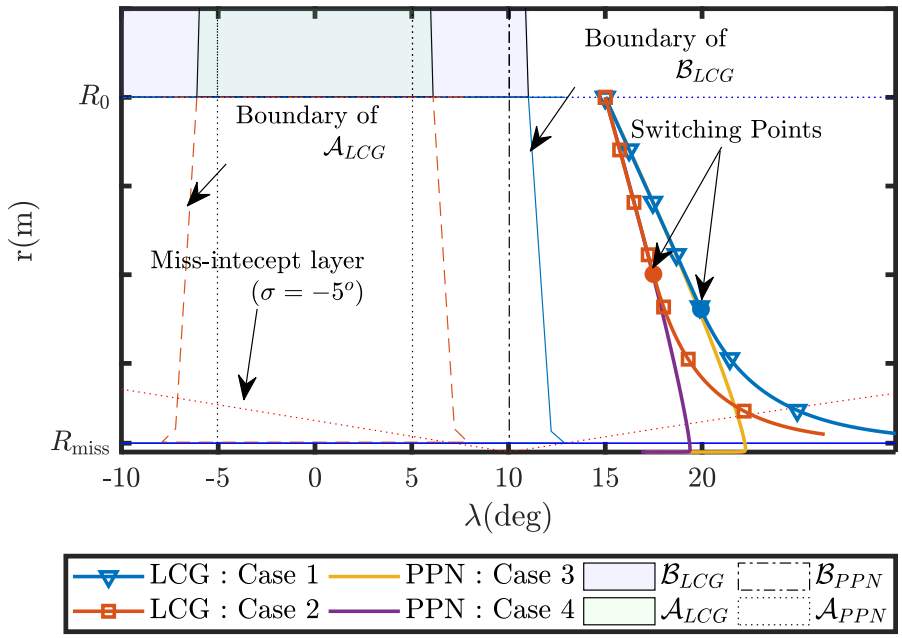

(c) Relative Trajectory of the Missile in LOS Coordinate (Scenario 1-2)

Figure 6.2: Simulation Results (Head-on Engagement, Scenario 1-2: Outside the *Partially capturable Region of LCG*)

to the collision course while maintaining the lock-on condition. Otherwise, the equilibrium point of the PPN is located outside the admissible range as shown in Fig. 6.3-(b), and therefore the missile starting from the initial look angle (Cases 4) fails to lock-on the target as shown in Fig. 6.3-(a). From these results, it can be stated that successful interception depends on the initial look angle if the missile is inside the *partially capturable region*. By contrast, missiles guided by LCG can achieve interception while maintaining the lock-on condition for all initial directions.

Figure 6.4 shows the simulation results of the *partially capturable region of LCG*. When the initial position is located far from the *capturable region of PPN*, the terminal LOS lies outside the admissible LOS angle range, and the missile converges to the collision course by increasing the LOS angle. The look angle decreases greatly and exceeds its minimum, leading to failure to lock-on the target. Using LCG, the missile after switching the guidance command proceeds to interception by the pursuit maneuver. In Case 1, however, the missile intercepts the target using LCG. At the initial condition, i.e., $(r_0, \lambda_0) \in \mathcal{B}_{LCG}$ and $\sigma_0 = \bar{\sigma}$, the switching occurs inside the boundary of the *capturable region of LCG* as shown in Fig. 6.4-(c), and the trajectory by the deviated pursuit causes the miss distance to be smaller than R_{miss}. The results of the numerical simulations are summarized in Table 6.6.

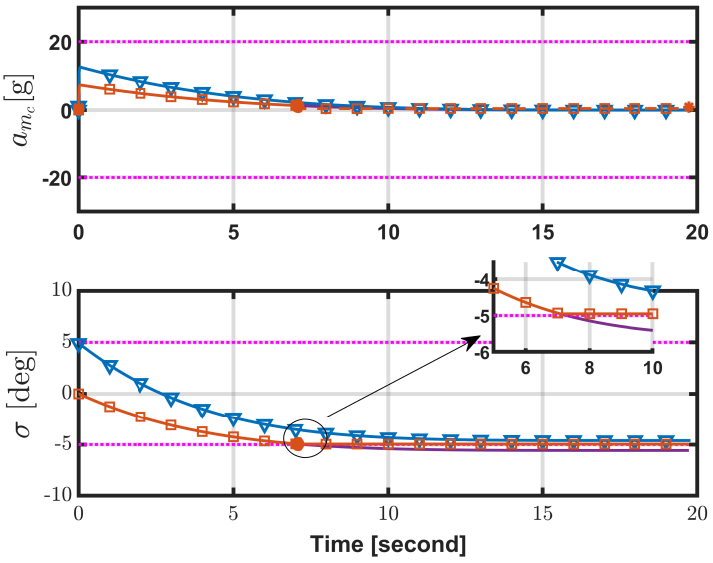

(a) Responses of Acceleration and Look Angle (Scenario 1-3)

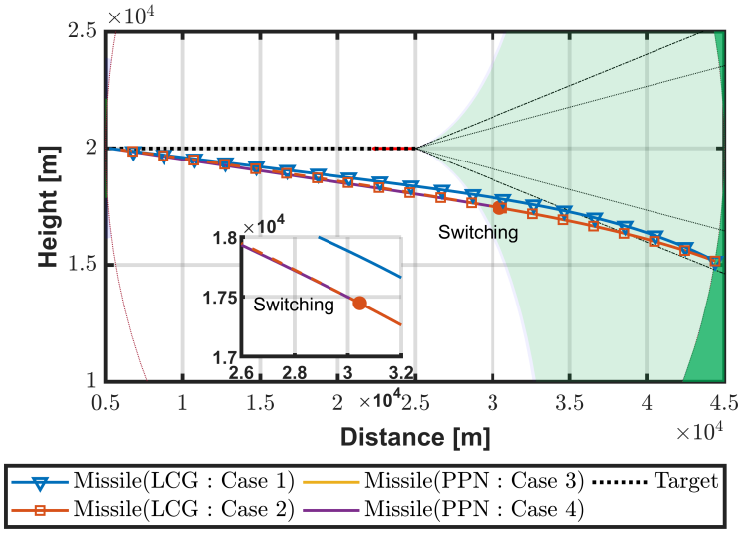

(b) Trajectories (Scenario 1-3)

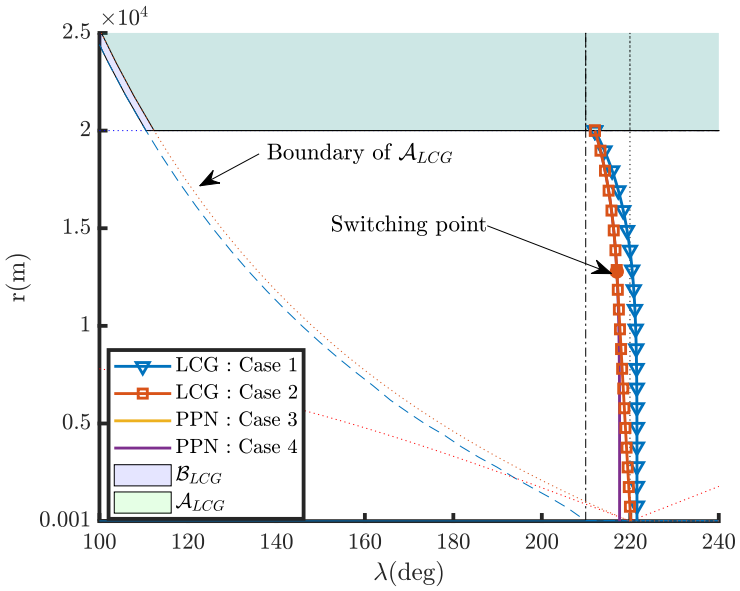

(c) Relative Trajectory of the Missile in LOS Coordinate (Scenario 1-3)

Figure 6.3: Simulation Results (Tail-chase Engagement, Scenario 1-3: *Partially capturable Region of PPN*)

Table 6.6: Miss Distance and Terminal Look Angle (Simulation 1, Tail-chase Engagement)

Case	Guidance scheme	Scenario 1-3: $\mathcal{B}_{PPN}$			Scenario 1-4: $\mathcal{B}_{LCG}$		
		r_f/R_{miss}	$\lvert\sigma_f/\sigma_{\text{lim}}\rvert$	$\lambda_f(^o)$	r_f/R_{miss}	$\lvert\sigma_f/\sigma_{\text{lim}}\rvert$	$\lambda_f(^o)$
1	LCG	0.0704	0.9900	170.75	0.67	0.993	168.96
2	LCG	0.0390	0.9902	170.05	2.84	0.992	169.87
3	PPN	0.0704	0.9900	170.75	0.081	4.185	134.41
4	PPN	0.081	1.1157	168.78	0.0551	4.591	128.73

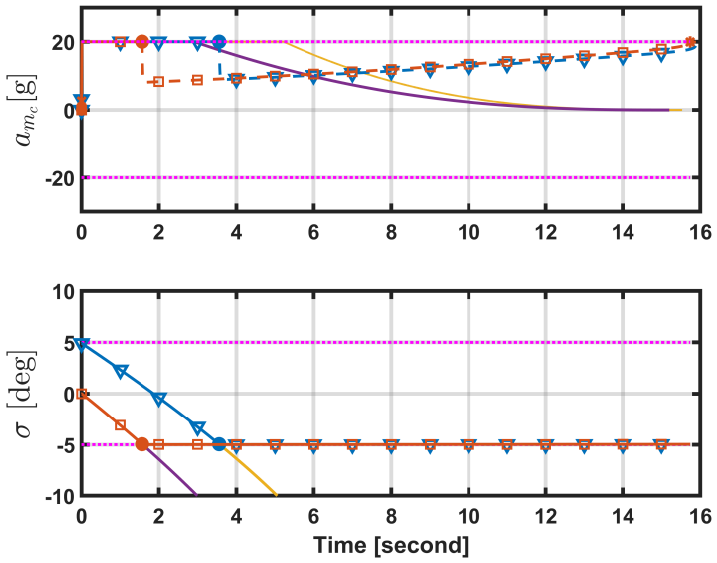

(a) Responses of Acceleration and Look Angle (Scenario 1-4)

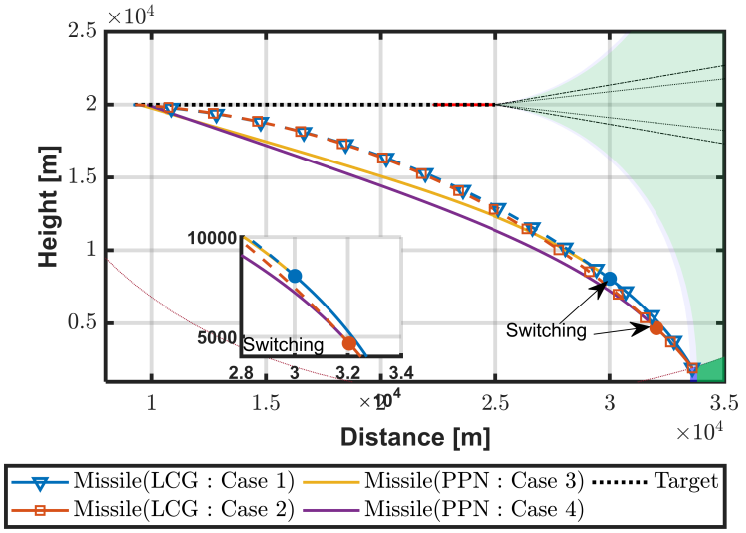

(b) Trajectories (Scenario 1-4)

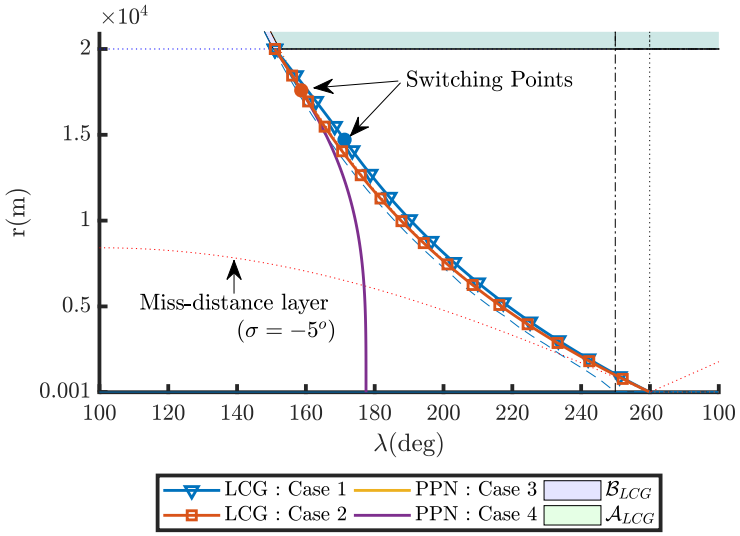

(c) Relative Trajectory of the Missile in LOS Coordinate (Scenario 1-4)

Figure 6.4: Simulation Results (Tail-chase Engagement, Scenario 1-4: *Partially capturable Region of LCG*)

6.2.2 Performance of IACCG

In this simulation, head-on interception is only considered where the missile is required to intercept the approaching target. It is assumed that the target keeps descending to a constant flight-path angle $\gamma_T = -150deg$.

Impact Angle Interception with Respect to Initial Distance

In the first scenario, the missile enters into a handover point lying on the predicted trajectory of the target with initial distance $r_0 = 10,000m$ and $r_0 = 20,000m$, and executes impact angle control guidance designated as $\gamma_{imp} = -160$ deg and -170 deg, respectively.

Figure 6.5 shows the simulation result. According to the initial condition, the cases are assigned to the capture region $\mathcal{C}_2$ as shown in Fig. 6.5-(a). If the un-achievable impact angle is selected (Cases 2-1 and 2-3), IACCG does not switch the command from DPP to PPN and fails to interception. Note that the impact angle $\gamma_{imp} = -160$ deg is only achieved for the case of $r_0 = 20,000m$. It is reflected that the impact angle interception can be much easier if initial launch distance is larger. Table 6.7 summarizes the simulation results of Scenario 2-1.

Comparative Performance of IACCG with LCG

In the second scenario, the missile enters into a handover point to intercept the target for exact head-on interception $\gamma_{imp} = -180$ deg. To evaluate the capture region, three initial positions are chosen as summarized in Table 6.3. Figure 6.6 shows the results of Scenario 2-2. As shown in Fig. 6.6, the missile guided by IACCG completes the mission only when the initial position of the missile lies in $\mathcal{C}_{\gamma_f}$ (Case 2-8). In this case, the guidance command is switched

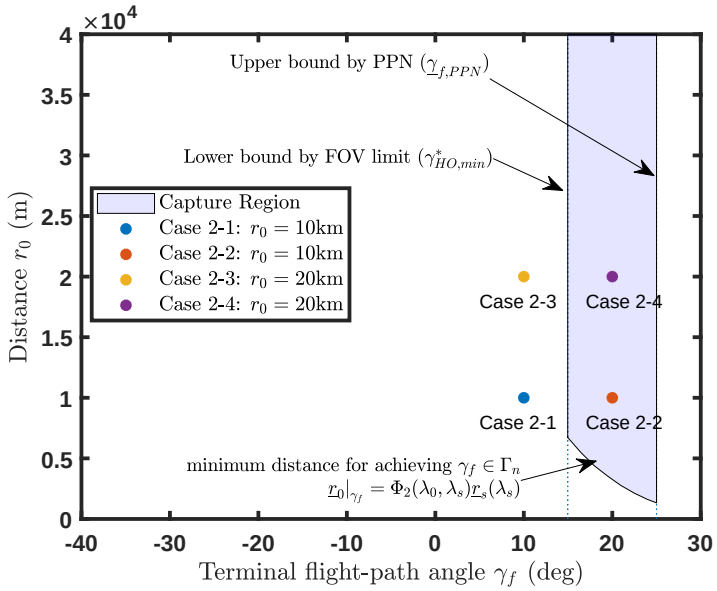

(a) Relative Trajectory of the Missile (represented in LOS Coordinate)

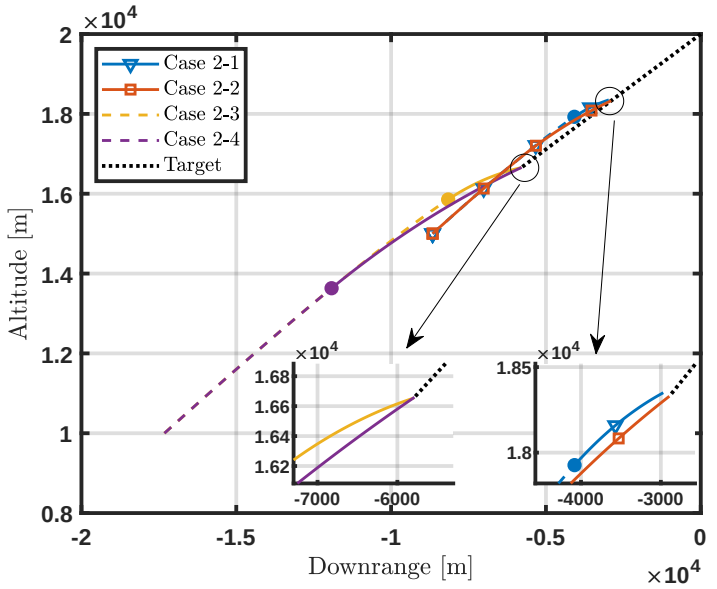

(b) Trajectories of the Missile and Target

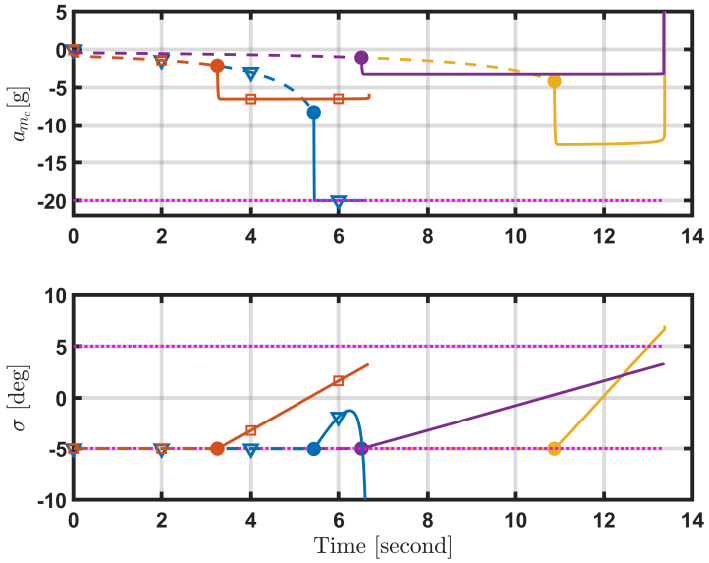

(c) Time Responses of the Acceleration and Look Angle

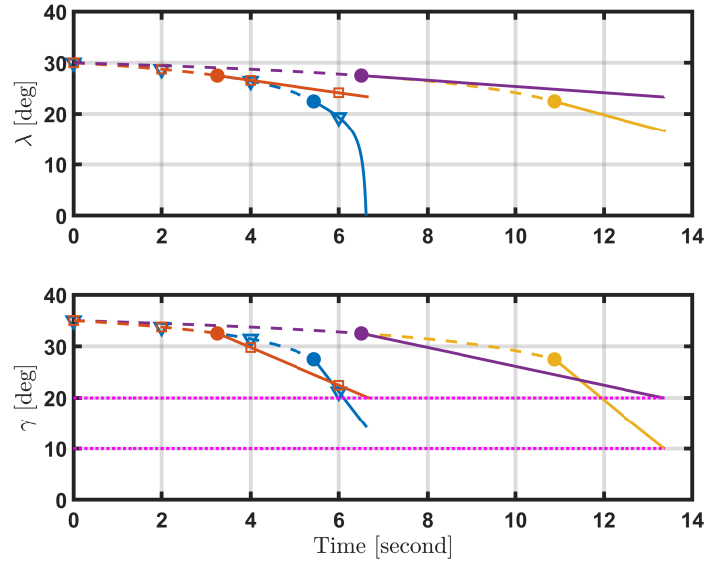

(d) Time Responses of the LOS Angle and Flight-Path Angle

Figure 6.5: Simulation Results (Scenario 2-1: Performance of Impact-Angle Interception)

Table 6.7: Miss Distance, Look Angle, and Impact Angle (Simulation 2-1)

Case	Guidance scheme	Scenario 2-1: $\lambda_0 = 30deg$		
		r_f/R_{miss}	$\lvert\sigma_f/\sigma_{\text{lim}}\rvert$	$\gamma_{imp} - \gamma_{imp}^d(^o)$
2-1	IACCG	16.59	17.89	-14.47
2-2	IACCG	9.967	11.92	-2.988
2-3	IACCG	23.0	17.50	-10.48
2-4	IACCG	0.172	0.827	0.01

at $t = 9.58$ sec., and the flight path angle converges to the desired value, $\gamma_f = \gamma_T - \gamma_{imp} = 30$ deg. For the other case, i.e., $\lambda_0 = 24.5$ deg, the guidance command is not switched, which fails the interception. Since the initial LOS angle in $\mathcal{C}_{\gamma_f}$ has the range of $[32.5, 37.27]$ (deg) as shown in Fig. 6.6-(d), the missile should start the mission from the position in $\mathcal{C}_{\gamma_f}$ to intercept the target while satisfying the impact angle constraint.

For comparative study, same simulation is performed for the missile with LCG guidance. Compared to the results of IACCG, the missile guided by LCG intercepts the target for all initial positions. In particular, LCG in Case switches the guidance command to DPP near the collision $t_{go} = 0.2sec$ and succeeds the interception. However, none of the cases satisfy the impact angle constraint. Note that the lower bound of the guaranteed initial range, 32.5 deg, is the switching line that satisfies the exact head-on by PPN, and therefore LCG and PPN can accomplish the mission only when the missile begins the mission at the position $\lambda_0 = 32.5$ deg. Table 6.8 summarizes the simulation results of scenario 2-2.

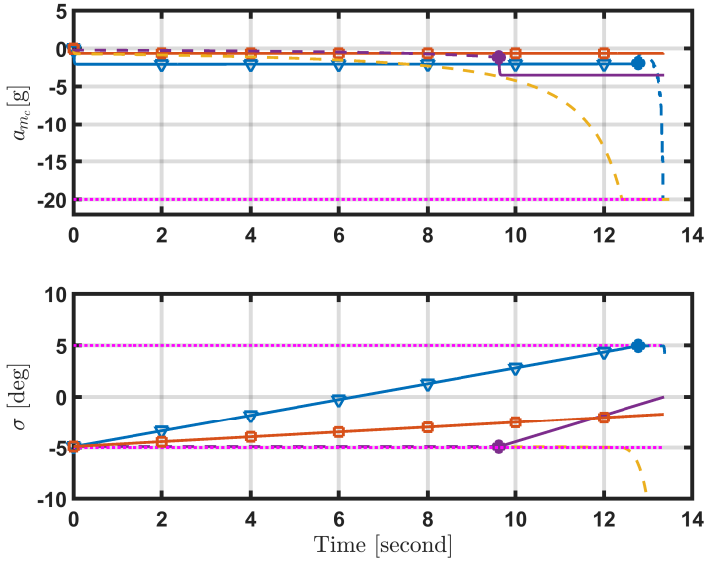

(a) Time Responses of the Acceleration and Look Angle

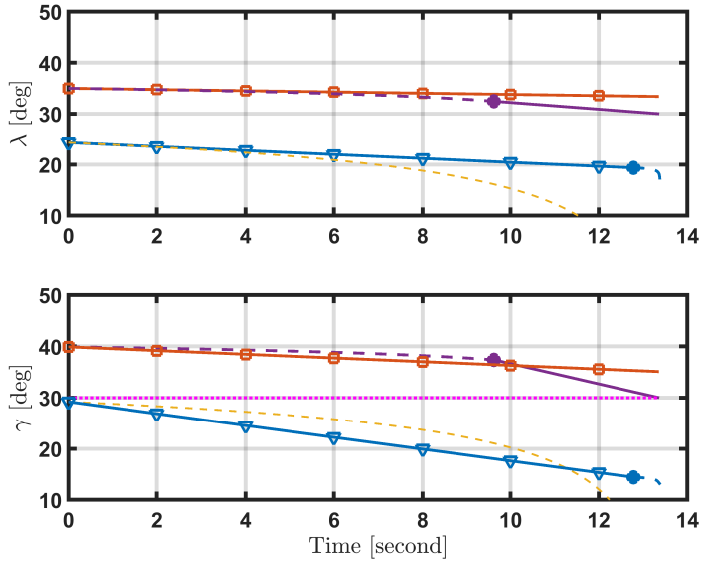

(b) Time Responses of the LOS Angle and flight-Path Angle

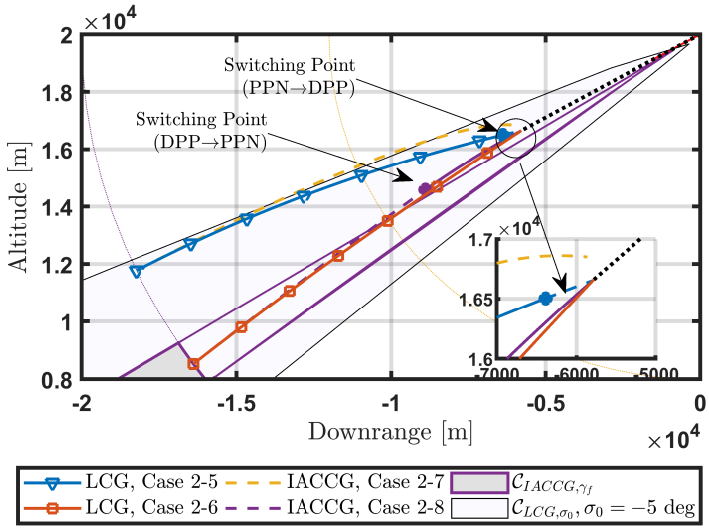

(c) Trajectories of the Missile and Target

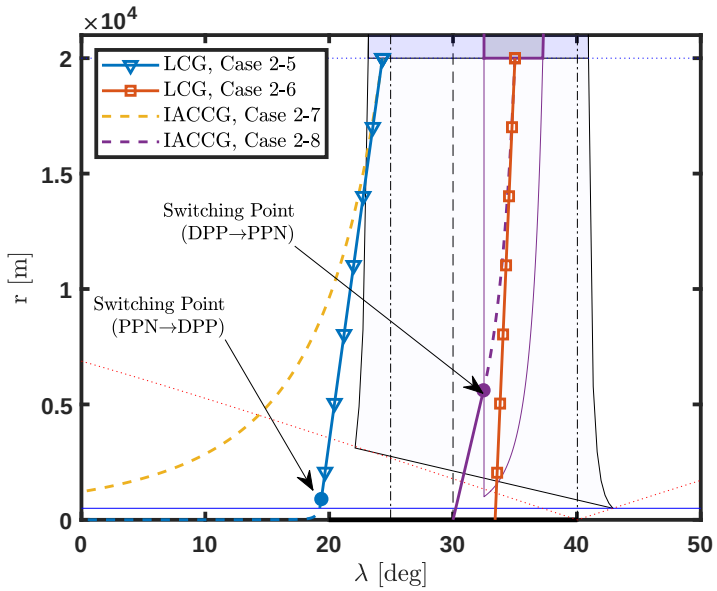

(d) Relative Trajectory of the Missile (represented in LOS Coordinate)

Figure 6.6: Simulation Results (Scenario 2-2: Comparative Study with LCG)

Table 6.8: Miss Distance, Look Angle, and Impact Angle (Simulation 2-2)

Case	Guidance scheme	Scenario 2-2: $r_0 = 20,000m$		
		r_f/R_{miss}	$\lvert\sigma_f/\sigma_{\text{lim}}\rvert$	$\gamma_{imp} - \gamma_{imp}^{d}(^o)$
2-5	LCG	0.099	0.9900	16.42
2-6	LCG	0.094	0.3351	-5.09
2-7	IACCG	44.8	16.80	19.33
2-8	IACCG	0.097	0.007	0.03

6.2.3 Performance of MIACCG

Numerical simulation is performed to demonstrate the effectiveness of the modified IACCG guidance law. Under the same situation as Scenario 2, the initial look angle is set to $\sigma_0 = 0$ by considering the lock-on before handover point. The existing composite guidance [29] law is conducted for comparative study.

Figures 6.7 show the simulation results of scenario 3. As shown in Fig. 6.7, the existing method (IACCG) intercepts the target only if the missile is initially in the capture region (Case 3-4). Otherwise, the guidance command steers the look-angle to the prescribed command in stage 1, and therefore the switching of the guidance phase does not occur. Consequently, the guidance law is only done by look angle control, which yields a large miss distance. Using the proposed algorithm, MACCG, on the other hand, the extended capture region can be seen as shown in Figs. 6.7-(c) and 6.7-(d). The look-angle command is properly corrected in stage 1 to satisfy the switching condition as shown in Fig. 6.7-(a). As a result, the missile intercepts the target while achieving specified impact angle in the extended initial positions. Table 6.9 summarizes the miss distance and the error of impact angle for the MACCG.

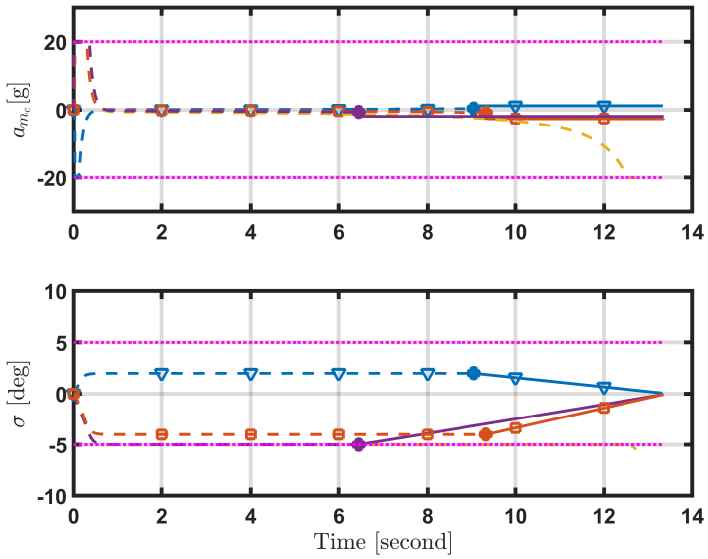

(a) Time Responses of the Acceleration and Look Angle

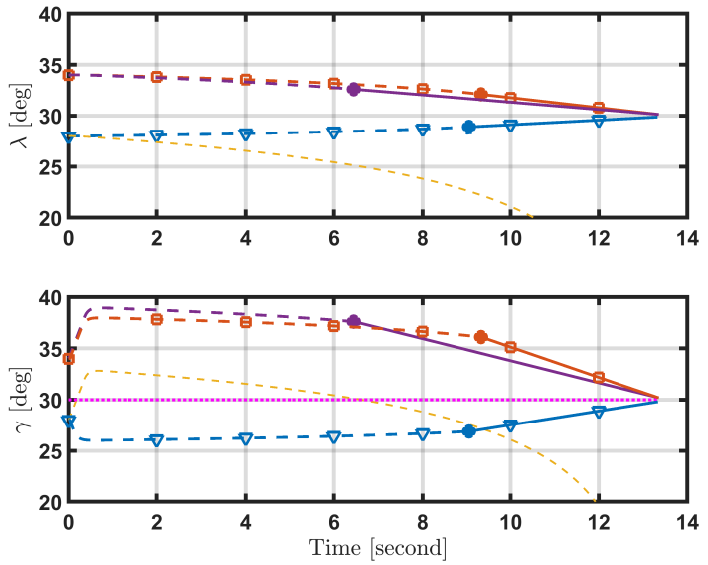

(b) Time Responses of the LOS Angle and Flight-Path Angle

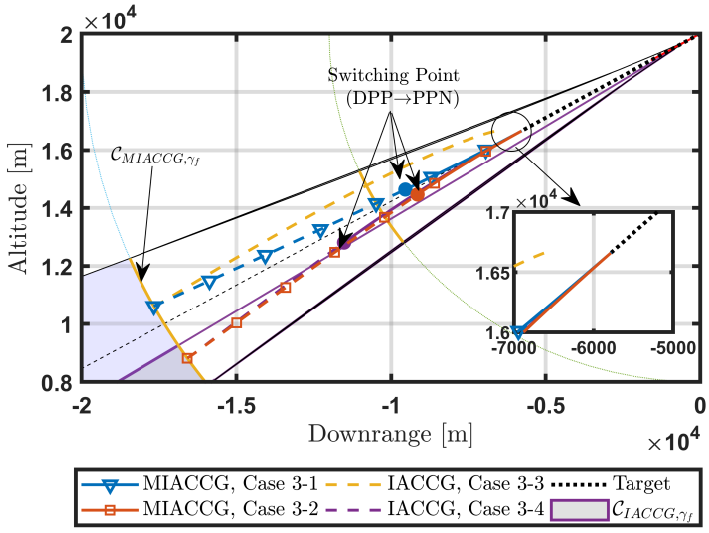

(c) Trajectories of the Missile and Target

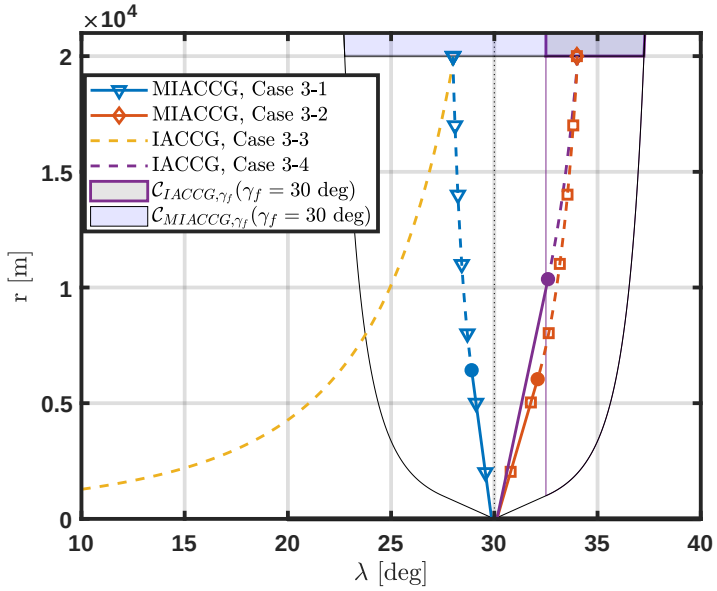

(d) Relative Trajectory of the Missile (represented in LOS Coordinate)

Figure 6.7: Simulation Results (Scenario 3: Performance of MIACCG)

Table 6.9: Miss Distance, Look Angle, and Impact Angle (Simulation 3)

Case	Guidance scheme	Scenario 3: $r_0 = 20,000m$		
		r_f/R_{miss}	$\lvert\sigma_f/\sigma_{\text{lim}}\rvert$	$\gamma_{imp} - \gamma_{imp}^{d}(^o)$
3-1	MIACCG	0.193	0.0127	0.194
3-2	MIACCG	0.066	0.0113	-0.172
3-3	IACCG	99.94	2.525	9.043
3-4	IACCG	0.172	0.011	-0.180

Chapter 7

Conclusion

7.1 Concluding Remarks

A capturability analysis on the field-of-view constrained guidance laws was performed. The analysis was motivated from the investigation of the applicability of existing guidance laws to air-to-air engagement situations where the seeker's field-of-view is too narrow to restrict the maneuver of the missile and closing speed between the target and missile is high. The proposed capture region was obtained in terms of initial positions and field-of-view, which makes easy to apply the results to the midcourse guidance. The existing guidance laws were classified into two categories depending on the guidance purposes, and the capture regions of the representative guidance laws were derived and investigated.

Based on the capture region, several meaningful findings can be addressed. First, it was shown that capture regions could be significantly affected by the reduction of the field-of-view limit. When the field-of-view is narrow, the capture region is divided into head-on and tail-chase engagement regions, and the capture region in the head-on engagement is formed relatively narrower. The capture region of the proportional navigation guidance is considerably reduced

in regard to reduction of field-of-view limit compared to earlier result on Guelman [44]. Second, from the inclusion relations, the capture region of impact angle control is usually made much narrower than that of the guidance law for target interception. It was found that the capture region can be extended when the look angle control logic is exploited to prevent the look angle from exceeding the field-of-view limit. In this regard, it would be better to directly enter a collision course at the beginning of the homing phase and to use the FOV constraint logic as an auxiliary method instead of a turn maneuver. The results would be the fact that the impact angle control constraint is an additional requirement together with the primary objective, witch makes the mission much sophisticated.

The guidance mission is often required to achieve a specific interception with desired collision configuration, and the impact angle control scheme should be incorporated. In this respect, a guideline for designing FOV-constrained guidance with PPN was provided in this study. The initial position inside the capture region can be utilized to find the feasible predicted handover points (PHP) in the mid-course phase. Based on the capture region, the missile can achieve the guidance objective by entering the capture region at the beginning of terminal phase. In summary, this study provides an opportunity to apply the existing guidance law, which had been designed for surface targets, to the air-to-air engagement, and finally the proposed guidance law could extend the capture region and improve the interception performance.

7.2 Directions for Further Research

Following directions are some suggestions for the meaningful extension of the study presented in this study.

Consideration on Maneuvering and Higher-Speed Targets

In the study, the capture region is obtained for intercepting a non-maneuvering and slower-speed target. In the air-to-air engagement, various types of threat can be considered including evasive-maneuverable aircrafts and ballistic missiles. Capturablitiy analysis of variants of the proportional navigation without considering the field-of-view limit was conducted for maneuvering target [39,47] and higher-speed target [46, 49], where the capture region was only realized in the velocity space not in the position space. The closed-form solution of the guidance law under maneuvering and higher-speed assumption is left unsolved, and therefore it would be better to derive the capture region for the maneuvering target by combining numerical and analytical ways.

One the other hand, it would be interesting to design a new guidance law for intercepting the maneuvering targets while considering the seeker's field-of-view limit. Only a few studies dealt with the seeker's field-of-view limit on the guidance design for intercepting the maneuvering target. In particular, for higher-speed target, retro-proportional navigation method was proposed as the head-pursuit concept. However, the retro-proportional navigation cannot be applied to narrow field-of-view case, because the target should be always outside the seeker's field-of-view. Instead, a proper guidance law could be designed to guarantee the lock-on condition and interception of the higher-speed target.

Consideration of Angle-of-Attack on FOV-constrained Guidance

When the missile travels in the atmospheric region, angle-of-attack mainly affects the missile dynamics. Most of the missile guidance studies have performed assuming that the angle-of-attack is negligible. The assumption may not be valid if the guidance law generates large acceleration command, which involves excessive maneuver and considerable angle of attack. Even a small angle of attack may be significant when the field-of-view is narrow. Consideration of the angle of attack effect on the guidance design process may improve the performance of the guidance law.

FOV-constrained Guidance Law with Multiple Constraints

In this study, FOV-constrained guidance laws are classified into guidance law for target interception and impact angle control guidance. The advanced FOV-constrained guidance can be improved by considering multiple constraints including impact angle, impact time control, and varying speed constraints, simultaneously.

Bibliography

[1] Fleeman, E. L., "Technologies for Future Precision Strike Missile Systems," *RTO SCI Lecture Series*, Atlanta, GA, March 2000.

[2] Hong, J.-H., and Ryoo, C.-K., "Homing Loop Design for Missiles with Strapdown Seeker," *Journal of the Korean Society for Aeronautical & Space Sciences*, Vol. 42, No. 4, 2014, pp. 317–325.
DOI:J.ICROS.2013.12.1809

[3] Felix, S., "US Navy Spike Missile System: a New Generation of Miniature Precision Guided Weapons," Technical report, OBM NO. 0704-0188, Naval Air Warfare Center Weapon Division, China Lake, CA, May 2006.

[4] Lee, C. H., *Missile Guidance Laws for a Strapdown Seeker with a Narrow Field of View*, Ph.D. Dissertation, Seoul National University, Seoul, Korea, 2013.

[5] Kim, K.-S., and Ra, S.-W., "Robust Least Squares Motion Deblurring Using Inertial Sensor for Strapdown Image IR Sensors," *Journal of Institute of Control, Robotics and Systems*, Vol. 18, No. 4, 2012, pp. 314–320.
DOI:10.5302/J.ICROS.2012.18.4.314

[6] Montoya, M., "Standard Missile: A Cornerstone of Navy Theater Air Missile Defense," *Johns Hopkins APL Technical Digest*, Vol. 22, No. 3, 2001, pp. 234–247.

[7] Vergez, P. L., and McClendon, J. R., "Optimal Control and Estimation for Strapdown Seeker Guidance of Tactical Missiles," *Journal of Guidance, Control, and Dynamics*, Vol. 5, No. 3, 1982, pp. 225–226.
DOI:10.2514/3.19767

[8] Tomas. R., C., "Guidance Law Design for Tactical Weapons with Strapdown Seekers," *AIAA Guidance and Control Conference*, Boulder ,CO, August 1979.
DOI:10.2514/6.1979-1732

[9] Mehra, R. K., and Ehrich, R. D., "Air-To-Air Missile Guidance For Strapdown Seeker," *IEEE Conference on Decision and Control*, Las Vegas, NV, December 1984.
DOI:10.1109/CDC.1984.272186

[10] Willman, W. W., "Effects of Strapdown Seeker Scale-Factor Uncertainty on Optimal Guidance," *Journal of Guidance, Control, and Dynamics*, Vol. 11, No. 3, 1988, pp. 199–206.
DOI:10.2514/3.20294

[11] Kim, T.-H., Park, B.-G., Kwon, H.-H., Kim, Y.-H., and Tahk, M.-J., "Stability Analysis of Missiles with Strapdown Seeker," *Journal of the Korean Society for Aeronautical & Space Sciences*, Vol. 39, No. 4, 2011, pp. 332–

340.
DOI:10.5139/JKSAS.2011.39.4.332

[12] Jianmei, S., Gaohua, C., Xianxiang, C., and Lixia, K., "Stability Region Analysis of the Parasitic Loop of the Semi-Strapdown Homing Seeker," *Proceedings of the Institution of Mechanical Engineers, Part I: Journal of Systems and Control Engineering*, Vol. 226, No. 4, 2012, pp. 550–562.
DOI:10.1177/0959651811421710

[13] Oh, S.-M., "Terminal Homing Guidance of Tactical Missiles with Strapdown Seekers Based on an Unscented Kalman Filter," *Journal of the Korean Society for Aeronautical & Space Sciences*, Vol. 38, No. 3, 2010, pp. 221–227.
DOI:10.5139/JKSAS.2010.38.3.221

[14] Jang, S.-A., Ryoo, C.-K., Choi, K., and Tahk, M.-J., "Guidance Loop Design for Portable Tactical Missiles with Strapdown Seeker," *Korean Society for Aeronautical and Space Sciences Spring Conference*, Pyung Chang, Gangwon-do, Korea, April 2008.

[15] Shneydor, N. A., *Missile Guidance and Pursuit: Kinematics, Dynamics and Control*, Woodehead, Cambridge, UK, 1998.

[16] Kim, D., Park, W., and Ryoo, C.-K., "Look-Angle-Control Guidance for Missiles with Strapdown Seeker," *Journal of Institute of Control, Robotics and Systems*, Vol. 19, No. 3, 2013, pp. 275–280.
DOI:10.5302/J.ICROS.2013.12.1809

[17] Ann, S., Lee, S., and Kim, Y., "Reference Shaping for Impact Angle and Time Control under Field-of-View Limit," *IFAC-PapersOnLine*, Vol. 50, No. 1, 2017, pp. 15191–15196.
DOI:10.1016/j.ifacol.2017.08.2355

[18] Manchester, I. R., and Savkin, A. V., "Circular-Navigation-Guidance Law for Precision Missile/Target Engagements," *Journal of Guidance, Control, and Dynamics*, Vol. 29, No. 2, 2006, pp. 314–320.
DOI:10.2514/1.13275

[19] Sang, D.-K., and Tahk, M.-J., "Guidance Law Switching Logic Considering the Seeker's Field-of-View Limits," *Proceedings of the Institution of Mechanical Engineers, Part G: Journal of Aerospace Engineering*, Vol. 223, No. 8, 2009, pp. 1049–1058.
DOI:10.1243/09544100JAERO614

[20] Zhang, Y., Wang, X., and Wu, H., "Impact Time Control Guidance with Field-of-View Constraint Accounting for Uncertain System Lag," *Proceedings of the Institution of Mechanical Engineers, Part G: Journal of Aerospace Engineering*, Vol. 230, No. 3, 2016, pp. 515–529.
DOI:10.1177/0954410015594401

[21] Jeon, I.-S., and Lee, J.-I., "Impact-Time-Control Guidance Law with Constraints on Seeker Look Angle," *IEEE Transactions on Aerospace and Electronic Systems*, Vol. 53, No. 5, 2017, pp. 2621–2627.
DOI:10.1109/TAES.2017.2698837

[22] Chen, X., and Wang, J., "Nonsingular Sliding-Mode Control for Field-of-View Constrained Impact Time Guidance," *Journal of Guidance, Control, and Dynamics*, Vol. 41, No. 5, 2018, pp. 1214–1222.
DOI:10.2514/1.G003146

[23] Shim, S., Hong, S., Moon, G., and M.J., T., "Impact Angle and Time Control Guidance under Field-of-View Constraints and Maneuver Limits," *International Journal of Aeronautical and Space Sciences*, Vol. 19, No. 1, 2018, pp. 217–226.
DOI:10.1007/s42405-018-0004-8

[24] Tekin, R., Erer, K. S., and Holzapfel, F., "Impact Time Control with Generalized-Polynomial Range Formulation," *Journal of Guidance, Control, and Dynamics*, Vol. 41, No. 5, 2018, pp. 1190–1195.
DOI:10.2514/1.G003279

[25] Kim, H.-G., and Kim, H. J., "Backstepping-Based Impact Time Control Guidance Law for Missiles with Reduced Seeker Field-of-View," *IEEE Transactions on Aerospace and Electronic Systems*, Vol. 55, No. 1, 2019, pp. 82–94.
DOI:10.1109/TAES.2018.2848319

[26] Lee, C. H., Hyun, C., Lee, J. G., Choi, J. Y., and Sung, S., "A Hybrid Guidance Law for a Strapdown Seeker to Maintain Lock-on Conditions against High Speed Targets," *Journal of Electrical Engineering and Technology*, Vol. 8, No. 1, 2013, pp. 190–196.
DOI:10.5370/JEET.2013.8.1.190

[27] Tekin, R., and Erer, K. S., "Switched-Gain Guidance for Impact Angle Control under Physical Constraints," *Journal of Guidance, Control, and Dynamics*, Vol. 38, No. 2, 2015, pp. 205–216.
DOI:10.2514/1.G000766

[28] Ratnoo, A., "Analysis of Two-Stage Proportional Navigation with Heading Constraints," *Journal of Guidance, Control, and Dynamics*, Vol. 39, No. 1, 2016, pp. 156–164.
DOI:10.2514/1.G001262

[29] Park, B.-G., Kwon, H.-H., Kim, Y.-H., and Kim, T.-H., "Composite Guidance Scheme for Impact Angle Control against a Nonmaneuvering Moving Target," *Journal of Guidance, Control, and Dynamics*, Vol. 39, No. 5, 2016, pp. 1132–1139.
DOI:10.2514/1.G001547

[30] Park, B.-G., Kim, T.-H., and Tahk, M.-J., "Biased PNG with Terminal-Angle Constraint for Intercepting Nonmaneuvering Targets Under Physical Constraints," *IEEE Transactions on Aerospace and Electronic Systems*, Vol. 53, No. 3, 2017, pp. 1562–1572.
DOI:10.1109/TAES.2017.2667518

[31] Park, B.-G., Kim, T.-H., and Tahk, M.-J., "Optimal Impact Angle Control Guidance Law Considering the Seeker's Field-of-View Limits," *Proceedings of the Institution of Mechanical Engineers, Part G: Journal of Aerospace Engineering*, Vol. 227, No. 8, 2012, pp. 1347–1364.
DOI:10.1177/0954410012452367

[32] Park, B.-G., Kim, T.-H., and Tahk, M.-J., "Range-to-Go Weighted Optimal Guidance with Impact Angle Constraint and Seeker's Look Angle Limits," *IEEE Transactions on Aerospace and Electronic Systems*, Vol. 52, No. 3, 2016, pp. 1241–1256.
DOI:10.1109/TAES.2016.150415

[33] Kim, T.-H., Park, B.-G., and Tahk, M.-J., "Bias-Shaping Method for Biased Proportional Navigation with Terminal-Angle Constraint," *Journal of Guidance, Control, and Dynamics*, Vol. 36, No. 6, 2013, pp. 1810–1816.
DOI:10.2514/1.59252

[34] Shaferman, V., "Optimal Guidance with an in Route Look-Angle Constraint," *AIAA Guidance, Navigation, and Control Conference*, Grapevine, TX, January 2017.
DOI:10.2514/6.2017-1507

[35] He, S., and Lin, D., "A Robust Impact Angle Constraint Guidance Law with Seeker's Field-of-View Limit," *Transactions of the Institute of Measurement and Control*, Vol. 37, No. 3, 2015, pp. 317–328.
DOI:10.1177/0142331214538278

[36] Kim, H.-G., Lee, J.-Y., and Kim, H. J., "Look Angle Constrained Impact Angle Control Guidance Law for Homing Missiles with Bearings-Only Measurements," *IEEE Transactions on Aerospace and Electronic Systems*, Vol. 54, No. 6, 2018, pp. 3096–3107.
DOI:10.1109/TAES.2018.2843600

[37] Turetsky, V., "Capture Zones of Linear Feedback Pursuer Strategies," *Automatica*, Vol. 44, No. 2, 2008, pp. 560–566.
DOI:10.1016/j.automatica.2007.06.014

[38] Guelman, M., "The Closed-Form Solution of True Proportional Navigation," *IEEE Transactions on Aerospace and Electronic Systems*, Vol. 12, No. 4, 1976, pp. 472–482.
DOI:10.1109/TAES.1976.308328

[39] Ghose, D., "True Proportional Navigation with Maneuvering Target," *IEEE Transactions on Aerospace and Electronic Systems*, Vol. 30, No. 1, 1994, pp. 229–237.
DOI:10.1109/7.250423

[40] Dhar, A., and Ghose, D., "Capture Region for a Realistic TPN Guidance Law," *IEEE Transactions on Aerospace and Electronic Systems*, Vol. 29, No. 3, 1993, pp. 995–1003.
DOI:10.1109/7.220946

[41] Kuo, C.-Y., and Chiou, Y.-C., "Geometric Analysis of Missile Guidance Command," *IEE Proceedings - Control Theory and Applications*, Vol. 147, No. 2, 2000, pp. 205–211.
DOI:10.1049/ip-cta:20000294

[42] Kuo, C.-Y., Soetanto, D., and Chiou, Y.-C., "Geometric Analysis of Flight Control Command for Tactical Missile Guidance," *IEEE Transactions on Control Systems Technology*, Vol. 9, No. 2, 2001, pp. 234–243.
DOI:10.1109/87.911375

[43] Dhananjay, N., Ghose, D., and Bhat, M. S., "Capturability of a Geometric Guidance Law in Relative Velocity Space," *IEEE Transactions on Control Systems Technology*, Vol. 17, No. 1, 2009, pp. 111–122.
DOI:10.1109/TCST.2008.924561

[44] Guelman, M., "A Qualitative Study of Proportional Navigation," *IEEE Transactions on Aerospace and Electronic Systems*, Vol. 7, No. 4, 1971, pp. 637–643.
DOI:10.1109/TAES.1971.310406

[45] Oh, J.-H., and Ha, I.-J., "Capturability of the 3-Dimensional Pure PNG Law," *IEEE Transactions on Aerospace and Electronic Systems*, Vol. 35, No. 2, 1999, pp. 491–503.
DOI:10.1109/7.766931

[46] Tyan, F., and Shen, J. F., "Capture Region of a Three Dimensional PPN Guidance Law Against a High Speed-Nonmaneuvering Target," *2008 American Control Conference*, Seattle, WA.
DOI:10.1109/ACC.2008.4587033

[47] Ghosh, S., Ghose, D., and Raha, S., "Capturability of Augmented Proportional Navigation (APN) Guidance with Nonlinear Engagement Dynamics," *American Control Conference*, Washington, DC, June 2013.
DOI:10.1109/ACC.2013.6579805

[48] Becker, K., "Closed-Form Solution of Pure Proportion Navigation," *IEEE Transactions on Aerospace and Electronic Systems*, Vol. 26, No. 3, 1990,

pp. 526–533.
DOI:10.1109/7.106131

[49] Ghosh, S., Ghose, D., and Raha, S., "Capturability Analysis of a 3-D Retro-PN Guidance Law for Higher Speed Nonmaneuvering Targets," *IEEE Transactions on Control Systems Technology*, Vol. 22, No. 5, 2014, pp. 1864–1874.
DOI:10.1109/TCST.2013.2289014

[50] Lee, S., Ann, S., Cho, N., and Kim, Y., "Capturability of Guidance Laws for Interception of Nonmaneuvering Target with Field-of-View Limit," *Journal of Guidance, Control, and Dynamics*, Vol. 42, No. 4, 2019, pp. 869–884.
DOI:10.2514/1.G003860

[51] Kumar, S. R., Rao, S., and Ghose, D., "Nonsingular Terminal Sliding Mode Guidance with Impact Angle Constraints," *Journal of Guidance, Control, and Dynamics*, Vol. 37, No. 4, 2014, pp. 1114–1130.
DOI:10.2514/1.62737

[52] Lee, S., Kim, Y., and Um, T.-Y., "Capture Region Analysis for Missile Guidance With Field-of-View Constraint against Moving Target," *30th Congress of the International Council of the Aeronational Sciences*, Daejeon, Korea, September 2016.

[53] Erer, K. S., Tekin, R., and Ozgoren, M. K., "Look Angle Constrained Impact Angle Control Based on Proportional Navigation," *AIAA Guidance, Navigation, and Control Conference*, Kissimmee, FL, January 2015.
DOI:10.2514/6.2015-0091

[54] Khalil, H. K.,, and Grizzle, J., *Nonlinear Systems*, Vol. 3, Prentice hall, Upper Saddle River, NJ, 1996.

Appendix A

Derivation of the deviated pursuit trajectory for RN-FOV

The nonlinear kinematics, Eq. (2.2), can be converted to the differential equation with respect to r as

$$\frac{dr}{r} = \frac{V_T \cos(\gamma_T - \lambda) - V_m \cos\sigma}{V_T \sin(\gamma_T - \lambda) + V_m \sin\sigma} d\lambda \tag{A.1}$$

Note that Eq.(A.1) depends only on λ because γ_T and σ are constant. Integrating by parts gives the analytic solution of the trajectory as

$$\ln\frac{r}{r_0} = \int_{\lambda_o}^{\lambda} \frac{V_T \cos(\gamma_T - \lambda)}{V_T \sin(\gamma_T - \lambda) + V_m \sin\sigma} d\lambda + \int_{\lambda_0}^{\lambda} \frac{-V_m \cos\sigma}{V_T \sin(\gamma_T - \lambda) + V_m \sin\sigma} d\lambda \tag{A.2}$$

Considering $\eta = V_T/V_m$ and $\zeta = \eta/\sin\sigma$, the terms inside the integration of the right hand side of Eq. (A.2) can be expressed as

$$\frac{V_T \cos(\gamma_T - \lambda)}{V_T \sin(\gamma_T - \lambda) + V_m \sin\sigma} = \frac{\zeta \cos(\gamma_T - \lambda)}{\zeta \sin(\gamma_T - \lambda) + 1} \tag{A.3}$$

$$\frac{-V_m \cos\sigma}{V_T \sin(\gamma_T - \lambda) + V_m \sin\sigma} = \frac{-\cot\sigma}{\zeta \sin(\gamma_T - \lambda) + 1} \tag{A.4}$$

By changing the variable $\zeta \sin(\gamma_T - \lambda) + 1 = t$, the first term of the right-hand side of Eq. (A.2) can be obtained as follows:

$$\int_{\lambda_0}^{\lambda} \frac{\zeta \cos(\gamma_T - \lambda)}{\zeta \sin(\gamma_T - \lambda) + 1} d\lambda = \int_{t}^{t_0} \frac{1}{t} dt = \ln\frac{\zeta \sin(\gamma_T - \lambda_0) + 1}{\zeta \sin(\gamma_T - \lambda) + 1} \tag{A.5}$$

By introducing the variable $x = \gamma_T - \lambda$, the trigonometric integral in the second term of the right-hand side of Eq. (A.2) can be expressed as follows:

$$\int_{\lambda_0}^{\lambda} \frac{1}{\zeta \sin(\gamma_T - \lambda) + 1} d\lambda = -\int_{x_0}^{x} \frac{1}{\zeta \sin x + 1} dx \tag{A.6}$$

To obtain the solution of Eq. (A.6), let us introduce an additional variable, $u = \tan\left(\frac{x}{2}\right)$. The variables x and u have the following relationship: $dx = 2du/(1+u^2)$ and $\sin x = 2u/(1+u^2)$. Note that $\int \frac{2}{(u)^2-(\zeta^2-1)} du = \frac{1}{\sqrt{\zeta^2-1}} \ln\left(\frac{\left|u+\zeta-\sqrt{\zeta^2-1}\right|}{\left|u+\zeta+\sqrt{\zeta^2-1}\right|}\right) + C$ in case $\zeta > 1$, and Eq. (A.6) can be rewritten as

$$\begin{aligned}
\int_{\lambda_0}^{\lambda} \frac{1}{\zeta \sin(\gamma_T - \lambda) + 1} d\lambda &= -\int_{u_0}^{u} \frac{2}{u^2 + 2\zeta u + 1} du = -\int_{u_0}^{u} \frac{2}{(u+\zeta)^2 - (\zeta^2 - 1)} du \\
&= \frac{-2}{\sqrt{\zeta^2 - 1}} \left(\frac{1}{2} \ln \left| \frac{u + \zeta - \sqrt{\zeta^2 - 1}}{u + \zeta + \sqrt{\zeta^2 - 1}} \right| \right) \Bigg|_{u_0}^{u} \\
&= \frac{2}{\sqrt{\zeta^2 - 1}} \left(\frac{1}{2} \ln \left| \frac{\frac{u+\zeta}{\sqrt{\zeta^2-1}} + 1}{\frac{u+\zeta}{\sqrt{\zeta^2-1}} - 1} \right| \right) \Bigg|_{u_0}^{u}
\end{aligned} \tag{A.7}$$

For a real axis, $x \in (-\infty, \infty)$, the inverse hyperbolic function $\tanh^{-1} x$ is defined as

$$\tanh^{-1} x = \begin{cases} \frac{1}{2} \ln\left(\frac{1+x}{1-x}\right) & x \in (-1,\, 1) \\ \pm\frac{1}{2}\pi i + \frac{1}{2} \ln\left(\frac{x+1}{x-1}\right) & x \in (-\infty, -1) \bigcup (1, \infty) \end{cases} \tag{A.8}$$

Therefore, the second term in Eq. (A.2) can be rewritten as

$$\begin{aligned}
&\int_{\lambda_0}^{\lambda} \frac{-\cos\sigma}{\eta \sin(\gamma_T - \lambda) + \sin\sigma} d\lambda \\
&= -\frac{2\cot\sigma}{\sqrt{\zeta^2 - 1}} \left\{ \tanh^{-1} \left(\frac{\tan\left(\frac{\gamma_T - \lambda}{2}\right) + \zeta}{\sqrt{\zeta^2 - 1}} \right) - \tanh^{-1} \left(\frac{\tan\left(\frac{\gamma_T - \lambda_0}{2}\right) + \zeta}{\sqrt{\zeta^2 - 1}} \right) \right\}
\end{aligned} \tag{A.9}$$

By substituting Eqs. (A.5) and (A.9) into Eq. (A.2), the analytic solution can be obtained as follows:

$$\frac{r}{r_0} = \frac{\zeta \sin(\gamma_T - \lambda_0) + 1}{\zeta \sin(\gamma_T - \lambda) + 1} \exp\left(-\frac{2 \cot \sigma}{\sqrt{\zeta^2 - 1}} \left(\tanh^{-1}\left(\frac{\tan\left(\frac{\gamma_T - \lambda}{2}\right) + \zeta}{\sqrt{\zeta^2 - 1}} \right) - \tanh^{-1}\left(\frac{\tan\left(\frac{\gamma_T - \lambda_0}{2}\right) + \zeta}{\sqrt{\zeta^2 - 1}} \right) \right) \right) \tag{A.10}$$

Appendix B

Proof of Corollary 3.1 and 3.2

B.1 Proof of Corollary 3.1

By Proposition 3.1, it can be proved by showing whether an equilibrium $\sigma_f \in [\underline{\sigma}, \bar{\sigma}]$ exists in its interval of initial LOS, where the conditions of the *partially capturable* and *capturable regions* depend on the condition of the initial look angle. Let $f(\sigma) = \lambda_0 - \frac{1}{N-1}(\sigma - \sigma_0)$ be the transition of λ by PPN and $g_H(\sigma) = \gamma_T - \pi - \sin^{-1}\left(\frac{V_m}{V_T}\sin\sigma\right)$ be the collision condition in the head-on engagement case. Considering the initial condition (λ_0,σ_0) as parameters, the equilibrium point of PPN σ_f can be obtained by solving $h_H(\sigma; \lambda_0, \sigma_0) = f(\sigma) - g_H(\sigma) = 0$.

First, let us examine a case in which the solution of h_H is in the FOV range $\sigma_f \in (\underline{\sigma}, \bar{\sigma})$. Because h_H is a strictly increasing function with respect to $\sigma \in [\underline{\sigma}, \bar{\sigma}]$, by Proposition 3.1, it can be stated that the location of an equilibrium point is $\sigma_f \in (\underline{\sigma}, \bar{\sigma})$ by the intermediate value theorem if and only if $h_H(\underline{\sigma}) < 0$, and $h_H(\bar{\sigma}) > 0$. Using $\sin\bar{\sigma}/\eta = 1/\zeta_{\lim}$ and $\sin\underline{\sigma}/\eta = -1/\zeta_{\lim}$, h_H gives

$$h_H(\underline{\sigma}; \lambda_0, \sigma_0) = \lambda_0 - \frac{1}{N-1}(\underline{\sigma} - \sigma_0) - (\gamma_T + \pi) - \sin^{-1}\left(\frac{1}{\zeta_{\lim}}\right) < 0 \quad \text{(B.1)}$$

$$h_H(\bar{\sigma}; \lambda_0, \sigma_0) = \lambda_0 - \frac{1}{N-1}(\bar{\sigma} - \sigma_0) - (\gamma_T + \pi) + \sin^{-1}\left(\frac{1}{a}\right) > 0 \quad \text{(B.2)}$$

For the *capturable* region, Eqs. (B.1) and (B.2) should be satisfied regardless of $\sigma_0 \in [\underline{\sigma}, \bar{\sigma}]$. Because h_H is increasing with respect to σ_0, substituting $\sigma_0 = \bar{\sigma}$ into Eq. (B.1) and $\sigma_0 = \underline{\sigma}$ into Eq. (B.2) yields

$$\begin{aligned} h_H(\underline{\sigma}; \lambda_0, \sigma_0 = \bar{\sigma}) &= \lambda_0 - (\gamma_T + \pi) - \sin^{-1}\left(\frac{1}{\zeta_{\lim}}\right) - \frac{1}{N-1}(\underline{\sigma} - \bar{\sigma}) < 0 \\ h_H(\bar{\sigma}; \lambda_0, \sigma_0 = \underline{\sigma}) &= \lambda_0 - (\gamma_T + \pi) + \sin^{-1}\left(\frac{1}{\zeta_{\lim}}\right) - \frac{1}{N-1}(\bar{\sigma} - \underline{\sigma}) > 0 \end{aligned} \tag{B.3}$$

Equation (B.3) means that h_H has a solution $\sigma_f \in (\underline{\sigma}, \bar{\sigma})$ for any initial look angle $\sigma_0 \in [\underline{\sigma}, \bar{\sigma}]$ if $\bar{\lambda}^c_{PPN,HO} < \lambda_0 < \underline{\lambda}^c_{PPN,HO}$. To examine the existence of the solution σ_f including $\sigma_f = \underline{\sigma}$ or $\sigma_f = \bar{\sigma}$ at the initial LOS boundary $\lambda_0 = \underline{\lambda}^c_{PPN,HO}$, substituting ($\underline{\sigma}$,$\lambda_0 = \underline{\lambda}^c_{PPN,HO}$) and ($\bar{\sigma}$, $\lambda_0 = \underline{\lambda}^c_{PPN,HO}$) of Eq. (3.11) into h_H respectively gives the following inequalities.

$$\begin{aligned} h_H(\underline{\sigma}; \lambda_0 = \underline{\lambda}^c_{PPN,HO}, \sigma_0) &= -\frac{1}{N-1}(\bar{\sigma} - \sigma_0) \le 0 \\ h_H(\bar{\sigma}; \lambda_0 = \underline{\lambda}^c_{PPN,HO}, \sigma_0) &= 2\sin^{-1}\left(\frac{1}{\zeta_{\lim}}\right) - \frac{1}{N-1}(2\bar{\sigma} - \underline{\sigma} - \sigma_0) \\ &\ge 2\sin^{-1}\left(\frac{1}{\zeta_{\lim}}\right) - \frac{2}{N-1}(\bar{\sigma} - \underline{\sigma}) > 0 \end{aligned} \tag{B.4}$$

Note from $N > 2(1+\eta)$ and $\sigma_{\lim} = \bar{\sigma} = -\underline{\sigma} \in (0, \sin^{-1}(1/\eta))$ that Eq. (B.1) is always greater than zero. By introducing $\varphi(\sigma_{\lim}) = \sin^{-1}\left(\frac{1}{\eta}\sin\sigma_{\lim}\right) - \frac{2}{N-1}\sigma_{\lim}$, it can be shown that $\phi(\sigma_{\lim}) > 0$ since $\varphi'(\sigma_{\lim}) > \varphi'(0) = 1/\eta - 2/(N-1) > 0$ and $\varphi(0) = 0$. From Eq. (B.4), $h(\sigma_f = \underline{\sigma}; \lambda_0 = \underline{\lambda}^c_{PPN,HO}, \sigma_0 = \bar{\sigma}) = 0$ implies that when $\lambda_0 = \underline{\lambda}^c_{PPN,HO}$, $\sigma_f \in (\underline{\sigma}, \bar{\sigma})$ if $\underline{\sigma} \le \sigma_0 < \bar{\sigma}$ and $\sigma_f = \underline{\sigma}$ if $\sigma_0 = \bar{\sigma}$. Similarly, substituting ($\underline{\sigma}$,$\lambda_0 = \bar{\lambda}^c_{PPN,HO}$) and ($\bar{\sigma}$, $\lambda_0 = \bar{\lambda}^c_{PPN,HO}$) of Eq. (3.11)

into h_H respectively gives

$$\begin{aligned} h_H(\underline{\sigma}; \lambda_0 = \bar{\lambda}^c_{PPN,HO}, \sigma_0) &= -2\sin^{-1}\left(\frac{1}{\zeta_{\lim}}\right) + \frac{1}{N-1}\left(2\bar{\sigma} - \underline{\sigma} - \sigma_0\right) \\ &\leq -2\sin^{-1}\left(\frac{1}{\zeta_{\lim}}\right) + \frac{2}{N-1}\left(\bar{\sigma} - \underline{\sigma}\right) < 0 \\ h_H(\bar{\sigma}; \lambda_0 = \bar{\lambda}^c_{PPN,HO}, \sigma_0) &= \frac{1}{N-1}\left(\sigma_0 - \underline{\sigma}\right) \geq 0 \end{aligned} \tag{B.5}$$

Therefore, for $\lambda_0 = \bar{\lambda}^c_{PPN,HO}$, $\sigma_f \in (\underline{\sigma}, \bar{\sigma})$ if $\underline{\sigma} < \sigma_0 \leq \bar{\sigma}$ and $\sigma_f = \bar{\sigma}$ if $\sigma_0 = \underline{\sigma}$. Equations (B.3)-(B.5) show that $\lambda_0 \in [\bar{\lambda}^c_{PPN,HO}, \underline{\lambda}^c_{PPN,HO}]$ is the *capturable* region of PPN.

For the *partially capturable region*, the necessary condition of the initial LOS can be obtained by substituting $\sigma_0 = \underline{\sigma}$ into Eq. (B.1) and $\sigma_0 = \bar{\sigma}$ into Eq. (B.2), respectively, as

$$\begin{aligned} h_H(\underline{\sigma}; \lambda_0, \sigma_0 = \underline{\sigma}) &= \lambda_0 - (\gamma_T + \pi) - \sin^{-1}\left(\frac{1}{a}\right) < 0 \\ h_H(\bar{\sigma}; \lambda_0, \sigma_0 = \bar{\sigma}) &= \lambda_0 - (\gamma_T + \pi) + \sin^{-1}\left(\frac{1}{a}\right) > 0 \end{aligned} \tag{B.6}$$

For the solution at the FOV limit $\sigma_f = \underline{\sigma}$ and $\sigma_f = \underline{\sigma}$, substituting the initial condition at the boundary $\lambda_0 = \lambda^*_{\bar{\sigma},HO} = \bar{\lambda}^{pc}_{PPN,HO}$ and $\lambda_0 = \lambda^*_{\underline{\sigma},HO} = \underline{\lambda}^{pc}_{PPN,HO}$ and the final condition into h_H yields

$$\begin{aligned} h_H(\underline{\sigma}; \lambda_0 = \underline{\lambda}^{pc}_{PPN,HO}, \sigma_0) &= \frac{1}{N-1}\left(\sigma_0 - \underline{\sigma}\right) \leq 0 \\ h_H(\bar{\sigma}; \lambda_0 = \bar{\lambda}^{pc}_{PPN,HO}, \sigma_0) &= -\frac{1}{N-1}\left(\bar{\sigma} - \sigma_0\right) \geq 0 \end{aligned} \tag{B.7}$$

Note that the equality condition of Eq. (B.7) only guarantees the existence of the solution. That is, $h_H(\sigma_f = \underline{\sigma}; \lambda_0 = \underline{\lambda}^{pc}_{PPN,HO}, \sigma_0 = \underline{\sigma}) = 0$ and $h_H(\sigma_f = \bar{\sigma}; \lambda_0 = \bar{\lambda}^{pc}_{PPN,HO}, \sigma_0 = \bar{\sigma}) = 0$ are the only solutions for each initial condition, respectively. Therefore, $\lambda_0 \in [\bar{\lambda}^{pc}_{PPN,HO}, \underline{\lambda}^{pc}_{PPN,HO}]$ is the *partially capturable region* of PPN.

B.2 Proof of Corollary 3.2

Sufficient conditions for capture in the tail-chase engagement case can be obtained in a similar manner to the head-on engagement case by showing whether the terminal look angle exists within the FOV. By introducing a strictly decreasing function of σ, $h_T(\sigma;\lambda_0,\sigma_0) = f(\sigma) - g_T(\sigma) = 0$, where $f(\sigma) = \lambda_0 + \frac{1}{1-N}(\sigma - \sigma_0)$ and $g_T(\sigma) = \gamma_T + \sin^{-1}\left(\frac{V_m}{V_T}\sin\sigma\right)$, the necessary condition for the existence of a solution can be obtained as follows:

$$\begin{aligned} h_T(\bar{\sigma};\lambda_0,\sigma_0 = \underline{\sigma}) &= \lambda_0 - \gamma_T + \sin^{-1}\left(\frac{1}{\zeta_{\lim}}\right) - \frac{1}{1-N}\left(\bar{\sigma} - \underline{\sigma}\right) \geq 0 \\ h_T(\underline{\sigma};\lambda_0,\sigma_0 = \bar{\sigma}) &= \lambda_0 - \gamma_T - \sin^{-1}\left(\frac{1}{\zeta_{\lim}}\right) + \frac{1}{1-N}\left(\bar{\sigma} - \underline{\sigma}\right) \leq 0 \end{aligned} \tag{B.8}$$

The initial LOS angle satisfying the above inequalities is *partially capturable.* Furthermore, the solution always exists when the following inequalities hold.

$$\begin{aligned} \lambda_0 - \gamma_T + \sin^{-1}\left(\frac{1}{\zeta_{\lim}}\right) &\geq 0 \\ \lambda_0 - \gamma_T - \sin^{-1}\left(\frac{1}{\zeta_{\lim}}\right) &\leq 0 \end{aligned} \tag{B.9}$$

The terminal LOS lies within the admissible LOS range whenever $\lambda_0 \in [\underline{\lambda}^c_{PPN,TC}, \bar{\lambda}^c_{PPN,TC}]$, $\forall\sigma_0 \in [\underline{\sigma}, \bar{\sigma}]$.

Appendix C

Proof of Corollary 5.1 and 5.2

The LOS kinematics of Eq. (A.1) can be rearranged as

$$\frac{d\lambda}{dr} = \frac{\eta \sin(\gamma_T - \lambda) + \sin\sigma}{\eta \cos(\gamma_T - \lambda) - \cos\sigma} \frac{1}{r} \tag{C.1}$$

Since $\frac{\partial}{\partial \sigma}\frac{d\lambda}{dr} < 0$ for $\sigma \in [\underline{\sigma}, \bar{\sigma}]$, we have

$$\frac{\eta \sin(\gamma_T - \lambda) + \sin\underline{\sigma}}{\eta \cos(\gamma_T - \lambda) - \cos\underline{\sigma}} \frac{1}{r} \leq \frac{d\lambda}{dr} \leq \frac{\eta \sin(\gamma_T - \lambda) + \sin\bar{\sigma}}{\eta \cos(\gamma_T - \lambda) - \cos\bar{\sigma}} \frac{1}{r} \tag{C.2}$$

Note from Eq. (C.2) that the boundaries are equivalent to the deviated-pursuit trajectories. By the comparison principle [54], the solution is bounded by the deviated pursuit trajectories that maintain maximum or minimum look angles. Note that the maximal trajectory $(\bar{r}, \bar{\lambda})$ and minimal trajectory $(\underline{r}, \underline{\lambda})$ can be obtained from Eq. (A.2) instead of integrating Eq.(C.2).

C.1 Proof of Corollary 5.1

By Proposition 3.3, any trajectory in the complimentary LOS angle domain $[\gamma_T - \frac{3\pi}{2}, \bar{\lambda}^{pc}_{HO}) \bigcup (\underline{\lambda}^{pc}_{HO}, \gamma_T - \frac{\pi}{2}]$ has a larger miss-intercept distance than that of the deviated pursuit $\bar{r} = \Phi(\bar{\lambda}, \lambda_0; \bar{\sigma}) r_0$ or $\underline{r} = \Phi(\underline{\lambda}, \lambda_0; \underline{\sigma}) r_0$. The initial LOS is farther from the equilibrium point than the boundaries of the *partially capturable region* of LCG, i.e., $\bar{\lambda}_0 < \bar{\lambda}(r_0) < \lambda^*_{\bar{\sigma},HO}$ or $\underline{\lambda}_0 > \underline{\lambda}(r_0) > \lambda^*_{\underline{\sigma},HO}$, and therefore the miss distance is always greater than R_{miss}.

To show the sufficiency of the *capturable region*, let us examine the domain of λ_0 with fixed r_0. The initial LOS angle domain $[\bar{\lambda}^{pc}_{HO}, \underline{\lambda}^{pc}_{HO}]$ can be divided into $[\bar{\lambda}^{pc}_{HO}, \bar{\lambda}^{pc}_{PPN,HO})$, $[\bar{\lambda}^{pc}_{PPN,HO}, \underline{\lambda}^{pc}_{PPN,HO}]$, and $(\underline{\lambda}^{pc}_{PPN,HO}, \underline{\lambda}^{pc}_{HO}]$. If $\lambda_0 \in (\underline{\lambda}^{pc}_{PPN,HO}, \underline{\lambda}^{pc}_{HO}]$, there exists $\sigma_0 = \underline{\sigma}$ such that the trajectory of the guidance is equivalent to that of the deviated pursuit while keeping $\underline{\sigma}$. Since λ_0 is closer to the equilibrium point $\lambda^*_{\underline{\sigma},HO}$ than is $\underline{\lambda}^{pc}_{HO}$, i.e., $\lambda^*_{\underline{\sigma},HO} < \lambda_0 \leq \underline{\lambda}^{pc}_{HO}$, the miss-intercept value is less than R_{miss}, i.e., $\underline{r}_f = \Phi(\underline{\lambda}(\underline{r}_f), \lambda_0; \underline{\sigma}) r_0 \leq \Phi(\underline{\lambda}_{HO,f}, \lambda^{pc}_{HO}; \underline{\sigma}) r_0 = R_{\text{miss}}$. Similarly, it can be shown that in $\lambda_0 \in [\bar{\lambda}^{pc}_{HO}, \bar{\lambda}^{pc}_{PPN,HO})$, there exist an initial look angle $\sigma_0 = \bar{\sigma}$ such that $\bar{r}_f = \Phi(\bar{\lambda}(\bar{r}_f), \lambda_0; \bar{\sigma}) r_0 \leq R_{\text{miss}}$. By Corollary. 3.1, there exists $\lambda_0 \in \mathcal{L}_{adm,HO}$ satisfying $\lambda_f \in \mathcal{L}_{adm,HO}$, which means that the missile guided by LCG can intercept the target without switching of the command. Therefore, there exist some initial velocity directions to guarantee interception only if λ_0 is in the interval $[\bar{\lambda}^{pc}_{HO}, \underline{\lambda}^{pc}_{HO}]$.

For the capturable region, without loss of generality, consider a region $\bar{\lambda}^{c}_{HO} \leq \lambda_0 < \bar{\lambda}^{c}_{PPN,HO}$. For any $\bar{\lambda}^{c}_{HO} \leq \lambda_0 < \bar{\lambda}^{c}_{PPN,HO}$, there exists an initial look angle $\sigma_0 = \sigma_c \in [\underline{\sigma}, \bar{\sigma})$ such that the missile finally reaches engagement by converging the collision course to $\lambda^*_{\bar{\sigma},HO}$, which can be expressed as

$$\lambda_{PPN} = \lambda_0 - \frac{1}{N-1}(\bar{\sigma} - \sigma_c) = \lambda^*_{\bar{\sigma},HO} \tag{C.3}$$

Then, the missile finally achieves homing by PPN if $\sigma_c \leq \sigma_0 < \bar{\sigma}$. Otherwise, the guidance command is switched from PPN to look angle control because the terminal LOS by PPN λ_{PPN} is constructed outside the admissible LOS. Let us define $\lambda^*_{sw} = \lambda_0(r_0) - \frac{1}{N-1}(\bar{\sigma} - \underline{\sigma})$; then, the LOS angle λ_{sw} at the switching time is

$$\lambda^*_{sw} \leq \lambda_{sw} < \lambda^*_{\bar{\sigma},HO} \tag{C.4}$$

Equation (C.4) means that the trajectory starting from the initial look angle $\sigma_0 = \underline{\sigma}$ has the switching point farthest from the equilibrium condition. Substituting the initial condition, $\bar{\lambda}^c_{HO} \le \lambda_0$, into λ^*_{sw} yields

$$\bar{\lambda}^{pc}_{HO} = \bar{\lambda}^c_{HO}(r_0) - \frac{1}{N-1}(\bar{\sigma} - \underline{\sigma}) \le \lambda_0(r_0) - \frac{1}{N-1}(\bar{\sigma} - \underline{\sigma}) \tag{C.5}$$

Note that $\bar{\lambda}^{pc}_{HO}$ defined in Eq. (3.32) is the switching point of the "*worst*"-case solution when $\lambda_0 = \bar{\lambda}^c_{HO}$. Therefore, any trajectory starting from the initial position with $\underline{\sigma} \le \sigma_0 < \sigma_c$ has $\bar{\lambda}^{pc}_{HO} < \lambda^*_{sw} \le \lambda(r_{sw}) < \lambda^*_{\bar{\sigma},HO}$, and the miss distance is always less than R_{miss}.

C.2 Proof of Corollary 5.2

To verify the *capturable region*, let us consider a domain of λ_0. The initial LOS angle domain $[\underline{\lambda}^c_{TC}, \bar{\lambda}^c_{TC}]$ can be divided into $[\underline{\lambda}^c_{TC}, \underline{\lambda}^c_{PPN,TC})$, $[\underline{\lambda}^c_{PPN,TC}, \bar{\lambda}^c_{PPN,TC}]$, and $(\bar{\lambda}^c_{PPN,TC}, \bar{\lambda}^c_{TC}]$. It is obvious that the missile can intercept the target if $\lambda_0 \in [\underline{\lambda}^c_{PPN,TC}, \bar{\lambda}^c_{PPN,TC}]$, which is the *capturable region* of PPN for the tail-chase engagement case. Without loss of generality, suppose that the initial LOS is in the domain $(\bar{\lambda}^c_{PPN,TC}, \bar{\lambda}^c_{TC}]$. By Proposition 3.4, the trajectory yielding the maximum miss distance is the deviated pursuit trajectory with initial $\sigma_0 = \bar{\sigma}$. The initial LOS is closer to the equilibrium point such that $\lambda^*_{\bar{\sigma},TC} < \bar{\lambda}_0 < \bar{\lambda}^c_{TC}(r_0)$, which provides a miss distance smaller than R_{miss}. As a result, the missile intercepts the target with any initial look angle.

The *partially capturable region* can be proved by showing that the trajectory of Eq. (3.47) is the marginal trajectory of the *capturable region*. Without loss of generality, the domain $(\bar{\lambda}^c_{TC}, \bar{\lambda}^{pc}_{TC}]$ can be considered. Suppose that the initial LOS satisfies $\bar{\lambda}^c_{TC} \le \lambda_0 \le \bar{\lambda}^{pc}_{TC}$ with $\sigma_0 = \underline{\sigma}$; then, the LOS angle at the

switching of the guidance command has $\lambda_{\bar{\sigma},TC} < \lambda_{sw} \leq \bar{\lambda}^{pc}_{TC}(\bar{r}_2)$. Because λ_{sw} is close to the equilibrium point, $\lambda_{\bar{\sigma},TC}$, compared to $\bar{\lambda}^{pc}_{TC}(\bar{r}_2)$, the trajectory generated by the look angle control yields a miss-intercept distance smaller than R_{miss}.

국문초록

본 논문에서는 이동표적 요격을 목적으로 한 스트랩다운 탐색기를 탑재한 유도탄의 시계제한을 고려한 유도기법 요격영역을 분석하였다. 유도탄의 유도기법은 임무 목적에 따라 표적요격을 위한 유도기법과 충돌각제어 유도기법으로 분류된다. 중기유도와의 유도기법 적용이 용이하도록 유도기법의 요격영역은 초기위치로 나타내었고, 유도탄의 물리적 특성으로 탐색기의 시계제한, 가속도 제한 등을 고려하였다. 산출된 요격영역을 바탕으로 시계제한 유도기법의 성능과 시계제한에 따른 특성을 분석하였다.

본 논문에서는 표적요격 유도기법의 요격영역 분석을 위해 순수비례항법 유도기법과 시계제한을 고려한 관측각제어기법, 그리고 순수비례항법 유도를 결합한 복합유도기법을 고려하였다. 각 유도기법의 요격영역은 순수비례항법 유도기법과 추적유도기법의 궤적 특성과 해석해를 이용하여 산출하였다. 순수비례항법 유도법칙은 탐색기 시계제한의 영향으로 협소한 교전영역이 발생하였고, 정면 및 후면 교전상황에 따라 교전영역이 분할되었다. 시계제한을 고려한 복합유도기법의 경우, 관측각제어에 의해 시계제한을 유지하는 기동을 수행한 효과로 순수비례항법에 비해 요격영역이 확장되었다. 특히, 추적유도기법의 특성에 따라 정면요격보다 후면요격 상황에서 보다 넓은 교전영역이 발생하였다.

한편, 충돌각 제어 유도기법의 요격영역 분석을 위해 초기구간에는 추적유도를 수행하고, 종말구간에는 비례항법 유도기법을 수행하는 복합 유도기법을 고려하였다. 산출된 요격영역은 탐색기의 협시계 제한에 의해 정면 및 후면 교전상황에 대해 분할된 교전영역이 발생하였고, 달성가능 충돌각은 시계제한 구속조건에 의해 영역이 제한되었다. 충돌각 복합유도의 요격영역은 초기거리에 따른 충돌각,

초기시선각에 따른 달성가능 충돌각, 특정 충돌각 구속조건을 만족하기 위한 초기 위치 및 달성가능한 충돌각과 같은 세부영역을 기반으로 영역특성을 해석하였다. 또한, 본 연구에서는 기존에 제안된 충돌각 제어 복합유도기법의 성능을 개선하기 위해 발사 초기구간에 설정된 관측각 명령을 수정하는 유도기법을 제안하였다. 제안된 유도기법은 기존 충돌각 복합 유도기법에 비해 넓은 요격영역이 산출되었다.

본 연구에서 유도한 요격영역을 검증하기 위해 수치 시뮬레이션을 수행하였다. 공대공 교전상황에 대한 정면 및 후면 교전 시나리오를 고려한 시뮬레이션 결과는 본 연구에서 제시한 수학적 해석의 결과를 뒷받침하였다. 각 유도기법의 성능을 비교하여 협시계 제한 기동에 의해 비례항법 유도기법의 표적요격 성능이 향상되고, 본 연구에서 제안한 충돌각 유도기법의 경우 기존 유도기법에 비해 넓은 영역에서 충돌각 유도성능이 나타남을 보였다.

주요어: 미사일유도, 요격영역분석, 비례항법유도, 관측각제어, 시계제한
학번: 2012-20690